Journal of Medicinal Chemistry

Article

Discovery of Marinoquinolines as Potent and Fast-Acting Plasmodium falciparum Inhibitors with In Vivo Activity

Anna Caroline Campos Aguiar, Michele Panciera, Eric Francisco Simão dos Santos, Maneesh Kumar Singh, Mariana Lopes Garcia, Guilherme Eduardo de Souza, Myna Nakabashi, José Luiz Costa, Célia R.S. Garcia, Glaucius Oliva, Carlos Roque Duarte Correia, and Rafael Victorio Carvalho Guido

J. Med. Chem., **Just Accepted Manuscript** • DOI: 10.1021/acs.jmedchem.8b00143 • Publication Date (Web): 07 Jun 2018

ACS Publications

is published by the American Chemical Society. 1155 Sixteenth Street N.W., Washington, DC 20036

Discovery of Marinoquinolines as Potent and Fast-Acting *Plasmodium falciparum* Inhibitors with In Vivo Activity

Anna Caroline Campos Aguiar[1‡], *Michele Panciera*[2‡], *Eric Francisco Simão dos Santos*[2], *Maneesh Kumar Singh*[3,4], *Mariana Lopes Garcia*[1], *Guilherme Eduardo de Souza*[1], *Myna Nakabashi*[4], *José Luiz Costa,*[5] *Célia R.S. Garcia*[3], *Glaucius Oliva*[1], *Carlos Roque Duarte Correia*[2]*, *Rafael Victorio Carvalho Guido*[1]*

1 Sao Carlos Institute of Physics, University of Sao Paulo, Av. Joao Dagnone, 1100 Jardim Santa Angelina, São Carlos, SP, 13563-120, Brazil

2 Institute of Chemistry, State University of Campinas, Josue de Castro St., Campinas, SP, 13083-970, Brazil

3 Faculty of Pharmaceutical Sciences, University of Sao Paulo, Av. Prof. Lineu Prestes, 580 Cidade Universitária, São Paulo, SP, 05508-900, Brazil

4 Department of Physiology, University of Sao Paulo, Rua do Matão 101, travessa 14, São Paulo, SP, 05508-090, Brazil

5 Faculty of Pharmaceutical Sciences, State University of Campinas, Rua Oswaldo Cruz, 2º andar, bloco F3, Cidade Universitária, Campinas, SP, 13083-859, Brazil

‡These authors contributed equally to the work

*Corresponding authors: (RVCG) rvcguido@ifsc.usp.br; (CRDC) roque@iqm.unicamp.br

ABSTRACT

We report the discovery of marinoquinoline (3*H*-pyrrolo[2,3-*c*]quinoline) derivatives as new chemotypes with antiplasmodial activity. We evaluated their inhibitory activities against *P. falciparum* and conducted a structure-activity relationship study, focusing on improving their potency and maintaining low cytotoxicity. Next, we devised quantitative structure activity relationship models (QSAR), which we prospectively validated, to discover new analogues with enhanced potency. The most potent compound, **50** (IC_{50}^{3d7} = 39 nM; IC_{50}^{K1} = 41 nM), is a fast-acting inhibitor with dual-stage (blood and liver) activity. The compound showed considerable selectivity (SI > 6410), an additive effect when administered in combination with artesunate, excellent tolerability in mice (all mice survived after an oral treatment with a 1000 mg/kg dose) and oral efficacy at 50 mg/kg in a mouse model of *P. berghei* malaria (62% reduction in parasitemia on day 5 post-infection); thus, compound **50** was considered a lead compound for the discovery of new antimalarial agents.

INTRODUCTION

Malaria is one of the most prevalent parasitic infections in the world. The disease affects 216 million people each year, and in 2016, it was estimated to have caused 445,000 deaths. In humans, malaria is caused by *Plasmodium falciparum*, *Plasmodium knowlesi*, *Plasmodium malariae*, *Plasmodium ovale*, and *Plasmodium vivax*, of which *P. falciparum* is responsible for highest mortality, particularly in children under 5 years old in Africa.[1]

The human malaria parasite has a complex life cycle that includes several developmental stages in the human host and the mosquito vector, which tremendously contributes to the challenge of eradicating malaria.[2–5] Disease control still relies on chemotherapy; however, drug resistance is a limiting factor, and the emergence of artemisinin resistance in southeast Asia and China is a serious threat to the global control of *P. falciparum* malaria.[6–9] Therefore, the discovery and development of new and efficacious drugs for the treatment and prevention of malaria are urgently needed to both overcome resistance and meet the challenge of eradicating malaria.[10–13] Due to the limitations of available chemotherapies, several efforts have focused on expanding the range of new antimalarial compounds to thwart parasite growth.[14–23] In this context, ideal new drugs should (1) not exhibit cross-resistance to existing drugs, (2) be administered as a single dose, (3) prevent transmission (active against the sexual stages of the parasite), and (4) provide chemoprotection (active against liver stages).[24]

Marinoquinolines (**MQ**) were first isolated from the marine gliding bacteria *Rapidithrix thailandica* (**MQ A**) and exhibit acetylcholinesterase-inhibiting activity.[25] Subsequently, some new MQ derivatives (**MQ B-F**) were isolated from another gliding bacteria, *Ohtaekwangia kribbensis* (Figure 1). All natural MQs contain the 3*H*-pyrrolo[2,3-*c*]quinoline core and exhibit moderate antiprotozoal activity against the chloroquine-resistant *P. falciparum* K1 lineage (IC_{50} = 1.7 – 15 μM) and *Trypanosoma cruzi* (IC_{50} = 22 – 53 μM) as

well as cytotoxic activity against the tumor cell lines L929, MCF-7 and KB-3-1.[26] Recently, other natural marinoquinoline analogs were isolated from bacterial strains of the species *Mooreia alkaloidigena* and *Catalinimonas alkaloidigena*. Five novel natural compounds were isolated from these cell cultures (**MQ G-K**). **MQ I** showed activity against the bacterial strain CNJ-912 (*Pontibacillus* sp.), whereas **MQ J** and **MQ K**, were tested against chloroquine-resistant strain of *P. falciparum* (K1) and showed IC_{50} values of 3.2 and 6.4 μM, respectively.[27,28] Based on these findings, which indicate that marinoquinolines have promising biological activity against the malaria parasite, here, we report the use of an integrated approach, including assessments of structure-activity relationships (SAR), quantitative structure-activity relationships (QSAR), mechanistic assessments, parasitological profiling and in vivo evaluation, to identify a frontrunner compound as a lead candidate for the discovery of new antimalarial agents.

RESULTS

Structure-activity Relationships

Chemistry. Effective routes were developed for the synthesis of several marinoquinoline derivatives from readily available starting materials or from intermediates synthesized as indicated in Schemes 1a-1c and Equations 1a-1c. The pinacol borane reagent 3-(4,4,5,5-tetramethyl-[1,3,2]dioxaborolan-2-yl)-1-(triisopropyl-silanyl)-1*H*-pyrrole **2** was synthesized on the gram scale by adapting procedures reported by Buchwald and Billingsley,[29] and Muchowski and coworkers,[30,31] and an overall yield of 58% was obtained in three steps. For the synthesis of iodobenzenes **25** and **26**, anilines **23** and **24** were first converted into their corresponding aryl diazonium salts, followed by iodination with NaI to provide the desired iodobenzenes **25** and **26** at 82% and 73% yields, respectively (Equation 1a).[32] The key

intermediate aryl pyrroles **3, 28** and **31** were synthesized using Suzuki-Miyaura cross-coupling reactions between pyrrole boronate ester **2** and the respective iodo- and bromo-aryl compounds **1, 25** and **26**, producing moderate to good yields (Schemes 1a and 1b). The nitro-containing aryl pyrrole **30**, which was obtained by another Suzuki-Miyaura coupling reaction followed by removal of the TIPS protecting group by TBAF, as indicated in Scheme 1c, was reduced by catalytic hydrogenation to provide the pyrroloaniline **31**. After obtaining pyrroloanilines **3, 28** and **31**, several marinoquinolines analogues were then synthesized using modified Pictet-Spengler reactions employing aliphatic and aromatic aldehydes. Two Pictet-Spengler protocols were devised to improve the effectiveness of the cyclization reactions. Methods A (using trifluoroacetic acid) and B (using benzotriazole and *p*-toluene sulfonic acid) generated marinoquinoline analogues **4-22** (Scheme 1a), **32-44** (Scheme 1c), and **48-50** (Equation 1c) in moderate to good isolated yields. Finally, the bromo-marinoquinolines **45-47** were prepared by a regioselective bromination reaction of marinoquinolines **19, 33** and **35** using NBS, as indicated in Scheme 1b.

Scheme 1: General scheme for the preparation of marinoquinolines (MQ).

Scheme 1a: Preparation of the marinoquinolines using Suzuki Coupling and Pictet-Spengler ring closure

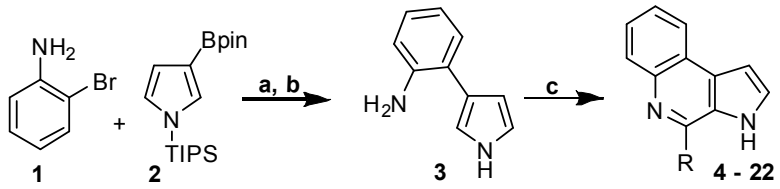

4 - methyl
5 - isobutyl
6 - benzyl
7 - ethyl
8 - phenyl
9 - 4-methoxy
10 - 3,5-dimethoxy
11 - 3,4,5-trimethoxy
12 - 4-chloro
13 - 4-bromo
14 - 4-nitro
15 - 4-amino
16 - 4-dimethylamino
17 - 4 - CO_2H
18 - 4- CO_2Me
19 - indole-3-yl
20 - 5-bromo-indol-3-yl
21 - 6-bromo-indol-3-yl
22 - indol-2-yl

Equation 1a: Preparation of the Iodobenzenes

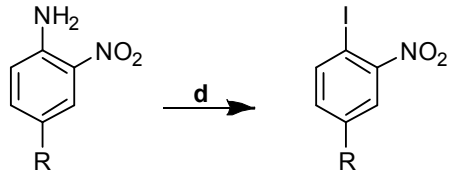

23: R= Br
24: R= OMe

25: R= Br
26: R= OMe

Scheme 1b: Preparation of the brominated marinoquinoline using Suzuki Coupling and Pictet-Spengler ring closure

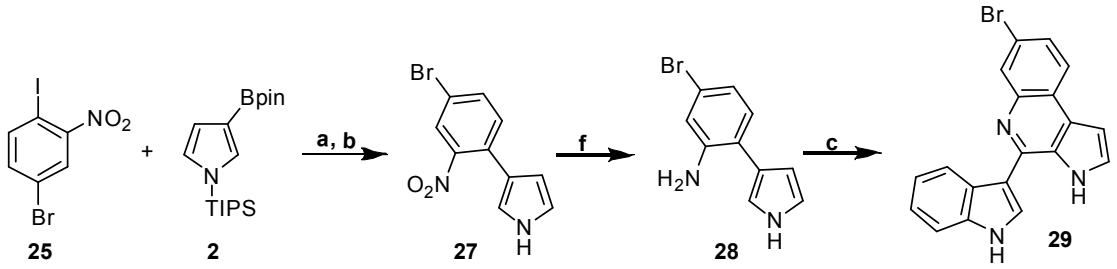

25 **2** **27** **28** **29**

Scheme 1c: Preparation of the methoxylated marinoquinoline using Suzuki Coupling and Pictet-Spengler ring closure

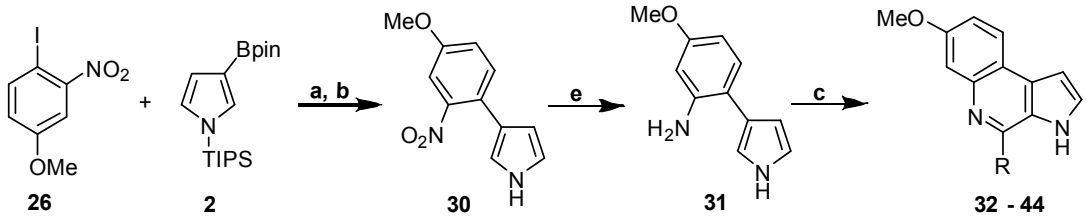

26 **2** **30** **31** **32 - 44**

32 - isobutyl
33 - methyl
34 - ethyl
35 - phenyl
36 - 3,5-dimethoxy
37 - 3,4,5-trimethoxy
38 - nitrophenyl
39 - aminophenyl
40 - 4-dimethylamino phenyl
41 - 4-carboxyphenyl
42 - 4-CO_2Me-phenyl
43 - 4-chlorophenyl
44 - benzyl

Equation 1b: Regioselective bromination of marinoquinolines **19** and 33

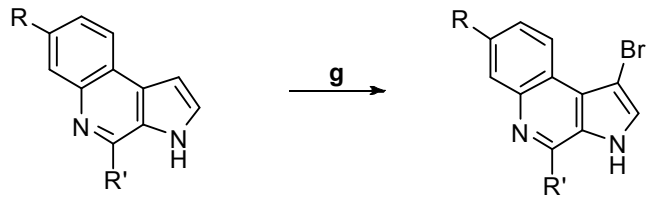

19: R= H, R' = indole-3-yl
33: R= OMe, R' = methyl
35: R= OMe, R' = phenyl

45: R= H, R' = indole3-yl
46: R= OMe, R' = methyl
47: R= OMe, R' = phenyl

Equation 1c: Preparation of the theoretically predicted marinoquinolines derivatives

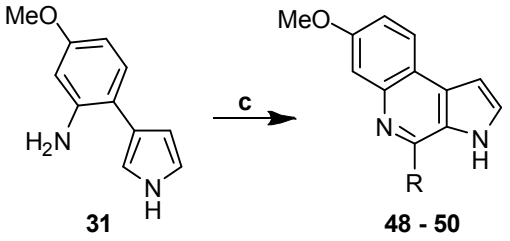

31 **48 - 50**

48 - 4-*N*-phenyacetamida
49 - indole-3-yl
50 - 4-*tert*-butylphenyl carbamate

[a] Reaction conditions: (a) $Pd(OAc)_2$, SPhos, K_3PO_4, *n*-BuOH, H_2O, 80 °C, 12 h; (b) TBAF (1.0 M), THF, 25 °C; (c) Corresponding aldehyde, CH_2Cl_2, TFA, 25 °C, 1 h.; d) (*i*) *t*-BuONO, $BF_3.OEt_2$, (*ii*) NaI, I_2; (e) 10% Pd/C, MeOH, H_2, 25 °C; (f) $SnCl_2.2\ H_2O$, $HCl_{(conc)}$, MeOH, reflux, 1 h.; (g) NBS, THF/H_2O 4:1, 25 °C, 15 min.

Biological Activity. We used the SYBR green method to perform the primary screening[33] and showed that natural marinoquinolines **4** and **6** were not active against the *P. falciparum* 3D7 strain at the highest concentration evaluated (IC_{50} > 10 μM) (Table 1). However, **5** showed antiplasmodial activity in the low micromolar range (IC_{50} = 4 μM, LE = 0.44). Moreover, the cytotoxic effect of **5** was evaluated against a human hepatic cell (HepG2) using the MTT assay, and no toxic activity was observed against HepG2 cells (EC_{50} > 250 μM and SI > 70). Based on these results, we selected **5** as a privileged scaffold for the SAR investigation.

The initial optimization efforts were focused on the R1 substituents. Replacing the isobutyl substituent with an ethyl (**7**) or phenyl (**8**) group provided slightly less potent compounds, with IC_{50} values of 7.3 and 9.9 μM, respectively, whereas the low cytotoxicity profile was retained. Despite the reduced potency of compound **8**, the selectivity index was > 75, suggesting that this compound displayed an attractive safety profile. Subsequently, the SAR of the 4-phenyl substituent was explored, as shown in Table 2. Various substituents, such as 4-OMe (**9**), 3,5-OMe (**10**), 3,4,5-OMe (**11**), Cl (**12**), Br (**13**), NO_2 (**14**), NH_2 (**15**), NMe_2 (**16**), COOH (**17**), and COOMe (**18**), were tolerated at the 4-phenyl substituent of the marinoquinoline; however, none of them improved potency. On the other hand, compound **16**, a dimethylaniline derivative, showed a significant improvement in the selectivity index (SI > 104). Due to structural similarities between indoloquinoline[34] and marinoquinoline derivatives, we tested whether the addition of an indole substituent improved the inhibitory activity of the series. Thus, an indole derivative was introduced in the 4-position of the marinoquinoline to explore the potential of this moiety for improving potency (**19**-**22**) (Table 3). In general, the replacement was tolerated but did not enhance the inhibitory activity of the corresponding 4-phenyl derivatives.

After initial tentative optimization of the R1 groups, the reference compound **5** proved to be the most active compound of this set. We then turned our attention to the R2 substituent, with the goal of improving potency while maintaining cytotoxicity at a moderate level (SI > 50) (Table 4). Introducing a methoxy group in the 7-position of the marinoquinoline ring in **5** yielded compound **32**, which exhibited improved potency (IC_{50} = 0.5 μM) and maintained the ligand efficiency (LE = 0.46) and low cytotoxicity (SI > 70) compared with the hit compound **5**. Subsequent analogues were obtained using the 7-methoxy-linked substituent at R2 (Table 4). Overall, the 7-methoxy-substituted derivatives were 2- to 18-fold more active than the 7-hydrogen analogues, leading to the discovery of submicromolar *P. falciparum* inhibitors. For

example, compounds **40** (IC_{50} = 0.4 μM; LE = 0.37) and **43** (IC_{50} = 0.6 μM; LE = 0.39) showed 15- and 18-fold increases in the inhibitory activity compared to the related compounds **16** (IC_{50} = 5.8 μM; LE = 0.33) and **12** (IC_{50} = 10.5 μM; LE = 0.35), respectively. Additionally, the most potent inhibitors, **32**, **40** and **43**, consistently exhibited acceptable SI values (> 50).

2D- and 3D-QSAR Studies

With the aim of obtaining insights into the structure-activity relationships underlying this series, we devised both 2D- and 3D-QSAR analyses to systematically describe the antiplasmodial activity of our series at the structural level and to prospectively test our hypotheses. The 2D- and 3D-QSAR analyses were performed using the hologram QSAR (HQSAR)[35] and CoMFA[36] methods, respectively. From the original data set, 31 marinoquinoline derivatives were selected as members of the training set for model generation, and the other 3 inhibitors were selected as members of the test set for external model validation. The compounds of both the training and test sets were selected according to the structural diversity and coverage on the range of the pIC_{50} values. A structure similarity map analysis confirmed that both training and test sets composition included compounds representative of the whole data set (Figure S1). Hence, the training and test sets were appropriated for the purpose of QSAR model development. HQSAR descriptors and CoMFA molecular fields were used as independent variables, whereas the pIC_{50} values were used as dependent variable in the PLS regression analyses to build QSAR models. The same training set was employed for all QSAR analysis, and the internal and external predictive ability of the models was assessed by their q^2 and predictive r^2 values (external test set predictions), respectively.

HQSAR employs a specialized fragment fingerprint, the molecular holograms, and PLS to generate fragment-based structure-activity relationships.[37] The studies require specific values to be selected for parameters, such as the distinction, size and type of the fragments, and the length of the hologram, to build predictive models. Hence, 14 HQSAR models were constructed using different combinations of fragment distinction and the default fragment size of 4-7. The best model used a combination of atoms, bonds, connections and hydrogen as fragment distinction parameters (Supporting Information Table S1). Next, the model was selected for further investigations of the influence of fragment size on the internal predictive power. The statistical quality of models was not improved as a function of increasing/decreasing the fragment size (2–5, 3–6, 5–8, 6–9, and 7–10) (Supporting Information Table S2). The best HQSAR model comprised the following parameters: fragment distinction A/B/C/H, fragment size 4–7, hologram length 53; and statistical parameters: $q^2 = 0.50$, $r^2 = 0.74$, SEE = 0.23, and N = 3 (Figure 2A and 2B). The model was submitted to leave-many-out (LMO) cross-validation employing 10 or 5 groups (LMO_{10} or LMO_5, respectively) of compounds as a more rigorous test for assessing the stability and statistical significance of the model. The results confirmed the stability and reliability of the best HQSAR model ($q^2_{LMO5} = 0.48 \pm 0.04$; $q^2_{LMO10} = 0.49 \pm 0.03$, Table S4). Moreover, the Receiver Operating Characteristic (ROC) analysis was used to confirm the performance of the model (Figure S2). The area under the curve (AUC) for the best model was 0.74, which indicated a reasonable discriminating power. The predictive power of the best HQSAR model was assessed by predicting the inhibitory activity of 3 test set compounds (**18**, **20** and **36**). This step evaluates the true predictive power of QSAR models by calculating the biological activity of compounds that were not included in the model training step.[38] The results of the external evaluation are shown in Table 5, and the graphical results for the predicted versus

experimental activities of both the training set and test set are displayed in Figure 2A. The satisfactory agreement between experimental and predicted values and r^2_{pred} (0.85) indicate that the best HQSAR model exhibited good predictive capability for external compounds.

In addition to predicting properties, HQSAR models provided contribution maps that were useful for the identification of the impact of fragments on biological activity. In this map, atoms represented in red and orange indicate negative contributions to the biological activity, atoms in yellow and green indicate positive contributions, and atoms in white represent neutral contributions. The contribution map for the most potent compound of the series, **40** (IC_{50} = 0.4 μM → pIC_{50} = 6.4), suggests that substitutions at the 4-positiion of the phenyl substituent and the presence of a pyrrole ring on the marinoquinoline moiety improve inhibitory activity Figure 2C).

HQSAR maps are useful tools for indicating which groups exhibit the greatest contributions to the inhibitory activity; however, these maps do not provide insights into the physicochemical properties of the new substituents. Thus, we investigated this series using QSAR 3D to obtain further insights into antiplasmodial activity and generate new analogues with enhanced inhibitory activity. The 3D-QSAR analyses were performed using comparative molecular field analysis (CoMFA).[36] The dataset of 34 molecules was structurally aligned to the lowest energy conformer of compound **40** using the database alignment protocol in SYBYL X. Molecular alignments and the maximal common substructure of marinoquinoline derivatives used for structural superimposition and alignment are shown in Figure 3A. The initial CoMFA model was derived for the same training set compounds used in the HQSAR analysis (31 inhibitors) using the default parameters of grid spacing and lattice point weight. However, the model showed an unsatisfactory cross-validation coefficient (**model 1**, q^2 = 0.41; SEP = 0.34; r^2 = 0.65; SEE = 0.26, Supporting Information Table S3). Thus, we applied a region focusing protocol to

obtain models with improved internal consistency and predictive power. Table S3 summarizes the statistical parameters for the models constructed. The best CoMFA model was built with a focusing region weight by Stdev*Coefficients of 1.5 and grid spacing of 1 Å (**model 10**, $q^2 = 0.60$, SEP = 0.30, $r^2 = 0.76$, SEE = 0.23). Moreover, we assessed the stability and performance of the CoMFA model by applying the leave-many-out (LMO) cross-validation and ROC analysis, respectively, as described for HQSAR model validation. Again, the results demonstrated the consistency of the best model ($q^2_{LMO5} = 0.57 \pm 0.04$; $q^2_{LMO10} = 0.59 \pm 0.02$, Table S4), and a reasonable discriminating power (AUC = 0.78, Figure S2). The values of the statistical parameters suggest that the model displayed internal consistency and reasonable predictive ability. Then, the best model was selected for the external validation by predicting the pIC_{50} of the 3 test set compounds that were not used for QSAR model development (Table 5). Figure 3B presents a plot of experimental versus predicted pIC_{50} values. The r^2_{pred} value calculated using this method was 0.92, suggesting good predictive power for external compounds.

CoMFA models provide structural information as contour maps, thereby allowing the identification of favorable and unfavorable regions for bulky, electropositive and electronegative substituents. Briefly, the green regions in the steric contour maps indicate areas where bulky substituents may enhance biological activity, while the yellow contours indicate areas where bulky substituent are detrimental for activity. In case of the electrostatic contour maps, regions in blue and red indicate electropositive and electronegative substituents associated with increased activity, respectively. The contour maps of the most potent compound, **40** ($pIC_{50} = 6.4$), are presented in Figure 3C. As shown in the maps, bulky substituents in the 4-position of the phenyl substituent and in the 7-position of the marinoquinoline moiety improve biological activity. These data are highly consistent with the HQSAR maps, suggesting that substitutions at the 4-position of the phenyl ring improve

inhibitory activity. Moreover, electropositive substituents at the 2- and 4-positions of the phenyl substituent and electronegative substituents in the 7-position of the marinoquinoline moiety might increase the inhibitor potency. According to the structural and physicochemical features provided by QSAR models, new compounds were synthetized and assessed.

Prospective Validation of the QSAR Models

To prospectively assess our hypothesis and verify the SAR data for marinoquinoline derivatives, we designed three new compounds based on the 2D- and 3D-QSAR maps and used both HQSAR and CoMFA models to predict their activities as *P. falciparum* inhibitors (Table 6). This strategy is particularly relevant because our model was generated from a dataset containing a limited number of molecules (i.e., 34 compounds) and range of pIC_{50} values (i.e., 2 orders of magnitude). Our design was focused on substitutions of compound **40** to increase potency while retaining low cytotoxicity. Thus, bulky and electronegative substituents such as carbamate and acetamide were introduced in the 4-position of the phenyl substituent and an indole group was introduced in the 4-position of the marinoquinoline moiety. The predicted inhibitory activities of compounds **48–50** were in the highest potency activity range in both HQSAR and CoMFA models (predicted pIC_{50} values ≥ 6.0) (Table 5). Therefore, we then synthetized and assessed these compounds. For **48**, the predicted biological activity was overestimated. Based on the experimental data, compound **48** was poor inhibitor of *P. falciparum* ($IC_{50} > 10$ μM). On the other hand, for compounds **49** and **50**, the evaluated inhibitory activities matched the predictions reasonably well (Figures 2A and 3B). Interestingly, the evaluated inhibitory potencies for compounds **49** ($IC_{50} = 0.061$ μM; LE = 0.42) and **50** ($IC_{50} = 0.039$ μM; LE = 0.36) were higher than the predicted values (Table 5). According to the results of the cytotoxicity assay, compound **49** was toxic to HepG2 cells in the micromolar range ($EC_{50} = 20$ μM); however, the selectivity index was reasonable (SI =

328). On the other hand, compound **50** exhibited very low cytotoxicity and a remarkably high selectivity index (SI > 6400). In summary, the prospective assessment of our hypothesis additionally strengthened the external validation of the models and confirmed the SAR underlying this series. Hence, the models have limited predictive power, however, they did capture the essential SAR features which gave us useful insights for the discovery of new derivatives with enhanced inhibitory potency.

Marinoquinoline Derivatives are Fast-Acting Inhibitors with Additive Effects in Combination with Artesunate, are Active Against Resistant Strain, but have no Activity on Male and Female Gametocytes

To better characterize the antiplasmodial activity of the series, the most potent and selective compounds (i.e., **32**, **43** and **50**) were selected as representatives for this series for further evaluation using inocula with rings, schizonts or asynchronous as predominant starting *P. falciparum* forms. As shown in Table 7, the calculated IC_{50} values against asynchronous, rings, trophozoites, and schizont were equivalent to the values observed for the ring stages, suggesting that the compounds are potent inhibitors of all erythrocytic forms of *P. falciparum*. Next, to determine the speed of action of the marinoquinoline derivatives, we incubated synchronized cultures (presenting at least 90% of parasites at ring stage) with the compounds at a concentration 10-fold greater than IC_{50} values and observed the morphological changes under the microscope at 8, 24, 32 and 42 h post-synchronization (Figure 4A). Compounds **32**, **43** and **50** showed activity toward the early ring stages, inducing alterations in *P. falciparum* morphology between 8 and 16 h after incubation. These data suggest a fast-acting mechanism in which the young forms of *P. falciparum* in the intraerythrocytic cycle are susceptible to the effects of the compounds. Additionally, we

assessed the potential drug interactions of these molecules with artesunate to inhibit *P. falciparum* in vitro using concentration-response assays. The assay aimed to elucidate the potential benefits and limitations of candidate molecules administered in combination with antimalarial drugs.[39] The concentration of the marinoquinoline derivatives corresponding to the IC_{50} values applied in combination with artesunate was first evaluated in a fixed ratio of 1:1; then, the fractional inhibitory concentration index (FIC index) was determined. The FIC index was calculated for each fixed ratio. An FIC index = 1 indicates an additive drug interaction, an FIC index < 1 indicates a synergistic interaction, and an FIC index > 1 indicates an antagonistic interaction.[40] As shown in Table 8, the FIC indexes for the selected inhibitors ranged from 0.9 ± 0.1 to 1.3 ± 0.1, suggesting an additive effect when applied in combination with artesunate. Additionally, the isobologram plot for the representative inhibitor **50** confirmed the additive interaction with artesunate (ΣFIC = 0.8 ± 0.2) (Figure 4B).

We selected the most potent compound, **50**, and evaluated its inhibitory activity toward the *P. falciparum* K1 strain, a multidrug-resistant strain that does not respond to the antimalarial drugs chloroquine, pyrimethamine and sulfadoxine. Compound **50** was active at nanomolar concentrations and effectively maintained its potency when tested against the resistant cell line (IC_{50}^{K1} = 41 nM) (Figure 4C).

To further evaluate the antimalarial potential of this series, we evaluated the in vitro killing profile by determining the capability of treated parasites to undergo new invasions. The 3D7 *P. falciparum* strain was cultivated in the presence of compound **50** at a 10x IC_{50} concentration for 24 and 48 h. The untreated parasites and standard antimalarials chloroquine, pyrimethamine, atovaquone and artesunate were used as a control. Compound **50** exerted effects on parasite viability that were comparable to the fast-acting agents chloroquine and artesunate (Figure 4D and 4E). These results are highly consistent with the results of speed of

action studies, which indicated that compound **50** displayed inhibitory activity toward the parasite at a very young stage in the intraerythrocytic cycle (Figure 4A). Since few compounds are effective against the gametocyte stage of the parasite and thus prevent disease transmission,[41] further experiments were conducted using compound **50** to test whether the compound was active against late stage (IV–V) gametocytes in a *P. falciparum* dual gamete formation assay (DGFA).[42] Compound **50** showed very low activity against male (inhibition = 7 ± 1% at 1 μM) and female (inhibition = 2.0 ± 0.4% at 1 μM) gametocytes.

We also tested the in vitro prophylactic potential of compound **50** against the liver stages of *P. berghei* (*Pb*EEF), which precede symptomatic blood-stage infection, using a luciferase-expressing transgenic *P. berghei* line.[43] The inhibitory potency of compound **50** against *Pb*EEF was similar to the potency determined for the erythrocytic form of *P. falciparum*, namely, the compound was active in the nanomolar range against both forms (IC_{50}^{Pb} = 76 nM; IC_{50}^{Pf} = 39 nM, respectively). Moreover, the activity of compound **50** toward *Pb*EEF and is relation to HepG2 cytotoxicity indicates that the compound is highly selective for *P. berghei* exo-erythrocytic stages (SI = 50), thereby emphasizing the safety profile of this series.

Marinoquinoline Derivatives Interfere with Heme Species Sequestration

Resistance to antimalarial drugs is associated with mutations in the chloroquine resistance transporter (PfCRT) and multidrug resistant protein (PfMDR1), both of which are located at the digestive vacuole (DV) membrane.[44,45] The DV is a bilayer membrane compartment in *P. falciparum* where host hemoglobin is metabolized.[46] In the DV, free heme is sequestered as inert crystalline hemozoin (Hz). In most instances, chloroquine (CQ) accumulates inside the DV and interferes with Hz formation, leading to parasite death. Mutations in PfCRT impair

CQ accumulation, resulting in drug resistance. Concentration-dependent assays designed to monitor heme species (Hb, free heme and Hz) in both CQ-susceptible (CQS) and CQ-resistant *Plasmodium* strains have shown distinct distribution patterns.[47,48] We performed a calorimetric estimation of heme species following treatment with compound **50** to investigate if this representative compound also possesses a similar mechanism of action as aminoquinolines. In this assay, cellular fractionation was performed to collect the heme species in the presence of pyridine and their distributions were determined spectrophotometrically. Notably, Fe(III)PPIX forms a low-spin complex with pyridine and exhibits a very peculiar spectral property in UV-visible spectroscopy, thus allowing the estimation of heme species.[49] Ring-stage parasites were incubated with compound **50** at 20–160x IC_{50} doses for 32 h and then the heme fractionation assay was conducted. A final analysis was conducted to estimate both the percentage of total heme and amount of heme in the iron (Fe) form in single cells (Figure 6). Parasites of the control group showed a significant reduction in levels of free heme (Figure 6A and 6D) and a simultaneous increase in Hz accumulation (Figure 6B and 6E). On the other hand, parasites treated with compound **50** exhibited the opposite results for the distribution of total heme. Significant sequestration of Hb was observed at higher concentrations (Figure 6C and 6F). Our results showed the concentration-dependent distribution of the percentage of heme species in parasites and quantitation of the levels of the heme-iron form per cell, thereby indicating that compound **50** interfered with hemoglobin metabolism. Nonetheless, the required concentration to inhibit hemozoin formation was 100 times higher than the IC_{50} value, suggesting that this product is not the main target of marinoquinolines.

Marinoquinoline Derivatives are Well Tolerated and Active in In Vivo Model

Motivated by the in vitro results, we tested the in vivo activity of representative marinoquinoline derivatives (**32**, **43** and **50**). We initially conducted in vivo toxicity assays to assess unpredicted toxic effects of this series. The in vivo toxicity of compounds **32**, **43** and **50** was evaluated in mice receiving the compounds administered by gavage or intraperitoneal injections (3 mice per group).[50] The inhibitors were administered at a single dose of 1000 mg/kg, and the survival rate was evaluated for 30 days of observation. The compounds were well tolerated and did not display apparent signs of toxicity; all mice survived for up to 30 days (the last day of observation). Moreover, all animals gained weight in the same proportion as untreated controls. Next, we tested the in vivo activity of marinoquinoline inhibitors in *P. berghei*-infected mice (Figure 7A).[51] Three infected mice were treated with 50 mg/kg of an inhibitor via the oral route (po) or intraperitoneal (ip) injections for three consecutive days after infection. Parasitemia was evaluated on days 5, 7 and 9 post-infection. Compounds that reduced parasitemia by greater than 50% on day 5 post-infection were considered active. The antimalarial chloroquine (CQ) was used as positive control (20 mg/kg). Compound **50** reduced parasitemia by 60% on day 5 and 55% on day 9 post-infection via both administration routes (Figure 7B and 7C). Additionally, animals treated with compound **50** showed increased survival (25 ± 3 days) compared to the untreated controls (19 ± 5 days) (Table 9). Conversely, compounds **32** and **43** were not active.

To shed some light on the lack of in vivo activity for compounds **32** and **43**, we conducted an investigation of the metabolic stability of compounds **32**, **43** and **50** in rat liver microsomes (Figure 8). Compounds **32** and **43** displayed poor metabolic stability, similar to the verapamil control, with levels of compounds remaining after 30 min of incubation as low as 24%, 15% and 10%, respectively. On the other hand, nearly half of the initial amount of compound **50** was still detected after a 30-min incubation with rat liver microsomes, indicating that this compound displayed a relatively higher metabolic stability. The poor metabolic stability and

modest in vitro potency of compounds **32** (IC_{50}^{Pf} = 0.5 μM) and **43** (IC_{50}^{Pf} = 0.6 μM) may have contributed to the lack of in vivo activity (Figure 7B and 7C). On the other hand, the combination of the structural and biological properties of compound **50**, such as increased metabolic stability, the enhanced in vitro potency (IC_{50}^{Pf} = 0.039 μM) and the presence of a labile carbamate group, which generates compound **39** (IC_{50}^{Pf} = 1.3 μM) as a potential pharmacologically active metabolite following hydrolysis, favorably contributed to the observed in vivo efficacy (Figure 7B and 7C).

DISCUSSION AND CONCLUSIONS

In the present study, we used a combination of organic synthesis, SAR studies and molecular modeling strategies to synthesize and identify marinoquinoline derivatives as new lead candidates for antimalarial drug development. The best compounds showed very low cytotoxicity, with an SI > 6140, and in vitro inhibitory activity against the erythrocytic form of the parasite (sensitive and resistant strains) in the nanomolar range. Furthermore, these compounds showed a fast-acting mechanism and potential additive effect when administered in combination with artesunate. The representative marinoquinoline compound (**50**) interferes with heme species sequestration at a concentration 100 times higher than the evaluated IC_{50} value, thereby suggesting that hemozoin metabolism is not the main target of marinoquinolines. Moreover, compound **50** showed excellent correlations with the potencies against asexual and hepatic (which do not display hemozoin metabolism) forms, indicating that the mechanism of action is shared by the liver and blood forms. Inhibitors with dual actions against liver and blood forms have been discovered for dihydroorotate dehydrogenase (DHODH),[52] cytochrome bc1 complex (cyt bc1),[53] phosphatidylinositol-4-OH kinase (PI4K),[54] and cyclic amine resistance locus (CARL)[55]. These enzymes are validated molecular targets for new antimalarials and attractive starting points to investigate the

mechanism of action underlying this series. In summary, the most promising compound within this series (**50**) is potent against sensitive and resistant strains, well tolerated, and a fast-acting inhibitor of parasite growth, with noticeable in vitro activity against both the early stage of intraerythrocytic cycle and liver stages of development, and it has modest in vivo activity. The discovery of compound **50** as a new chemotype will enable us to rationally design derivatives with improved drug-like properties aimed at developing the next generation of antimalarial drugs.

EXPERIMENTAL SECTION

1. Chemistry. Synthesis of compounds

All reagents were commercially available and were used without further purification. Nuclear magnetic resonance spectra were recorded in $CDCl_3$, $(CD_3)_2CO$ or MeOD solutions. Hydrogen and Carbon-13 spectra (^1H and ^{13}C NMR) were recorded at Bruker spectrometers operating at 250, 400, 500, 600 MHz for ^1H, using tetramethylsilane (TMS) as internal standard. Data are reported as follows: chemical shift (δ), multiplicity, integrated intensity and coupling constant (J) in Hertz. HRMS analysis was performed using an Agilent 6550 Accurate-Mass Q-TOF LC/MS system with Agilent Jet Stream technology for electrospray ionization. Flash column chromatography was performed using silica gel (230-400 mesh) and mixtures of EtOAc:hexanes; DCM:MeOH; EtOAc:MeOH. Thin layer chromatography (TLC) was performed using silica gel employing Merck® Silica gel 60 F254 plates. Air- and moisture-sensitive reactions were conducted in oven dried glassware under dry nitrogen atmosphere, using freshly distilled solvents from the appropriate desiccant agent. Melting points (mp) were determined on a capillary melting point apparatus, and are uncorrected. The

chemical purity of compounds **32**, **43** and **50** were confirmed by quantitative ^{1}H NMR (qNMR), with the values determined as 99,0%, 99,6%, and 98,9% respectively. All the other compounds tested were confirmed to be ≥95% by ^{1}H NMR.

General Produce A: Synthesis of 1-iodo-2-nitrobenzene compounds from nitroanilines:[29] To a round-bottomed flask containing boron trifluoride diethyl etherate (9.95 mL, 78.53 mmol) at -30 °C, it was added 2-nitroaniline (18.67 mmol) dissolved in 50 mL of THF and 90% *tert*-butyl nitrite (8.17 mL, 68.72 mmol) dissolved in 50 mL of THF. The reaction mixture was allowed to warm to -5 °C when 100 mL of diethyl ether was added and the mixture was allowed to stir at -5 °C for 30 min until a solid precipitated. The solid was filtered and washed with ether to provide the intermediate aryldiazonium tetrafluoroborate, which was used in the next step without further purification.

The crude aryldiazonium salt was then added in one portion to a 500 mL round bottomed flask containing a stir bar, potassium iodide (4.40 g, 26.53 mmol), iodine (3.37 g, 13.27 mmol), and 75 mL of acetonitrile. The reaction was allowed to stir at room temperature for 30 min., followed by the addition of 150 mL of a saturated aqueous solution of sodium thiosulfate and 150 mL of CH_2Cl_2. The mixture was stirred for 5 min, the layers were separated, and the combined organic layers were dried with anhydrous $MgSO_4$. The solvent was removed in vacuum to give the corresponding aryl iodides.

General Produce B: Suzuki-Miyaura Couplings: A round-bottomed flask was charged with a mixture of $Pd(OAc)_2$ (0.013 g, 0.059 mmol, 0.5 mol%), SPhos (0.048 g, 0.119 mmol, 1 mol%), K_3PO_4 (10.13 g, 47.70 mmol), pyrrole-borane **2** (5.00 g, 14.31 mmol), the corresponding 2-haloanilines (11.92 mmol), and 17 mL of *n*-BuOH, 6.85 mL of H_2O. The resulting mixture was then stirred at 80 °C for 12 h. The mixture was cooled to r.t. and

extracted with three portions (50 mL) of ethyl acetate. The organic layer was separated, washed with brine, dried over sodium sulfate, filtered and the solvent was removed under reduced pressure. The crude product was purified by column chromatography on silica gel using 5 to 10% ethyl acetate:hexanes to provide analytical samples of the corresponding arylpyrroles.

General procedure C: preparation of marinoquinolines analogues by Pictet-Spengler Reaction:

Method A: To a stirred solution of the aryl pyrroles (0.5 mmol) in 3.5 mL CH_2Cl_2 it was added the corresponding aldehyde (0.6 mmol) and TFA (0.25 mmol). The reaction mixture was submitted to vigorous stirring for 1 h. Next, the crude reaction mixture was transferred to a separatory funnel followed by addition of saturated $NaHCO_3$ until pH = 9 and extracted with three portions of CH_2Cl_2 (10 mL). The combined organic phases were dried over anhydrous sodium sulfate, filtrated, and the filtrate was concentrated under reduced pressure. The residue was then purified by flash chromatography using EtOAc/Hexanes, EtOAc/CH_2Cl_2 or EtOAc/MeOH as eluent to give the corresponding marinoquinolines in good yields. Analytical samples were obtained from a middle cut from the purification process by flash chromatography.

Method B:[56] To a stirred solution of the aryl pyrroles (0.5 mmol) and benzotriazole (0.5 mmol) dissolved in 2.0 mL in dry toluene it was added the corresponding aldehyde (0.6 mmol), followed by addition of *p*-TsOH (10 mol %). The reaction mixture was then stirred overnight at room temperature. After 12 h, the reaction mixture was diluted with CH_2Cl_2 and extracted with water. The organic layer was washed with brine and dried over anhydrous sodium sulfate. The solvent was concentrated under reduced pressure and purified by flash

chromatography using EtOAc/Hexanes, EtOAc/CH_2Cl_2 or EtOAc/MeOH as eluent to give the corresponding marinoquinolines. Analytical samples were obtained from a middle cut from the purification process by flash chromatography.

General procedure D: preparation of 1-bromomarinoquinolines analogues: To a solution of corresponding marinoquinoline (0.3mmol) in THF/H_2O 4:1 (10 mL) it was added NBS (0.3 mmol). The reaction mixture was stirred vigorously at room temperature for 15 min. Next, water (5 mL) and AcOEt (20 mL) were added and the reaction mixture extracted with two portions of AcOEt. The organic layers were combined, dried over anhydrous sodium sulfate, and concentrated under reduced pressure. The crude product was purified via flash column chromatography on silica gel using hexane-ethyl acetate as eluent to afford the corresponding products.

2-(1*H*-pyrrol-3-yl)aniline (3): Prepared using the general procedure B starting from 2-bromoaniline (**1**) (4.10 g, 23.85 mmol) to afforded 2-(1-(triisopropylsilyl)-1*H*-pyrrol-3-yl)aniline (7.04 g, 94% yield) as a yellow oil. ^{1}H NMR (400 MHz, CD_2Cl_2) δ 7.22 (dd, *J* = 8.1, 1.4 Hz, 1H), 7.02 (td, *J* = 7.7, 1.6 Hz, 1H), 6.98 – 6.97 (m, 1H), 6.88 (t, *J* = 2.4 Hz, 1H), 6.74 (dd, *J* = 11.3, 4.4 Hz, 1H), 6.51 (dd, *J* = 2.6, 1.4 Hz, 1H), 3.98 (s, 1H), 1.50 (sept, *J* = 14.7, 7.4 Hz, 3H), 1.14 (d, *J* = 7.5 Hz, 18H). ^{13}C NMR (100 MHz, CD_2Cl_2) *δ* 144.51, 130.07, 127.41, 125.40, 124.52, 122.90, 122.81, 118.81, 115.82, 111.10, 18.20, 12.28. HRMS for $C_{19}H_{30}N_2Si$ $(M + H)^+$ calcd 315.2251, found 315.2269.

An oven dried 100 mL flask was charged with the crude product prepared in the previous reaction (7.04 g, 22.38 mmol). The flask was capped with a rubber septum and then evacuated and backfilled with nitrogen. Anhydrous THF (90 mL) was added via syringe,

followed by the addition of 1.0 M TBAF in THF (33.57 mL, 33.57 mmol) at room temperature. After 3 h, it was added 50 mL of water to quench the reaction followed by extraction with three portions of 50 mL of CH_2Cl_2. The combined organic layers were dried over anhydrous sodium sulfate and concentrated under reduced pressure. The crude product was purified via flash column chromatography on silica gel (10 - 40% EtOAc/Hexanes) to afforded 2-(1*H*-pyrrol-3-yl)aniline **3** (3.01 g, 85% yield) as a green oil. ^{1}H NMR (250 MHz, $CDCl_3$) δ 8.32 (br s, 1H); 7.22 (dd, 1H, *J*=7.5 and 1.3); 7.04 (td, 1H, *J*=7.8 and 1.3); 6.87 (m, 1H); 6.82-6.67 (m, 3H); 6.39 (m, 1H); 3.89 (br s, 2H). ^{13}C NMR (62.5 MHz, $CDCl_3$): δ 143.6, 129.8, 127.1, 122.3, 121.6, 122.3, 121.6, 118.6, 118.4, 116.1, 115.5, 108.4. HRMS for $C_{10}H_{10}N_2$ $(M + H)^+$ calcd 159.0917, found 159.0918.

4-Methyl-3*H*-pyrrolo[2,3-*c*]quinoline (Marinoquinoline A - 4). Prepared using general procedure C (Method A) from compound **3** and acetaldehyde. The crude product was purified by chromatography on silica gel (40% EtOAc/Hexanes) to provide the compound marinoquinoline A (**4**) (47.3 mg, 52% yield) as a white solid. Mp 235-236 ºC; lit. 233-235 ºC.[57]

^{1}H NMR (500 MHz, $(CD_3)_2CO$) δ 11.18 (br s, 1H), 8.24 – 8.20 (m, 1H), 8.02 – 7.98 (m, 1H), 7.58 (d, 1H, *J* = 2.5), 7.55 – 7.45 (m, 2H), 7.12 (d, 1H, *J* = 3.0), 2.83 (s, 3H). ^{13}C NMR (125 MHz, $(CD_3)_2CO$) δ 146.9, 143.7, 129.8, 128.4, 127.2, 126.1, 125.7, 124.2, 123.7, 102.0, 21.2. HRMS for $C_{12}H_{10}N_2$ $(M + H)^+$ calcd 183.0917, found 183.0917.

4-isobutyl-3*H*-pyrrolo[2,3-*c*]quinoline (Marinoquinoline B - 5): Prepared using general procedure C (Method A) from compound **3** and isovaleraldehyde. The crude product was purified by chromatography on silica gel (30% EtOAc/Hexanes) to provide marinoquinoline B (**5**) (61.7 mg, 55% yield) as a white solid. Mp 205-206 ºC; lit. 205-207 ºC. ^{1}H NMR (500

MHz, $(CD_3)_2CO$) δ 11.16 (br s, 1H), 8.25 – 8.21 (m, 1H), 8.04 – 8.01 (m, 1H), 7.56 (t, 1H, J = 2.5), 7.54 – 7.47 (m, 2H), 7.12 (dd, 1H, J = 2.5 and 1.5), 3.07 (d, 2H, J = 7.0), 2.45 (septuplet, 1H, J = 7.0), 1.00 (d, 6H, J = 6.5). ^{13}C NMR (125 MHz, $(CD_3)_2CO$) δ 150.1, 143.7, 130.1, 129.9, 128.6, 127.0, 126.0, 125.6, 124.1, 123.7, 101.9, 44.1, 29.0, 23.0. HRMS for $C_{15}H_{16}N_2$ $(M + H)^+$ calcd 225.1386, found 225.1397.

4-benzyl-3*H*-pyrrolo[2,3-*c*]quinoline (Marinoquinoline C - 6): Prepared using general procedure C (Method A) from compound **3** and 2-phenylacetaldehyde. The crude product was purified by chromatography on silica gel (30% EtOAc/Hexanes) to provide the marinoquinoline C (**6**) (76.2 mg, 59% yield) as a white solid. Mp 180-181 ºC; lit. 179-181 ºC. ^{1}H NMR (500 MHz, $(CD_3)_2CO$) δ 11.05 (br s, 1H), 8.26 – 8.22 (m, 1H), 8.08 – 8.04 (m, 1H), 7.56 – 7.49 (m, 3H), 7.42 (d, 2H, J = 7.0), 7.24 (t, 2H, J = 7.0), 7.18 – 7.11 (m, 2H), 4.56 (s, 2H). ^{13}C NMR (125 MHz, $(CD_3)_2CO$) δ 148.9, 143.7, 139.9, 130.2, 129.7, 129.3, 129.3, 129.1, 127.4, 127.0, 126.2, 125.9, 124.2, 123.7, 102.1, 42.6. HRMS for $C_{18}H_{14}N_2$ $(M + H)^+$ calcd 259,1230, found 259.1240.

4-ethyl-3*H*-pyrrolo[2,3-*c*]quinoline (7): Prepared using general procedure C (Method A) from compound **3** and propanal. The crude product was purified by chromatography on silica gel (40% EtOAc/Hexanes) to provide the marinoquinoline **7** (59.8 mg, 61% yield) as a yellow solid. Mp 184-186 ºC; lit. 185-186 ºC. ^{1}H NMR (500 MHz, $(CD_3)_2CO$) δ 11,12 (sl, 1H), 8.24 – 8.20 (m, 1H), 8.04 – 8.00 (m, 1H), 7.56 (t, 1H, J = 3.0), 7.54 – 7.47 (m, 2H), 7.12 (dd, 1H, J = 3.0 and 2.0), 3.21 (qt, 2H, J = 7.5), 1.45 (t, 3H, J = 7.5). ^{13}C NMR (125 MHz, $(CD_3)_2CO$) δ 151.5, 143.7, 130.0, 129.0, 128.6, 126.9, 126.0, 125.6, 124.1, 123.7, 102.0, 28.1, 12.6. HRMS for $C_{13}H_{12}N_2$ $(M + H)^+$ calcd 197.1073, found 197.1079.

4-phenyl-3*H*-pyrrolo[2,3-*c*]quinoline (8): Prepared using general procedure C (Method A) from compound **3** and benzaldehyde. The crude product was purified by chromatography on silica gel (25% EtOAc/Hexanes) to provide the marinoquinoline **8** (64.7 mg, 53% yield) as a white solid. Mp 211-212 ºC; lit. 212-214 ºC. ^{1}H NMR (500 MHz, $(CD_3)_2CO$) δ 11.09 (br s, 1H), 8.34 – 8.30 (m, 1H), 8.16 – 8.12 (m, 1H), 8.12 – 8.08 (m, 2H), 7.65 (t, 1H, J = 2.5), 7.62 – 7.51 (m, 5H), 7.24 (dd, 1H, J = 2.5 and 1.5). ^{13}C NMR (125 MHz, $(CD_3)_2CO$) δ 148.1, 144.6, 140.5, 131.4, 131.0, 130.6, 130.3, 130.3, 129.0, 128.9, 128.9, 127.3, 127.2, 125.0, 124.5. HRMS for $C_{17}H_{12}N_2$ $(M + H)^+$ calcd 245.1073, found 245.1085.

4-(4-methoxyphenyl)-3*H*-pyrrolo[2,3-*c*]quinoline (9): Prepared using general procedure C (Method A) from compound **6** and 4-methoxybenzaldehyde. The crude product was purified by chromatography on silica gel (25% EtOAc/Hexanes) to provide the marinoquinoline **9** (86.4 mg, 63% yield) as a white solid. Mp 173-175 ºC; lit. 173-174 ºC. ^{1}H NMR (600 MHz, $(CD_3)_2CO$) δ 11.09 (br s, 1H), 8.3 – 8.27 (m, 1H), 8.12 – 8.09 (m, 1H), 8.06 (distorted d, 2H, J~9.0), 7.63 (t, 1H, J = 3.0), 7.59 – 7.52 (m, 2H), 7.21 (dd, 1H, J = 3.0 and 1.8), 7.14 – 7.10 (distorted d, 2H, J ~ 8.4), 3.89 (s, 3H). ^{13}C NMR (150 MHz, $(CD_3)_2CO$) δ 160.6, 146.2, 143.1, 131.3, 130.0, 129.6, 129.3, 127.2, 127.2, 125.6, 125.2, 123.2, 122.8, 114.0, 101.2, 54.9. HRMS for $C_{18}H_{14}N_2O$ $(M + H)^+$ calcd 275.1179, found 275.1180.

4-(3,5-dimethoxyphenyl)-3*H*-pyrrolo[2,3-*c*]quinoline (10): Prepared using general procedure C (Method A) from compound **3** and 3,5-dimethoxybenzaldehyde. The crude product was purified by chromatography on silica gel (30% EtOAc/Hexanes) to provide marinoquinoline **10** (115.6 mg, 76% yield) as a brown solid. Mp 182-183 ºC; lit. 183-184 ºC. ^{1}H NMR (500 MHz, $(CD_3)_2CO$) δ 11.18 (br s, 1H), 8.33 – 8.28 (m, 1H), 8.16 – 8.11 (m, 1H), 7.64 (distorted t, 1H, J ~ 2.5), 7.61 (m, 2H), 7.23 (dd, 1H, J = 3.0 and 2.0), 7.19 (d, 2H, J =

2.0), 6.63 (t, 1H, J = 2.5), 3.87 (s, 6H). ^{13}C NMR (125 MHz, $(CD_3)_2CO$) δ 162.1, 147.4, 143.7, 141.7, 130.6, 130.2, 128.2, 126.5, 126.4, 124.3, 123.8, 107.4, 102.1, 101.8, 55.7. HRMS for $C_{19}H_{16}N_2O_2$ $(M + H)^+$ calcd 305.1285, found 305.1298.

4-(3,4,5-trimethoxyphenyl)-3*H*-pyrrolo[2,3-*c*]quinoline (11): Prepared using general procedure C (Method A) from compound **3** and 3,4,5-trimethoxybenzaldehyde. The crude product was purified by chromatography on silica gel (35% EtOAc/Hexanes) to provide the marinoquinoline **11** (120 mg, 72% yield) as a yellow solid. Mp 200-201 ºC; lit. 199-201 ºC. ^{1}H NMR (400 MHz, CD_3OD) δ 8.60 – 8.55 (m, 1H), 8.26 – 8.22 (m, 1H), 8.21 (d, 1H, J = 2.8), 7.88 (quintet of doublets, 2H, J = 7.6 and 1.6), 7.56 (d, 1H, J = 2.8), 7.34 (s, 2H), 4.00 (s, 6H); 3.93 (s, 3H). ^{13}C NMR (100 MHz, CD_3OD) δ 155.5, 145.0, 142.8, 139.3, 136.2, 134.6, 131.0, 129.5, 126.8, 125.9, 125.5, 123.1, 121.5, 108.3, 105.1, 61.3, 57.0. HRMS for $C_{20}H_{18}N_2O_3$ $(M + H)^+$ calcd 335.1390, found 335.1396.

4-(4-chlorophenyl)-3*H*-pyrrolo[2,3-*c*]quinoline (12): Prepared using general procedure C (Method A) from compound **3** and 4-chlorobenzaldehyde. The crude product was purified by chromatography on silica gel (20% EtOAc/Hexanes) to provide the marinoquinoline **12** (90.6 mg, 65% yield) as a yellow solid. Mp 181-182 ºC; lit. 182-184 ºC. ^{1}H NMR (500 MHz, $(CD_3)_2CO$) δ 11.15 (s, 1H), 8.35 – 8.30 (m, 1H), 8.15 – 8.09 (m, 3H), 7.67 (t, 1H, J = 2.5), 7.64 – 7.56 (m, 4H), 7.25 (dd, 1H, J = 3.0 and 2.0). ^{13}C NMR (125 MHz, $(CD_3)_2CO$) δ 146.0, 143.8, 138.5, 135.4, 131.2, 130.7, 130.5, 129.7, 128.4, 128.0, 126.7, 126.6, 124.3, 123.8, 102.3. HRMS for $C_{17}H_{11}ClN_2$ $(M + H)^+$ calcd 279.0683, found 279.0692.

4-(4-bromophenyl)-3*H*-pyrrolo[2,3-*c*]quinoline (13): Prepared using general procedure C (Method A) from compound **3** and 4-bromobenzaldehyde. The crude product was purified by

chromatography on silica gel (20% EtOAc/Hexanes) to provide the marinoquinoline **13** (96.9 mg, 60% yield) as a yellow solid. Mp 168-169 ºC; lit. 168-170 ºC. ^{1}H NMR (600 MHz, $(CD_3)_2CO$) δ 11,16 (sl, 1H), 8.34 – 8.30 (m, 1H), 8.15 – 8.11 (m, 1H), 8.04 (distorted d, 2H, J ~ 8.4), 7.76 (distorted d, 2H, J ~ 8.4), 7.55 (t, 1H, J = 2.4), 7.62 – 7.57 (m, 2H), 7.25 (dd, 1H, J = 3.0 and 1.8). ^{13}C NMR (150 MHz, $(CD_3)_2CO$) δ 145.2, 142.9, 138.0, 131.8, 130.6, 129.7, 129.6, 127.6, 127.1, 125.8, 125.8, 123.4, 123.0, 122.8, 101.4. HRMS for $C_{17}H_{11}BrN_2$ $(M + H)^+$ calcd 323.0178, found 323.0185.

4-(4-nitrophenyl)-3*H*-pyrrolo[2,3-*c*]quinoline (14): Prepared using general procedure C (Method A) starting from compound **3** and 4-nitrobenzaldehyde. The crude product was purified by chromatography on silica gel (20% EtOAc/Hexanes) to provide the marinoquinoline **14** (89.7 mg, 62% yield) as a yellow solid. Mp 220-222 ºC; lit. 220-221 ºC. ^{1}H NMR (600 MHz, $(CD_3)_2CO$) δ 11,33 (sl, 1H), 8.41 (d, 2H, J = 8.7), 8.37 – 8.33 (m, 3H), 8.18 – 8.14 (m, 1H), 7.70 (t, 1H, J = 3.0), 7.65 – 7.60 (m, 2H), 7.28 (dd, 1H, J = 3.0 and 1.8). ^{13}C NMR (150 MHz, $(CD_3)_2CO$) δ 149.0, 145.8, 144.9, 143.7, 130.9, 130.8, 130.7, 128.9, 128.0, 127.1, 127.0, 124.6, 124.5, 123.9, 102.4. HRMS for $C_{17}H_{11}N_3O_2$ $(M + H)^+$ calcd 290.0924, found 290.0919.

4-(3*H*-pyrrolo[2,3-*c*]quinolin-4-yl)aniline (15): Prepared by catalytic reduction of 4-(4-nitrophenyl)-3*H*-pyrrolo[2,3-*c*]quinoline (**14**) by the following procedure: To a stirred solution of (4-(4-nitrophenyl)-3*H*-pyrrolo[2,3-c]quinoline) (115.7 mg, 0.4 mmol) in MeOH (4.0 mL) it was added 42.5 mg of Pd/C 10% (10 mol% of Pd). The reaction mixture was purged with nitrogen for about 10 minutes and then maintained under H_2 atmosphere (balloon of hydrogen) for 6 h. The reaction mixture was then filtered through a short pad of Celite and washed with three portions of MeOH (10 mL). The filtrate was concentrated under reduced

pressure and the residue was purified by flash chromatography (5% MeOH/CH_2Cl_2) to furnish marinoquinoline **15** (89.19 mg, 86% yield) as a yellow solid. Mp 193-194 ºC. ^{1}H NMR (500 MHz, $CDCl_3$) δ 7.00 (s, 1H), 6.27 (t, J = 6.7 Hz, 2H), 5.87 (d, J = 8.3 Hz, 2H), 5.69 – 5.58 (m, 2H), 5.48 (s, 1H), 5.18 (s, 1H), 4.93 (d, J = 8.4 Hz, 2H), 1.95 (s, 2H). ^{13}C NMR (125 MHz, DMSO) δ 149.99, 146.72, 142.31, 129.62, 128.80, 128.56, 127.55, 126.42, 125.49, 124.61, 122.86, 122.54, 113.66, 100.99. HRMS for $C_{17}H_{13}N_3$ $(M + H)^+$ calcd 260.1182, found 260.1170.

***N*,*N*-dimethyl-4-(3*H*-pyrrolo[2,3-*c*]quinolin-4-yl)aniline (16):** Prepared using general procedure C (Method A) starting from compound **3** and 4-(dimethylamino)benzaldehyde. The crude product was purified by chromatography on silica gel (40% EtOAc/Hexanes) to provide marinoquinoline **17** (107.6 mg, 75% yield) as a red solid. Mp 172-173 ºC, lit 173-175 ºC. ^{1}H NMR (600 MHz, $(CD_3)_2CO$) δ 11.05 (br s, 1H), 8.26 (dd, 1H, J = 7.8 and 1.2), 8.09 (dd, 1H, J = 7.8 and 0.6), 8.01 (d, 2H, J = 9.0), 7.60 (d, 1H, J = 2.4), 7.57 – 7.48 (m, 2H), 7.18 (d, 1H, J = 2.4), 6.88 (d, 2H, J = 8.4), 3.03 (s, 6H). ^{13}C NMR (150 MHz, $(CD_3)_2CO$) δ 152.2, 147.7, 144.1, 130.4, 130.3, 129.9, 128.1, 127.7, 127.4, 126.3, 125.6, 124.0, 123.6, 112.9, 102.0, 40.4. HRMS for $C_{19}H_{17}N_3$ $(M + H)^+$ calcd 288.1495, found 288.1496.

4-(3*H*-pyrrolo[2,3-*c*]quinolin-4-yl) benzoic acid (17): Prepared using general procedure C (Method A) starting from compound **3** and 4-formylbenzoic acid. The crude product was purified by chromatography on silica gel (40% EtOAc/Hexanes) to provide marinoquinoline **17** (76.3 mg, 53% yield) as a yellow solid. Mp 223-224 ºC. ^{1}H NMR (500 MHz, DMSO) δ 13.32 (s, 1H), 12.59 (s, 1H), 8.52 (d, J = 6.4 Hz, 1H), 8.24 (d, J = 8.3 Hz, 2H), 8.22 – 8.19 (m, 1H), 8.16 (d, J = 8.3 Hz, 2H), 8.04 (s, 1H), 7.82 – 7.73 (m, 2H), 7.49 (s, 1H). ^{13}C NMR (100 MHz, DMSO) δ 166.9, 143.67, 137.45, 133.85, 132.55, 131.79, 129.77, 127.84, 127.10,

125.93, 125.11, 123.81, 122.26, 102.75. HRMS for $C_{18}H_{12}N_2O_2$ $(M + H)^+$ calcd 289.0971, found 289.0975.

Methyl 4-(3*H*-pyrrolo[2,3-*c*]quinolin-4-yl)benzoate (18): Prepared using general procedure C (Method A) from compound **3** and methyl 4-formylbenzoate. The crude product was purified by chromatography on silica gel (30% EtOAc/Hexanes) to provide marinoquinoline **18** as a yellow solid (77 mg, 51% yield). Mp 168-170 ºC. ^{1}H NMR (600 MHz, DMSO) δ 11.86 (s, 1H), 8.25 (d, J = 8.9 Hz, 1H), 8.20 – 8.18 (m, 3H), 7.68 – 7.64 (m, 1H), 7.54 (d, J = 2.5 Hz, 1H), 7.26 (dd, J = 8.8 e 2.5 Hz, 1H), 7.21 – 7.16 (m, 1H), 3.94 (s, 3H), 3.92 (s, 3H). ^{13}C NMR (150 MHz, DMSO) δ 166.10. 157.75, 144.79, 143.46, 142.66, 129.83, 129.79, 129.49, 129.02, 128.78, 126.02, 124.23, 117.54, 117.41, 108.79, 100.75, 55.23. HRMS for $C_{19}H_{14}N_2O_2$ $(M + H)^+$ calcd 303.1128, found 303.1139.

4-(1*H*-indol-3-yl)-3*H*-pyrrolo[2,3-*c*]quinoline (Marinoquinoline E - 19): Prepared using general procedure C (Method A) starting from compound **3** and 1*H*-indole-3-carbaldehyde. The crude product was purified by chromatography on silica gel (5% MeOH/Hexanes) to provide marinoquinoline E (**19**) (96.6 mg, 68% yield) as a yellow solid. Mp 266-267 ºC, lit 264-266 ºC. ^{1}H NMR (500 MHz, $(CD_3)_2CO$) δ 10.96 (br s, 1H), 10.83 (br s, 1H), 8.78 (d, 1H, J = 7.5), 8.27 (d, 1H, J = 8.0), 8.24 (d, 1H, J = 2.5), 8.17 (d, 1H, J = 8.0), 7.62 – 7.47 (m, 4H), 7.28 – 7.17 (m, 3H). ^{13}C NMR (125 MHz, $(CD_3)_2CO$) δ 144.5, 144.1, 138.0, 130.1. 129.5, 128.1, 127.8, 127.3, 126.8, 126.3, 125.5, 123.7, 123.6, 123.3, 121.1, 115.3, 112.2, 102.2. HRMS for $C_{19}H_{13}N_3$ $(M + H)^+$ calcd 284.1182, found 284.1193.

4-(5-bromo-1*H*-indol-3-yl)-3*H*-pyrrolo[2,3-*c*]quinoline (20): Prepared using general procedure C (Method A) starting from compound **3** and 5-bromo-1*H*-indole-3-carbaldehyde.

The crude product was purified by chromatography on silica gel (10% EtOAc/CH_2Cl_2) to provide marinoquinoline **20** (117.7 mg, 65% yield) as a brown solid. Mp 169-171 ºC. ^{1}H NMR (400 MHz, DMSO) δ 11.98 (s, 1H), 11.79 (s, 1H), 8.97 (s, 1H), 8.43 (s, 1H), 8.27 (d, J = 7.8 Hz, 1H), 8.06 (d, J = 8.1 Hz, 1H), 7.65 (s, 1H), 7.57 (t, J = 7.4 Hz, 1H), 7.54 – 7.47 (m, 3H), 7.37 (d, J = 8.6 Hz, 1H), 7.22 (s, 1H). ^{13}C NMR (100 MHz, DMSO) δ 142.83, 142.17, 135.31, 128.57, 128.42, 128.12, 127.47, 125.94, 125.68, 124.80, 124.72, 124.67, 122.88, 122.20, 113.63, 112.83, 101.29. HRMS for $C_{19}H_{12}BrN_3$ $(M + H)^+$ calcd 362.0287, found 362.0283.

4-(6-bromo-1*H*-indol-3-yl)-3*H*-pyrrolo[2,3-*c*]quinoline (21): Prepared using general procedure C (Method A) starting from compound **3** and 6-bromo-1H-indole-3-carbaldehyde. The crude product was purified by chromatography on silica gel (10% EtOAc/CH_2Cl_2) to provide marinoquinoline **21** (114.1 mg, 63% yield) as a light brown solid. Mp 175-176 ºC ^{1}H NMR (500 MHz, DMSO) δ 11.82 (s, 1H), 11.71 (s, 1H), 8.73 (d, J = 8.5 Hz, 1H), 8.35 (d, J = 2.7 Hz, 1H), 8.23 (d, J = 7.8 Hz, 1H), 8.08 (d, J = 8.1 Hz, 1H), 7.69 (d, J = 1.4 Hz, 1H), 7.59 (s, 1H), 7.56 – 7.52 (m, 1H), 7.49 (dd, J = 10.8, 4.0 Hz, 1H), 7.31 (dd, J = 8.5, 1.7 Hz, 1H), 7.16 (s, 1H). ^{13}C NMR (125 MHz, DMSO) δ 142.89, 142.20, 137.48, 128.61, 128.27, 127.74, 127.08, 126.13, 125.44, 125.38, 124.49, 124.28, 122.88, 122.65, 122.23, 114.90, 114.10, 113.22, 101.00. HRMS for $C_{19}H_{12}BrN_3$ $(M + H)^+$ calcd 362.0287, found 362.0284.

4-(1*H*-indol-2-yl)-3*H*-pyrrolo[2,3-*c*]quinoline (22): Prepared using general procedure C (Method A) starting from compound **3** and 1*H*-indole-2-carbaldehyde. The crude product was purified by chromatography on silica gel (5% EtOAc/CH_2Cl_2) to provide marinoquinoline **22** (80.7 mg, 57% yield) as a light yellow solid. Mp 260-261 ºC. ^{1}H NMR (500 MHz, DMSO) δ 11.95 (s, 1H), 11.76 (s, 1H), 8.32 (d, J = 8.0 Hz, 1H), 8.14 (d, J = 8.1 Hz, 1H), 7.73 – 7.67

(m, 2H), 7.65 – 7.60 (m, 3H), 7.57 (t, *J* = 7.4 Hz, 1H), 7.28 – 7.25 (m, 1H), 7.21 (t, *J* = 7.6 Hz, 1H), 7.08 (t, *J* = 7.4 Hz, 1H). ^{13}C NMR (125 MHz, DMSO) δ 141.70, 138.30, 136.83, 134.77, 129.28, 128.77, 128.60, 128.32, 126.07, 125.48, 125.43, 123.15, 122.98, 122.96, 120.86, 119.53, 112.22, 103.35, 101.34. HRMS for $C_{19}H_{14}N_3$ $(M + H)^+$ calcd 284.1182, found 284.1186.

4-bromo-1-iodo-2-nitrobenzene (25): Prepared using the general procedure A starting from 4-bromo-2-nitroaniline (**23**) (4.00 g, 12.2 mmol) to afford compound **25** (4.83 g, 82% yield) as a red solid. ^{1}H NMR (400 MHz, $CDCl_3$) δ 7.99 (d, *J* = 2.2 Hz, 1H), 7.89 (d, *J* = 8.4 Hz, 1H), 7.40 (dd, *J* = 8.4, 2.2 Hz, 1H). ^{13}C NMR (100 MHz, $CDCl_3$) δ 153.62, 143.05, 136.63, 128.60, 122.79, 84.52. HRMS for $C_6H_3BrINO_2$ $(M + H)^+$ calcd 327.8465, found 327.8451.

1-Iodo-4-methoxy-2-nitrobenzene (26): Prepared using the general procedure A starting from 4-methoxy-2-nitroaniline (**24**) (8.10 g, 37.34 mmol) to afford compound **26** (9.81 g, 73% yield) as a red solid. ^{1}H NMR (400 MHz, CD_2Cl_2) δ 7.87 (d, *J* = 3.6 Hz, 1H), 7.40 (d, *J* = 2.9 Hz, 1H), 6.89 (dd, *J* = 8.8, 2.9 Hz, 1H), 3.85 (s, 3H). ^{13}C NMR (100 MHz, CD_2Cl_2) δ 160.85, 154.14, 142.66, 120.82, 111.61, 74.66, 56.61. HRMS for $C_7H_6INO_3$ $(M + H)^+$ calcd 279.9465, found 279.9445.

5-Bromo-2-(1*H*-pyrrol-3-yl)aniline (28): Prepared using general procedure B from 4-bromo-1-iodo-nitrobenzene (**25**) (2.00 g, 6.00 mmol) and pyrrole-borane **2** (1.05 g, 3.00 mmol). The crude material was used in next step without purification.

An oven dried 50 mL round-bottomed flask was charged with the freshly prepared crude material. The flask was capped with a rubber septum and then evacuated and backfilled with nitrogen. Anhydrous THF (20 mL) was added via syringe, followed by the addition of 1.0 M

TBAF in THF (4.50 mL, 4.50 mmol) at room temperature. After 2 h, water was added to the reaction mixture and it was extracted with three portions of CH_2Cl_2. The organic layers were dried over sodium sulfate and concentrated under reduced pressure. The crude product was purified by flash column chromatography on silica gel (gradient 0 - 20% EtOAc/Hexanes) to afforded 3-(4-bromo-2-nitrophenyl)-1*H*-pyrrole **27** (506 mg, 63% yield) as a yellow solid. ^{1}H NMR (400 MHz, $CDCl_3$) δ 8.48 (s, 1H), 7.74 (s, 1H), 7.61 (dd, J = 8.3, 1.2 Hz, 1H), 7.39 (d, J = 8.4 Hz, 1H), 6.94 (s, 1H), 6.82 (d, J = 1.7 Hz, 1H), 6.29 (s, 1H). ^{13}C NMR (150 MHz, $CDCl_3$) δ 157.9, 149.5, 132.1, 122.4, 118.9, 118.7, 118.3, 116.4, 108.4, 108.2, 55.8. HRMS for $C_{10}H_7BrN_2O_2$ $(M + H)^+$ calcd 266.9764, found 266.9758.

To a solution of **27** (506 mg, 1.9 mmol) in methanol (8 mL) was added $SnCl_2.2H_2O$ (2.14 g, 9.5 mmol) and $HCl_{(conc)}$ (1.1 mL, 13.3 mmol). The reaction was refluxed for 1 h. The solvent was removed under reduced pressure and the crude residue was partitioned between ethyl acetate and 1M KOH. The organic layers were dried over sodium sulfate and concentrated under reduced pressure. The crude product was purified by flash column chromatography on silica gel (gradient 0 - 30% EtOAc/Hexanes) to afforded 5-bromo-2-(1*H*-pyrrole-3-yl)aniline **28** (198 mg, 44% yield) as a brown solid. ^{1}H RMN (500 MHz, CD_2Cl_2) δ 8,55 (s, 1H); 7,12 (d, J = 8,1 Hz, 1H); 7,06 – 7,00 (m, 1H); 6,96 – 6,91 (m, 2H); 6,90 (dd, J = 8,1 e 2,0 Hz, 1H); 6,44 (dd, J = 4,1 e 2,5 Hz, 1H); 4,12 (s, 2H). ^{13}C NMR (126 MHz, CD_2Cl_2) δ 145,98; 131,48; 127,42; 121,67; 121,48; 121,35; 120,61; 119,27; 118,15; 116,68; 110,54; 108,73. EMAR (ESI+) calcd para $C_{10}H_9BrN_2$ $(M + H)^+$: 237.0022; found 236.9998.

7-bromo-4-(1*H*-indol-3-yl)-3*H*-pyrrolo[2,3-*c*]quinoline (29). Prepared using general procedure C (Method A) from compound **28** and 1*H*-indole-3-carbaldehyde. The crude product was purified by chromatography on silica gel (40% EtOAc/Hexanes) to provide

marinoquinoline **29** as a brown solid (77 mg, 43% yield). Mp 155-156 ºC. ^{1}H NMR (500 MHz, CD_3OD) δ 8.29 (d, J = 1.9 Hz, 1H), 8.23 – 8.17 (m, 2H), 8.04 (s, 1H), 7.65 (dd, J = 8.6, 1.9 Hz, 1H), 7.60 (d, J = 2.9 Hz, 1H), 7.56 (d, J = 8.1 Hz, 1H), 7.31 – 7.27 (m, 1H), 7.25 – 7.21 (m, 1H), 7.19 (d, J = 2.9 Hz, 1H). ^{13}C NMR (125 MHz, CD_3OD) δ 146.38, 144.51, 138.48, 131.03, 130.27, 129.32, 129.04, 128.91, 127.70, 127.51, 125.76, 123.6, 122.98, 122.01, 121.58, 120.11, 114.17, 112.71, 102.36. HRMS for $C_{19}H_{12}BrN_3$ $(M + H)^+$ calcd 362.0287, found 362.02676.

5-methoxy-2-(1*H*-pyrrol-3-yl)aniline (31): Prepared using general procedure B from 1-iodo-4-methoxy-2-nitrobenzene (**26**) (3.32 g, 11.92 mmol) to provide the intermediate 3-(4-methoxy-2-nitrophenyl)-1-(triisopropylsilyl)-1*H*-pyrrole (4.45 g, 92% yield) as a yellow oil. ^{1}H NMR (400 MHz, $CDCl_3$) δ 7.43 (d, J = 8.6 Hz, 1H), 7.13 (d, J = 2.7 Hz, 1H), 7.05 (dd, J = 8.6, 2.7 Hz, 1H), 6.83 (d, J = 1.5 Hz, 1H), 6.77 (t, J = 2.4 Hz, 1H), 6.35 (dd, J = 2.6, 1.4 Hz, 1H), 3.85 (s, 3H), 1.45 (sept, J = 14.8, 7.5 Hz, 3H), 1.11 (d, J = 7.5 Hz, 18H). ^{13}C NMR (100 MHz, $CDCl_3$) δ 157.84, 152.21, 132.07, 124.96, 122.67, 120.79, 118.32, 110.59, 108.16, 55.94, 29.85, 17.92, 11.78. HRMS for $C_{20}H_{30}N_2O_3Si$ $(M + H)^+$ calcd 375.2098, found 375.2100.

An oven dried 100 mL round-bottomed flask was charged with the freshly prepared 3-(4-methoxy-2-nitrophenyl)-1-(triisopropylsilyl)-1*H*-pyrrole (4.45 g, 11.90 mmol). The flask was capped with a rubber septum and then evacuated and backfilled with nitrogen. Anhydrous THF (40 mL) was added via syringe, followed by the addition of 1.0 M TBAF in THF (17.85 mL, 17.85 mmol) at room temperature. After 2 h, water was added to the reaction mixture and it was extracted with three portions of CH_2Cl_2. The organic layers were dried over sodium sulfate and concentrated under reduced pressure. The crude product was purified by flash column chromatography on silica gel (gradient 0 - 25% EtOAc/Hexanes) to afforded 3-

(4-methoxy-2-nitrophenyl)-1*H*-pyrrole **30** (2.07 g, 80% yield) as a yellow solid. ^{1}H NMR (600 MHz, $CDCl_3$) δ 8.34 (sl, 1H), 7.41 (d, J = 8.6 Hz, 1H), 7.16 (d, J = 2.7 Hz, 1H), 7.07 (dd, J = 2.7 e 8.6 Hz, 1H), 6.90 (q ap., J = 2.0 Hz, 1H), 6.81 (q ap., J = 2.5 Hz, 1H), 6.28 (m, 1H). ^{13}C NMR (150 MHz, $CDCl_3$) δ 157.9, 149.5, 132.1, 122.4, 118.9, 118.7, 118.3, 116.4, 108.4, 108.2, 55.8. HRMS for $C_{11}H_{10}N_2O_3$ $(M + H)^+$ calcd 219.0764, found 219.0755.

A solution of intermediate **30** (2.07 g, 9.48 mmol) and Pd/C 10% (1 mol% of Pd, 0.095 mmol, 100.88 mg) in MeOH (95 mL) was degassed for 15 min with N_2, and then stirred under H_2 atmosphere (balloon of hydrogen) for 4 h. Next, the reaction mixture was filtered through a short pad of Celite and washed with MeOH several times. The filtrates were concentrated under reduced pressure and the residue was purified by flash chromatography (40% ethyl EtOAc/Hexanes) to afford the title compound **31** (1.55 g, 87% yield) as a yellow solid. ^{1}H NMR (500 MHz, $CDCl_3$) δ 8.33 (sl, 1H), 7.14 (d, J = 8.4 Hz, 1H), 6.89 (q ap., J = 1.5 Hz, 1H), 6.84 (q ap., J = 2.1 Hz, 1H), 6.36 (m, 2H), 3.96 (sl, 2H), 3.77 (s, 3H). ^{13}C NMR (125 MHz, $CDCl_3$) δ 159.3, 145.0, 130.8, 121.6, 118.4, 115.9, 115.5, 108.8, 104.1, 101.1, 55.2. HRMS for $C_{11}H_{12}N_2O$ $(M + H)^+$ calcd 189.1022, found 189.1029.

4-isobutyl-7-methoxy-3*H*-pyrrolo[2,3-*c*]quinoline (32). Prepared using general procedure C (Method A) from compound **31** and 3-methylbutanal. The crude product was purified by chromatography on silica gel (35% EtOAc/Hexanes) to provide marinoquinoline **32** as a white solid (76,5 mg, 60% yield). Mp 143-144 ºC. ^{1}H RMN (600 MHz, CD_2Cl_2) δ 9.27 (s, 1H), 8.07 (d, J = 8.8 Hz, 1H), 7.49 (d, J = 2.6 Hz, 1H), 7.43 (d, J = 3.0 Hz, 1H), 7.18 (dd, J = 8.9 e 2.6 Hz, 1H), 7.00 (d, J = 3.0 Hz, 1H), 3.91 (s, 3H), 2.97 (d, J = 7.4 Hz, 2H), 2.42 – 2.31 (m, 1H). 0.97 (d, J = 6.6 Hz, 6H). ^{13}C RMN (150 MHz, CD_2Cl_2) δ 158.70, 149.65, 144.60,

128.94, 128.67, 126.57, 124.36, 117.78, 117.25, 109.03, 101.72, 55.92, 44.29, 29.24, 23.12. HRMS for $C_{16}H_{18}N_2O$ $(M + H)^+$ calcd 255.1492, found 255.1504.

4-methyl-7-methoxy-3*H*-pyrrolo[2,3-*c*]quinoline (33). Prepared using general procedure C (Method A) from compound **31** and acetaldehyde. The crude product was purified by chromatography on silica gel (30% EtOAc/Hexanes) to provide marinoquinoline **33** as a white solid (53 mg, 50% yield). Mp 191-192 ºC. ^{1}H NMR (600 MHz, CD_2Cl_2) δ 9.49 (s, 1H), 8.05 (d, J = 8.8 Hz, 1H), 7.56 – 7.42 (m, 2H), 7.18 (d, J = 8.5 Hz, 1H), 6.99 (s, 1H), 3.91 (s, 3H), 2.83 (s, 3H). ^{13}C NMR (150 MHz, CD_2Cl_2) δ 158.27, 145.54, 143.32, 128.40, 127.84, 126.73, 123.88, 117.14, 116.74, 107.85, 101.27, 20.34. HRMS for $C_{13}H_{12}N_2O$ $(M + H)^+$ calcd 213.1022, found 213.1027.

4-ethyl-7-methoxy-3*H*-pyrrolo[2,3-*c*]quinoline (34). Prepared using general procedure C (Method A) from compound **31** and propionaldehyde. The crude product was purified by chromatography on silica gel (30% EtOAc/Hexanes) to provide marinoquinoline **34** as a white solid (58 mg, 51% yield). Mp 121-123 ºC. ^{1}H NMR (600 MHz, CD_2Cl_2) δ 9.34 (s, 1H), 8.06 (d, J = 8.8 Hz, 1H), 7.49 (d, J = 2.6 Hz, 1H), 7.42 (d, J = 3.0 Hz, 1H), 7.18 (dd, J = 8.9 e 2.6 Hz, 1H), 6.99 (d, J = 3.0 Hz, 1H), 3.91 (s, 3H), 3.14 (q, J = 7.6 Hz, 2H), 1.44 (t, J = 7.6 Hz, 3H). ^{13}C NMR (150 MHz, CD_2Cl_2) δ 158.75, 151.13, 144.44, 129.04, 127.80, 126.69, 124.38, 117.82, 117.23, 108.90, 101.79, 55.93, 28.18, 12.99. HRMS for $C_{14}H_{14}N_2O$ $(M + H)^+$ calcd 227.1179, found 227.1166.

4-phenyl-7-methoxy-3*H*-pyrrolo[2,3-*c*]quinoline (35). Prepared using general procedure C (Method B) from compound **31** and benzaldehyde. The crude product was purified by chromatography on silica gel (40% EtOAc/Hexanes) to provide marinoquinoline **35** as a

white solid (110 mg, 80% yield). Mp 82-83 ºC. ^{1}H NMR (500 MHz, $CDCl_3$) δ 8.07 (d, J = 8.8 Hz, 1H), 7.85 (dd, J = 1.2 e 6.9 Hz, 2H), 7.53 (m, 5H), 7.16 (dd, J = 2.4 e 8.8 Hz, 1H), 7.00 (d, J = 2.9 Hz, 1H), 3.89 (s, 3H).^{13}C RMN (125 MHz, $CDCl_3$) δ 158.5, 147.2, 143.2, 137.8, 130.4, 129.0, 128.61, 128.58, 128.5, 126.5, 123.8, 117.6, 117.1, 107.1, 100.3, 54.4. HRMS for $C_{18}H_{14}N_2O$ $(M + H)^+$ calcd 275.1179, found 275.1183.

4-(3,5-dimethoxyphenyl)-7-methoxy-3*H*-pyrrolo[2,3-*c*]quinoline (36). Prepared using general procedure C (Method B) from compound **31** and 3,5-dimethoxybenzaldehyde. The crude product was purified by chromatography on silica gel (40% EtOAc/Hexanes) to provide marinoquinoline **36** as a brown solid (132 mg, 79% yield). Mp 143-144 ºC. ^{1}H NMR (600 MHz, CD_2Cl_2) δ 9.13 (s, 1H), 8.12 (d, J = 8.9 Hz, 1H), 7.59 (d, J = 2.1 Hz, 1H), 7.46 (t, J = 2.7 Hz, 1H), 7.24 (dd, J = 15.6 e 7.8 Hz, 1H), 7.09 (d, J = 2.3 Hz, 2H); 7.08 – 7.06 (m, 1H); 6.60 (t, J = 2.2 Hz, 1H); 3.96 (s, 3H); 3.87 (s, 6H). ^{13}C NMR (150 MHz, CD_2Cl_2) δ 162.00, 158.97, 146.88, 144.82, 141.14, 130.10, 127.21, 127.17, 124.38, 118.19, 118.11, 109.55, 106.85, 101.90, 101.57, 56.12, 55.98. HRMS for $C_{20}H_{19}N_2O_3$ $(M + H)^+$ calcd 335.1390, found 335.1410.

7-methoxy-4-(3,4,5-trimethoxyphenyl)-3*H*-pyrrolo[2,3-*c*]quinoline (37). Prepared using general procedure C (Method A) from compound **31** and 3,4,5-trimethoxybenzaldehyde. The crude product was purified by chromatography on silica gel (5% EtOAc/CH_2Cl_2) to provide marinoquinoline **37** as a brown solid (123,9 mg, 68% yield). Mp 143-144 ºC. ^{1}H NMR (600 MHz, CD_2Cl_2) δ 9.25 (s, 1H), 8.13 (d, J = 8.9 Hz, 1H), 7.59 (d, J = 2.5 Hz, 1H), 7.49 (ap., J = 2.7 Hz, 1H), 7.24 (dd, J = 8.8 e 2.6 Hz, 1H), 7.15 (s, 2H); 7.10 – 7.07 (m, 1H), 3.96 (s, 3H), 3.89 (s, 6H), 3.86 (s, 3H). ^{13}C NMR (150 MHz, CD_2Cl_2) δ 158.98, 154.41, 147.17, 144.88,

139.54, 134.77, 130.08, 127.27, 124.40, 118.03, 109.52, 106.06, 101.96, 61.13, 56.78, 55.97. HRMS for $C_{21}H_{21}N_2O_4$ $(M + H)^+$ calcd 365.1501, found 365.1508.

7-methoxy-4-(4-nitrophenyl)-3*H*-pyrrolo[2,3-*c*]quinoline (38). Prepared using general procedure C (Method A) from compound **31** and 4-nitrobenzaldehyde. The crude product was purified by chromatography on silica gel (30% EtOAc/Hexanes) to provide marinoquinoline **38** as an orange solid (69 mg, 43% yield). Mp 148-149 ºC. ^{1}H NMR (600 MHz, CD_2Cl_2) δ 9.05 (s, 1H), 8.40 (d, J = 8.7 Hz, 2H), 8.17 (d, J = 8.7 Hz, 2H), 8.15 (d, J = 8.9 Hz, 1H), 7.58 (d, J = 2.5 Hz, 1H), 7.53 (ap., J = 2.8 Hz, 1H), 7.29 (dd, J = 8.9 e 2.6 Hz, 1H), 7.12 (dd, J = 2.9 e 2.0 Hz, 1H), 3.96 (s, 3H). ^{13}C NMR (150 MHz, CD_2Cl_2) δ 159.25, 148.71, 145.51, 144.96, 144.36, 130.86, 129.79, 127.81, 127.09, 124.78, 124.54, 119.11, 118.34, 109.51, 102.27, 56.03. HRMS for $C_{18}H_{13}N_3O_3$ $(M + H)^+$ calcd 320.1030, found 320.1022.

4-(7-methoxy-3*H*-pyrrolo[2,3-*c*]quinolin-4-yl)aniline (39). Prepared through of reduction of 7-methoxy-4-(4-nitrophenyl)-3*H*-pyrrolo[2,3-*c*]quinoline **(38)** according to the following procedure: To a stirred solution of 7-methoxy-4-(4-nitrophenyl)-3*H*-pyrrolo[2,3-*c*]quinoline (127.7 mg, 0.4 mmol) in MeOH (4.0 mL) it was added 42.5 mg of Pd/C 10% (10 mol% of Pd). The reaction mixture was purged with H_2 for about 10 minutes and then maintained under H_2 atmosphere for 6 h. Next, the reaction mixture was filtered through a short pad of Celite and washed with three portions of MeOH. The filtrate was concentrated under reduced pressure and the residue was purified by flash chromatography (5% MeOH/CH_2Cl_2) to afford marinoquinoline **39** (96.1 mg, 83% yield) as a yellow solid. Mp 238-239 ºC. ^{1}H NMR (400 MHz, CD_2Cl_2) δ 12.01 (s, 1H), 8.25 (d, J = 8.7 Hz, 1H), 7.93 – 7.67 (m, 3H), 7.56 (s, 1H), 7.33 –7.14 (m, 2H), 6.80 (d, J = 8.4 Hz, 2H), 5.79 (s, 2H), 3.91 (s, 3H). ^{13}C NMR (100 MHz,

CD_2Cl_2) 158.26, 130.33, 125.01, 124.52, 116.68, 113.68, 101.36, 55.31. HRMS for $C_{18}H_{14}N_3O$ $(M + H)^+$ calcd 290.1288, found 290.1262.

4-(7-methoxy-3*H*-pyrrolo[2,3-*c*]quinolin-4-yl)-*N*,*N*-dimethylaniline (40). Prepared using general procedure C (Method A) from compound **31** and 4-(dimethylamino)benzaldehyde. The crude product was purified by chromatography on silica gel (5% EtOAc/CH_2Cl_2) to provide marinoquinoline **40** as a yellow solid (98,4 mg, 62% yield). Mp 112-113 ºC. ^{1}H NMR (500 MHz, CD_2Cl_2) δ 9.07 (s, 1H), 8.06 (dd, J = 19.0 e 8.6 Hz, 1H), 7.90 (d, J = 8.8 Hz, 2H), 7.60 (s, 1H), 7.46 (d, J = 2.7 Hz, 1H), 7.19 (dd, J = 8.8 e 2.6 Hz, 1H), 7.05 (d, J = 2.9 Hz, 1H), 6.89 (d, J = 8.7 Hz, 2H), 3.96 (s, 4H); 3.06 (s, 6H). ^{13}C NMR (125 MHz, DMSO) δ 157.55, 150.92, 146.30, 143.42, 129.50, 129.23, 128.10, 125.78, 125.58, 123.97, 116.83, 116.12, 111.95, 108.43, 100.51, 55.14, 48.58. HRMS for $C_{20}H_{19}N_3O$ $(M + H)^+$ calcd 318.1601, found 318.1603.

4-(7-methoxy-3*H*-pyrrolo[2,3-*c*]quinolin-4-yl) benzoic acid (41). Prepared using general procedure C (Method A) from compound **31** and 4-formylbenzoic acid. The crude product was purified by chromatography on silica gel (10% EtOAc/CH_2Cl_2) to provide marinoquinoline **41** as a yellow solid (88 mg, 55% yield). Mp 129-130 ºC. ^{1}H NMR (400 MHz, DMSO) δ 13.02 (s, 1H), 11.86 (s, 1H), 8.24 (d, J = 8.9 Hz, 1H), 8.20 – 8.09 (m, 4H), 7.67 – 7.61 (m, 1H), 7.53 (d, J = 2.3 Hz, 1H), 7.25 (dd, J = 8.9 e 2.5 Hz, 1H), 7.20 – 7.14 (m, 1H), 3.92 (s, 3H). ^{13}C NMR (100 MHz, DMSO) δ 157.74, 145.11, 143.48, 142.04, 129.64, 128.79, 126.06, 124.25, 117.40, 115.81, 108.81, 100.73, 55.25. HRMS for $C_{19}H_{14}N_2O_3$ $(M + H)^+$ calcd 319.1077, found 319.1076.

Methyl 4-(7-methoxy-3*H*-pyrrolo[2,3-*c*]quinolin-4-yl) benzoate (**42**): Prepared using general procedure C (Method A) from compound **31** and methyl 4-formylbenzoate. The crude product was purified by chromatography on silica gel (40% EtOAc/Hexanes) to provide marinoquinoline 42 as a yellow solid (88 mg, 53% yield). Mp 173-174 ºC. ^{1}H RMN (600 MHz, DMSO) δ 11.86 (s, 1H), 8.25 (d, J = 8.9 Hz, 1H), 8.20 – 8.18 (m, 3H), 7.68 – 7.64 (m, 1H), 7.54 (d, J = 2.5 Hz, 1H), 7.26 (dd, J = 8.8 e 2.5 Hz, 1H), 7.21 – 7.16 (m, 1H), 3.94 (s, 3H), 3.92 (s, 3H). ^{13}C RMN (150 MHz, DMSO) δ 166.10, 157.75, 144.79, 143.46, 142.66, 129.83, 129.79, 129.49, 129.02, 128.78, 126.02, 124.23, 117.54, 117.41, 108.79, 100.75, 55.23, 52.32. HRMS calcd 333.1239, found 333.1213.

4-(4-chlorophenyl)-7-methoxy-3*H*-pyrrolo[2,3-*c*]quinoline (43). Prepared using general procedure C (Method B) from compound **31** and 4-chlorobenzaldehyde. The crude product was purified by chromatography on silica gel (35% EtOAc/Hexanes) to provide marinoquinoline **43** as a yellow solid (140 mg, 91% yield). Mp 154 ºC. ^{1}H NMR (600 MHz, CD_2Cl_2) δ 9.14 (s, 1H), 8.12 (d, J = 8.9 Hz, 1H), 7.91 (d, J = 8.3 Hz, 2H), 7.57 (d, J = 2.5 Hz, 1H), 7.52 (d, J = 8.3 Hz, 2H), 7.48 (d, J = 2.7 Hz, 1H), 7.25 (dd, J = 8.9 e 2.6 Hz, 1H), 7.08 (d, J = 2.9 Hz, 1H), 3.94 (s, 3H). ^{13}C NMR (150 MHz, CD_2Cl_2) δ 159.11, 145.70, 144.75, 137.55, 135.70, 130.49, 130.22, 129.77, 127.64, 127.09, 124.47, 118.41, 118.08, 109.29, 102.07, 55.99. HRMS for $C_{18}H_{13}ClN_2O$ $(M + H)^+$ calcd 309.0789, found 309.0788.

4-benzyl-7-methoxy-3*H*-pyrrolo[2,3-*c*]quinoline (44). Prepared using general procedure C (Method A) from compound **31** and 2-phenylacetaldehyde. The crude product was purified by chromatography on silica gel (40% EtOAc/Hexanes) to provide marinoquinoline **44** as a white solid (105.2 mg, 73% yield). Mp 216-218 ºC. ^{1}H NMR (600 MHz, CD_2Cl_2) δ 8.98 (s, 1H), 7.53 (d, J = 2.5 Hz, 1H), 7.30 – 7.20 (m, 7H), 6.96 (d, J = 2.9 Hz, 1H), 4.49 (s, 2H),

3.91 (s, 3H). ^{13}C NMR (150 MHz, CD_2Cl_2) δ 144.32, 133.73, 130.06, 124.45, 115.23, 114.88, 114.83, 113.74, 112.80, 112.45, 109.91, 103.58, 103.15, 94.66, 87.04, 41.45, 28.01. HRMS for $C_{19}H_{16}N_2O$ $(M + H)^+$ calcd 289.1335, found 289.1335.

1-bromo-4-(1*H*-indol-3-yl)-3*H*-pyrrolo[2,3-*c*]quinoline (45): Prepared using general procedure D from **19**. The crude product was purified by chromatography on silica gel (25% EtOAc/Hexanes) to provide marinoquinoline **45** (120 mg, 72% yield) as a yellow solid. Mp 142-143 ºC. ^{1}H NMR (500 MHz, DMSO) δ 12.12 (s, 1H), 11.78 (s, 1H), 8.98 (dd, J = 8.0, 1.1 Hz, 1H), 8.67 (d, J = 7.8 Hz, 1H), 8.29 (d, J = 2.8 Hz, 1H), 8.12 (d, J = 8.0 Hz, 1H), 7.81 (d, J = 2.8 Hz, 1H), 7.62 (t, J = 10.9 Hz, 1H), 7.58 (t, J = 11.0 Hz, 1H), 7.52 (d, J = 7.9 Hz, 1H), 7.24 (t, J = 10.9 Hz, 1H), 7.20 (t, J = 10.9 Hz, 1H). ^{13}C NMR (125 MHz, DMSO) δ 143.65, 142.70, 136.56, 129.00, 127.44, 126.3, 126.05, 124.59, 123.11, 122.32, 122.25, 121.46, 120.96, 120.18, 112.13, 111.61, 89.59. HRMS for $C_{19}H_{12}BrN_3$ $(M + H)^+$ calcd 362.0287, found 362.0283.

1-bromo-7-methoxy-4-methyl-3*H*-pyrrolo[2,3-*c*]quinoline (46): Prepared using general procedure D from **33**. The crude product was purified by chromatography on silica gel (35% EtOAc/Hexanes) to provide marinoquinoline **46** (59 mg, 68% yield) as a yellow solid. Mp 150-153 ºC. ^{1}H NMR (600 MHz, CD_2Cl_2) δ 8.89 (d, J = 9.0 Hz, 1H), 7.46 (d, J = 2.6 Hz, 1H), 7.43 (s, 1H), 7.22 (dd, J = 9.0 e 2.7 Hz, 1H), 3.94 (s, 3H), 2.79 (s, 3H). ^{13}C NMR (150 MHz, CD_2Cl_2) δ 158.33, 146.25, 143.91, 127.54, 126.78, 124.01, 122.86, 116.81, 116.38, 107.98, 90.25, 55.30, 19.69. HRMS for $C_{13}H_{11}BrN_2O$ $(M + H)^+$ calcd 291.0128, found 291.0128.

1-bromo-7-methoxy-4-phenyl-3*H*-pyrrolo[2,3-*c*]quinoline (47): Prepared using general procedure D from **35**. The crude product was purified by chromatography on silica gel (30% EtOAc/Hexanes) to provide marinoquinoline **47** (69 mg, 67% yield) as a light yellow solid. Mp 107 ºC. ^{1}H NMR (600 MHz, CD_2Cl_2) δ 9.16 (s, 1H), 8.99 (d, J = 9.0 Hz, 1H), 7.90 (dt, J = 3.0 e 1.8 Hz, 2H), 7.61 (d, J = 2.6 Hz, 1H), 7.58 (m, 2H), 7.55 – 7.51 (m, 1H), 7.47 (s, 1H), 7.29 (dd, J = 9.0 and 2.7 Hz, 1H), 3.96 (s, 3H). ^{13}C NMR (150 MHz, CD_2Cl_2) δ 158.56, 146.65, 145, 137.7, 129.47, 129.17, 128.24, 126.44, 126.34, 125.17, 122.84, 117.39, 116.99, 109.27, 90.92, 55.41. HRMS for $C_{18}H_{13}BrN_2O$ $(M + H)^+$ calcd 353.0284, found 353.0273.

***N*-(4-(7-methoxy-3*H*-pyrrolo[2,3-*c*]quinolin-4-yl)phenyl) acetamide (48).** Prepared using general procedure C (Method A) starting from compound **31** and N-(4-formylphenyl)acetamide. The crude product was purified by chromatography on silica gel (5% EtOAc/CH_2Cl_2) to provide marinoquinoline **48** as a yellow solid (106 mg, 64% yield). Mp 168-170 ºC. ^{1}H NMR (600 MHz, DMSO) δ 11.73 (s, 1H), 10.19 (s, 1H), 8.20 (d, J = 8.8 Hz, 1H), 8.01 (d, J = 8.5 Hz, 2H), 7.84 (d, J = 8.4 Hz, 2H), 7.62 – 7.56 (m, 1H), 7.49 (d, J = 2.4 Hz, 1H), 7.21 (dd, J = 8.8 e 2.5 Hz, 1H), 7.15 – 7.11 (m, 1H), 3.91 (s, 3H), 2.13 (s, 3H). ^{13}C NMR (150 MHz, DMSO) δ 168.57, 157.60, 145.75, 143.53, 140.17, 132.83, 129.42, 129.11, 128.28, 125.92, 124.09, 118.88, 117.12, 116.75, 108.73, 100.58, 55.18, 24.15. HRMS for $C_{20}H_{17}N_3O_2$ $(M + H)^+$ calcd 332.1394, found 332.1390.

4-(1*H*-indole-3-yl)-7-methoxy-3*H*-pyrrolo[2,3-*c*]quinoline (49). Prepared using general procedure C (Method A) from compound **31** and 1*H*-indole-3-carbaldehyde. The crude product was purified by chromatography on silica gel (5% MeOH/CH_2Cl_2) to provide marinoquinoline **49** as a yellow solid (88 mg, 56% yield). Mp 242 ºC. ^{1}H NMR (500 MHz, $CDCl_3$) δ 8.13 (d, J = 8.9 Hz, 1H), 8.08 (d, J = 8.0 Hz, 1H), 7.95 (s, 1H), 7.53 (m, 4H); 7.25

(t, J = 7.4 Hz, 1H), 7.18 (m, 1H), 7.06 (d, J = 2.8 Hz, 1H), 3.95 (s, 3H). ^{13}C NMR (125 MHz, $CDCl_3$) δ 158.5, 143.6, 143.2, 137.1, 129.8, 128.0, 126.9, 126.4, 125.8, 123.7, 122.2, 120.4, 120.0, 117.1, 116.3, 112.9, 111.3, 106.8, 100.3, 54.5. HRMS for $C_{20}H_{15}N_3O$ $(M + H)^+$ calcd 314.1288, found 314.1293.

***t*-Butyl (4-(7-methoxy-3*H*-pyrrolo[2,3-c]quinolin-4-yl)phenyl) carbamate (50 – Lead Compound)**. Prepared using general procedure C (Method A) starting from compound **31** and *tert*-butyl (4-formylphenyl)carbamate. The crude product was purified by chromatography on silica gel (30% EtOAc/Hexanes) to provide marinoquinoline **50** as a yellow solid (101.2 mg, 52% yield). Mp 214-215 ºC. ^{1}H NMR (400 MHz, CD_2Cl_2) δ 9.25 (s, 1H), 8.10 (d, J = 8.9 Hz, 1H), 7.88 (d, J = 8.6 Hz, 2H), 7.56 (d, J = 2.6 Hz, 1H), 7.53 (d, J = 8.6 Hz, 2H), 7.46 – 7.43 (m, 1H), 7.22 (dd, J = 8.9 e 2.6 Hz, 1H), 7.07 – 7.03 (m, 1H), 6.88 (s, 1H), 3.93 (s, 3H), 1.54 (s, 9H). ^{13}C NMR (100 MHz, CD_2Cl_2) δ 158.93, 153.14, 146.69, 144.93, 140.17, 133.55, 130.10, 129.47, 127.26, 127.26, 124.37, 119.12, 117.96, 117.88, 109.39, 101.82, 81.19, 55.96, 28.62. HRMS for $C_{23}H_{23}N_3O_3$ $(M + H)^+$ calcd 390.1812, found 390.1801.

2. Biology. Tests against P. falciparum blood parasites in vitro

The activity of the marinoquinolines was evaluated against *P. falciparum* blood parasites (3D7 – chloroquine-sensitive and K1 – multidrug-resistant (chloroquine, pyrimethamine and sulfadoxine) from MR4 (https://www.beiresources.org/)), which were cultured as previously described.[58] Parasites were synchronized twice in the week prior to the experiment using 5% D-sorbitol. The 5% D-sorbitol solution was incubated with the parasites for 10 min at 37 °C. Then, the iRBCs were washed once with RPMI medium to remove the

remaining sorbitol. The parasitemia of the culture and the morphology of the parasites were assessed daily using a Giemsa solution (Sigma, St. Louis, Missouri, EUA). A culture with approximately 5-10% parasitemia and a predominance of ring stage forms (> 80%) was used in the in vitro experiments. The parasite culture was diluted to 0.5% of parasitemia and 2% hematocrit, and incubated with various concentrations of the test compounds that had previously been solubilized in 0.05% dimethyl sulfoxide (DMSO) (v/v). Each test was performed in triplicate, and the results were compared with the control cultures grown in complete medium with no drugs. Artesunate and chloroquine were used in each experiment as antimalarial controls. The effects of the compounds were measured using a SYBR green assay.[33] Briefly, the plates were centrifuged at 700 g for 5 min at room temperature to remove the medium, washed with 1X PBS and incubated for 30 min with lysis buffer [2.4228 g of ultra-pure Tris (for a 20 mM solution), pH 7.5; 1.8612 g of ultrapure EDTA (for 5 mM solution); 80 μg of saponin (0.008% w/v); 800 μL of Triton X-100 (0.08% v/v); water Type I] and SYBR green I DNA stain (1:20000). The fluorescence of uninfected erythrocytes was considered background. Fluorescence was measured on a fluorimeter (SpectraMax340PC384) at 485/535 nm.

The half-maximal drug inhibitory concentration (IC_{50}) was estimated by curve fitting using software from the OriginLab Corporation (USA) and comparing the results to the parasite growth in drug-free medium.

3. Cytotoxicity tests using immortalized cells

The cytotoxicity of marinoquinolines was evaluated in a human hepatoma cell line (HepG2 from ATCC https://www.atcc.org/Products/All/HB-8065.aspx) cultured in 75-cm^2 sterile flasks containing RPMI-1640 medium (supplemented with 10% heat-inactivated fetal

bovine serum and 40 mg/L gentamicin) in a 5% CO_2 atmosphere at 37 °C. When cells were confluent, the monolayer was washed with culture medium, trypsinized, distributed in a flat-bottomed 96-well plate (5×10^3 cells/well) and incubated for 18 h at 37 °C to allow cells to adhere.[60] Various concentrations (400–6.2 μM) of the compounds (20 μL) were added to each well of the 96-well plates, incubated with the cultured cells for 24 h in a 5% CO2 atmosphere at 37 °C, and then the 3-(4,5-dimethylthiazol-2-yl)-2,5-diphenyltetrazolium bromide (MTT) solution (5 mg/mL; 20 μL/well for 3 h) was added to evaluate cell viability. Supernatants were carefully removed and 100 μL of DMSO were added to each well and mixed to solubilize the formazan crystals. The optical density was determined at 570 nm and 630 nm (background) (SpectraMax340PC384). Cell viability was expressed as the percentage of the absorbance measured in the control, untreated cells after subtracting the appropriate background.

4. In vitro association with artesunate

An isobologram was generated to analyze the effects of drug combinations with the aim of determining the additive, synergic or antagonistic effect. Briefly, the fractional half-maximum inhibitory concentration (FIC_{50}) was calculated for each drug pair combination. A stock drug solution was prepared for each compound using complete media, such that the final concentration was approximately three-fold higher than the the IC_{50} value. Using these stocks solutions, the following volume-volume (v/v) mixtures of "Compound A" and "Compound B" were prepared: 0:5, 1:4, 2:3, 1:4 and 5:0. These mixtures were then serially diluted two-fold to generate a range of 7 concentrations. The ΣFIC_{50} values were calculated

using the equation: FIC_{50} compound A (IC_{50} of compound A when combined with compound B/ compound A IC_{50}) + FIC_{50} compound B (IC_{50} of compound B when combined with compound A / compound B IC_{50}). Isobologram curves were constructed by plotting FIC_{50}, B vs FIC_50, A. A straight diagonal line ($\Sigma FIC_{50} = 1$) indicates an additive effect between Compound A and Compound B, a concave curve below the diagonal (FICindex < 1) indicates a synergistic effect and a convex curve above the diagonal (FICindex > 1) indicates antagonism.[40]

5. In vitro killing profile

The parasite killing profile was estimated by culturing unlabeled erythrocytes infected with *P. falciparum* (3D7A) with 3 μM compound **50** (10x in vitro IC_{50} value evaluated using a ^{1}H-hypoxanthine incorporation assay). Parasites were treated with drugs for 24 or 48 h. Drugs were replenished after the first 24 h of treatment by removing the spent media and replacing them with new culture media containing fresh drug. After treatment, the drug was removed and the culture was diluted (1/3 dilution) with fresh erythrocytes (2% hematocrit) that had previously been labeled with an intracellular dye (carboxylfluorescein diacetate succinimidyl ester, CFDA-SE). Following an additional 48-h incubation under standard conditions, the ability of treated parasites to an establish infection in freshly labeled erythrocytes was determined using two-color flow cytometry after labeling the parasite DNA (using Hoechst 33342). Cultures containing untreated parasites were used as controls. Parasite viability is reported as the percentage of infected CFDA-SE-stained erythrocytes in drug-treated samples measured at 24 or 48 h using untreated samples of the initial inoculum after a 48-h incubation with labeled erythrocytes and labeled parasite DNA as a reference. Four standard antimalarial drugs (e.g., chloroquine at 0.25 μM, pyrimethamine at 0.94 μM, atovaquone at 0.01 μM and

artesunate at 0.3 μM) were included in each assay to validate the results obtained with the test compounds and allow a comparative classification of the killing behavior of the drugs tested in the present study.

6. P. falciparum dual male and female gamete formation assay

Mature Pf NF54 gametocyte cultures exhibiting the ability to form gametes were divided into wells of a 384-well plate each containing the drug to be tested at a concentration of 1 μM. The final DMSO concentration of the microculture did not exceed 0.25%. Gametocytes in the wells were incubated in the presence of the drug for 24 or 48 h before being stimulated to form gametes by decreasing the temperature from 37 °C to 26 °C and adding the gametocyte activating factor xanthurenic acid (2.5 μM). At 20 min after induction, exflagellation in each well was recorded by automated time-lapse microscopy using a 6x objective and a custom algorithm. This process was repeated to obtain three readings from each well, and after image processing, the mean of each replicate was calculated. Typically, between 150 and 250 exflagellation centers from each field were recorded in the negative controls, depending on the overall exflagellation of the source parent culture. DMSO was used as a negative control and 20 μM Gentian Violet was used as a positive control. After data collection, the plate was returned to a 26 °C incubator for 24 h and then female gamete formation was assessed by staining live cultures with a Cy3-labeled anti-Pfs25 monoclonal antibody. Cells were resuspended when the antibody was added and then stained as they adhered for 2 h before being recorded by an automated microscope using the 6x objective and identified and counted using a custom algorithm. Four fields of view were captured and the mean value was recorded. Typically, 1300-2000 female gametes were recorded per field in the controls. The percent inhibition of male or female gamete formation was calculated with respect to the

positive and negative controls, and the entire experiment was repeated 4 times using independent cultures.

7. Evaluation of P. berghei liver forms

The in vitro prophylactic potential of compound **50** against the liver stages of *P. berghei* (*Pb*EEF) was tested using a luciferase-expressing transgenic *P. berghei* line.[43] Briefly, 3×10^3 hepatoma cells (HepG2) were incubated overnight, compound **50** (10^{-4} to 10^{-9} M) was added 18 h prior to infection. Cells were infected with 1×10^5 luciferase-expressing transgenic *P. berghei* sporozoites that had been freshly isolated from salivary glands of infected *Anopheles stephensi* mosquitoes. The cultures were grown for 48 h and the luciferase activity was measured and correlated to parasite viability. Atovaquone and puromycin were used as positive controls for the *P. berghei* liver stage assay and HepG2 cytotoxicity, respectively.

8. Heme fractionation assay

Heme species were measured using a recently published protocol.[61] The most active compound (**50**) was selected for further study. The antimalarial chloroquine was used as control. Sorbitol-synchronized early ring stage parasites were incubated with compound **50** at multiples of the IC_{50} value (20x, 40x, 80x, and 160x) for 32 h in a mixed gas environment. After 32 h, trophozoites were isolated with 1% saponin, followed by hypotonic lysis and

collection of the supernatant by centrifugation. The supernatant was further mixed with 4% SDS, 0.3 M NaCl and 25% pyrimidine to examine the hemoglobin (Hb) fraction. The pellet was further solubilized with 4% SDS, followed by the addition of 0.2 M HEPES (pH 7.2), 0.3 M NaCl and 25% pyrimidine. The supernatant was collected by centrifugation and represented free heme fraction. The pellet from this step was solubilized in 0.3 M NaOH, followed by addition of 0.2 M HEPES, 0.3 M HCl and 25% pyrimidine. This solubilized fraction corresponded to hemozoin (Hz). UV-visible spectra of heme components present in heme-pyrimidine complexes were recorded using a Flex Station 3 (Molecular Devices).

9. In vivo Assay against P. berghei

A suppressive parasite growth test was performed in mice infected with the *P. berghei* NK65 strain (originally received from the New York University Medical School), as described previously[51], with some modifications. Briefly, adult Swiss outbred mice (20±2 g weight) were intraperitoneally inoculated with 1×10^5 red blood cells infected with *P. berghei*. The infected mice were maintained together for at least 2 h and then randomly divided into groups of 6 animals per cage, which were subsequently administered 50 mg/kg of each compound diluted in 3% (v/v) DMSO by oral gavage or intraperitoneal (ip) injection daily for three days. Two control groups were used in parallel: one was treated with CQ (20 mg/kg), and the other was treated with the vehicle. Blood smears from mouse tails were prepared on days 5, 7 and 9 post-infection and then fixed with methanol, stained with Giemsa and examined under the microscope. Parasitemia was evaluated and the percent inhibition of parasite growth was calculated in relation to the untreated control group (considered 100% growth) using the following equation: [(C - T)/C] ×100; where C is the parasitemia in the control group and T is the parasitemia in the treated group. The use of laboratory animals was

approved by the Ethics Committee for Animal Use of Universidade Federal do Estado de São Paulo, UNIFESP (CEUA N 6630080816).

10. Microsomal Stability Test

The in vitro metabolic stability study was performed as previously described[62] using rat pooled liver microsomes (final protein concentration of 2 mg/mL) suspended in 0.1 M phosphate buffer (pH 7.4) containing 30 mM magnesium chloride. NADPH (10 mM) was used as cofactor, and verapamil (0.1 mM) was used as a positive control. Stock solutions of compounds (10 mM) were prepared separately in acetonitrile:water (1:1, v/v), except for compound **50**, which required at least 70% acetonitrile for solubilization. Final working solutions (4 μM) were prepared by sequentially diluting each stock solution in 0.1 M phosphate buffer (pH 7.4). At predetermined time points, the reactions were quenched by the addition of ice-cold acetonitrile. Samples were centrifuged and the supernatant was analyzed by liquid chromatography-tandem mass spectrometry (Agilent 1200 series HPLC coupled to AB SCIEX 3200Qtrap mass spectrometer). The relative loss of the parent compound over time was monitored and concentration versus time plots were prepared for each compound to determine the first-order rate constant for compound depletion, which was used to calculate the half-life of each compound.

11. Computational Method. Dataset

The series of 39 marinoquinoline derivatives designed as *P. falciparum* inhibitors were used as the dataset for the computational studies. The biological inhibitory values (IC_{50}) were converted into $pIC_{50} = -\log IC_{50}$. The compounds were manually divided into a training set

(**4–17**, **19**, **21**, **22**, **29**, **32–35**, **38–40**, **42**, **43**, and **45–47**) and a test set (**18**, **20** and **36**) as structural and biological representatives of the total dataset (Figure S1). Tables 1–4 show the structures and biological activities of each inhibitor. Compounds **37**, **41** and **44** were identified as outliers and removed from the dataset for QSAR analyses.

12. QSAR

QSAR modeling was performed using SYBYL-X 2.0 software (Tripos Inc., St. Louis, USA) running on a Red Hat Linux Workstation. The conformational state of each molecule in the dataset was energetically minimized using the Tripos force field and the Powell conjugate[62] gradient algorithm with a convergence criterion of 0.005 kcal/mol·Å, and the atomic partial charges were calculated using the Gasteiger-Hückel method.[63]

13. HQSAR

HQSAR is two-dimensional type of QSAR in which ligands are represented as unique molecular holograms (descriptors). For this purpose, the molecules are divided into structural fragments. Hologram generation is affected by the hologram length, fragment size, and fragment distinction parameters – atoms (A), bonds (B), connections (C), hydrogens (H), chirality (Ch) and hydrogen bond donor and acceptor (DA). Then, 14 different combinations of these parameters were considered during HQSAR model construction. Next, the impact of fragment size was evaluated by changing the minimum and maximum length of fragments to be included in the hologram using six distinct fragment sizes (i.e., 2–5, 3–6, 4–7, 5–8, 6–9, and 7–10) over the default series of hologram lengths, namely, 53, 59, 61, 71, 83, 97, 151, 199, 257, 307, 353, and 401 bins. The patterns of fragment counts from the

training set inhibitors were then related to the experimental biological data using the partial least squares (PLS) analysis.

14. CoMFA

CoMFA (Comparative Molecular Field Analysis) is a three-dimensional type of QSAR based on the interaction energies between a probe atom and the aligned ligand atoms inside a grid box.[36] All molecules in the dataset were aligned by the maximum common substructure method applied in the *align database* function of SYBYL. The steric and electrostatic fields were calculated at each lattice intersection of a grid box with 2 Å spacing. The lattice was defined with an extension of at least 4 Å from the ligand atoms in all directions. An sp^3 carbon atom with a charge of +1 was selected as the probe for the field calculations using standard SYBYL parameters (TRIPOS standard field, dielectric constant 1/r, and 30 kcal/mol cutoff). Region focusing, which was applied in the SYBYL PLS method, selectively re-weighted the grid intersection points in a region to create a new CoMFA model. Two procedures were used to derive weights: *Discriminant Power*, which determines weights according to the fraction of the variation of components attributable to each grid intersection point, and *Stdev*Coefficients*, which determines weights according to the product of the variation at each grid intersection point and its regression coefficient.

15. Model construction and validation

HQSAR and CoMFA descriptors were used as independent variables and the pIC_{50} as the dependent variable to develop the models. The data were linearly correlated using the partial least square (PLS) method and internal validation was performed using the cross-

validation analysis leave-one-out (LOO) method. The conventional correlation coefficient (r^2), cross-validation coefficient (q^2) and standard error of estimate (SEE) were analyzed to identify the model displaying the greatest predictive capability. To perform the Leave-many-out cross-validation the data set was divided into 10 and 5 randomly selected groups of equal size, and subsequently, each group was left out once during the cross-validation process. Each model was evaluated 25 times by measuring its accuracy in predicting the activity of the remaining 10% and 20% data set compounds. Models were considered acceptable if they satisfied the conditions: r^2>0.6 and q^2>0.5. To evaluate the performance of both the HQSAR and CoMFA models, the AUC-ROC analysis considered pIC_{50} = 5 (10 μM) as the activity cutoff. To assess the predictive ability of the QSAR models developed using the training sets, the external validation was performed by predicting pIC_{50} of test set compounds. The statistical parameter predictive r^2 (r^2_{pred}) expressed the predictive power of the models.

ACKNOWLEDGMENTS

We thank Sao Paulo Research Foundation – FAPESP (CEPID grant 2013/07600-3; 2011/51295-5; 2014/25770-6 to CRDC; 2013/25613-5 to MP; 2015/18192-9 to ACCA) for funding the research and fellowships; the National Council for Scientific and Technological Development – CNPq (grants 471509/2012-4 to RVCG, 405330/2016-2 to RVCG, 306901/2015-3 to RVCG and 305387/2013-8 to CRDC) for funding the research and fellowships, Coordination for the Improvement of Higher Education Personnel – CAPES for fellowships (grant 00.889.834/0001-08 to EFSS) and Serrapilheira Institute (grant number Serra-1708-16250 to RVCG) for funding the research. We are grateful to the MMV Foundation, particularly Dr. Paul Willis and Dr. Mélanie Rouillier, for providing support, allowing us access to their assay network, and their substantial expertise. We are thankful to Dr. Benigno Crespo, Dr. Laura Sans Alonso and Dr. Francisco Javier Gamo,

GlaxoSmithKline at DDW, Tres Cantos, Spain for performing the antimalarial killing profile tests. We thank Dr. Jake Baum, Dr. Michael Delves, Dr. Holly Matthews and Ms. Ursula Straschil, Imperial College London, UK for determining the transmission-blocking efficacy. We also thank Dr. Elizabeth Winzeler and Dr. Jenya Antonova, University of California San Diego, USA for performing the in vitro prophylactic evaluation against the liver stages of *P. berghei*. We are also indebted to Dr. Francisco Javier Gamo for thoroughly reviewing the manuscript.

AUTHOR INFORMATION

*Corresponding authors:

Phone: +55 19 3521 3086. E-mail: roque@iqm.unicamp.br (CRDC)

Phone: +55 16 3373 8673. E-mail: rvcguido@usp.br (RVCG)

AUTHORS' CONTRIBUTIONS

A.C.C.A. and M.P. contributed equally. R.V.C.G. and C.R.D.C. conceived the study. M.P. and E.F.S.S. designed and synthesized inhibitors. R.V.C.G. and M.L.G. performed the molecular modeling studies. A.C.C.A., G.E.S. M.K.S. and M.N.S. performed the in vitro studies. A.C.C.A. and G.E.S. performed the in vivo studies. A.C.C.A., C.R.S.G., G.O., C.R.D.C. and R.V.C.G. analyzed the data, contributed ideas and wrote the paper.

NOTE

The authors declare no competing financial interest.

ABBREVIATIONS USED

QSAR, quantitative structure–activity relationship; SI, selectivity index; MQ, marinoquinolines; SAR, structure-activity relationships; TIPS, triisopropylsilyl; TBAF, tetrabutylammonium fluoride; NBS, N-bromosuccinimide; MTT, 3-(4,5-dimethylthiazol-2-yl)-2,5-diphenyltetrazolium bromide; SYBR Green I, N',N'-dimethyl-N-[4-[(E)-(3-methyl-1,3-benzothiazol-2-ylidene)methyl]-1-phenylquinolin-1-ium-2-yl]-N-propylpropane-1,3-diamine; HepG2, human liver cancer cell line; EC_{50}, half maximal effective concentration; IC_{50}, half-maximum inhibitory concentration; LE, ligand efficiency; CoMFA, comparative molecular field analysis; HQSAR hologram quantitative structure–activity relationship; pIC_{50}, –log of the half-maximum inhibitory concentration; PLS, partial least squares; LMO, leave-many-out; ROC, receiver operating characteristic; AUC, area under the curve; SEE, standard error of estimation; SEP, standard error of prediction; FIC, fractional inhibitory concentration index; DFGA, dual gamete formation assay; EEF, exoerythrocytic form; CRT, chloroquine resistance transporter; MDR1, multidrug resistant protein 1; DV, digestive vacuole; CQ, chloroquine; Hz, hemozoin; Hb, hemoglobin; UV, ultraviolet; ip, intraperitoneally, po, oral administration; DHODH, dihydroorotate dehydrogenase; cyt bc1, cytochrome bc1 complex; PI4K, phosphatidylinositol-4-OH kinase; CARL, cyclic amine resistance locus; LC-MS, liquid chromatography mass spectrometry; NMR, nuclear magnetic resonance; TMS, tetramethylsilane; δ, chemical shift; J, coupling constant; HRMS, high-resolution mass spectrometry; TLC, thin layer chromatography; mp, melting points; qNMR, quantitative ^{1}H NMR; THF, tetrahydrofuran; iRBC, infected red blood cells; RPMI-1640, roswell park memorial institute medium; DMSO, dimethyl sulfoxide; PBS, phosphate buffered saline; EDTA, ethylenediaminetetraacetic acid; HEPES, (4-(2-hydroxyethyl)-1-piperazineethanesulfonic acid; NADPH, reduced nicotinamide adenine dinucleotide phosphate.

SUPPORTING INFORMATION

Additional details of the QSAR models, including Tables and Figures (PDF)

Molecular formula strings and biological activity data (CSV)

Copies of ^{1}H NMR and qNMR spectra for compounds **32**, **43** and **50** (PDF)

REFERENCES

(1) World Health Organization (WHO). World Malaria Report 2016. http://www.who.int/malaria/publications/world-malaria-report-2016/report/en/ (accessed September 24, **2016**).

(2) Burrows, J. N.; Burlot, E.; Campo, B.; Cherbuin, S.; Jeanneret, S.; Leroy, D.; Spangenberg, T.; Waterson, D.; Wells, T. N. C.; Willis, P. Antimalarial Drug Discovery - The Path towards Eradication. *Parasitology* **2014**, *141*, 128–139.

(3) Flannery, E. L.; Chatterjee, A. K.; Winzeler, E. A. Antimalarial Drug Discovery: Approaches and Progress towards New Medicines. *Nat. Rev. Microbiol.* **2013**, *11*, 849–862.

(4) Renslo, A. R. Antimalarial Drug Discovery: From Quinine to the Dream of Eradication. *ACS Med. Chem. Lett.* **2013**, *4*, 1126–1128.

(5) Phillips, M. A.; Burrows, J. N.; Manyando, C.; van Huijsduijnen, R. H.; Van Voorhis, W. C.; Wells, T. N. C. Malaria. *Nat. Rev. Dis. Prim.* **2017**, *3*, 17050.

(6) Dondorp, A. M.; Nosten, F.; Yi, P.; Das, D.; Phyo, A. P.; Tarning, J.; Lwin, K. M.; Ariey, F.; Hanpithakpong, W.; Lee, S. J.; Ringwald, P.; Silamut, K.; Imwong, M.; Chotivanich, K.; Lim, P.; Herdman, T.; An, S. S.; Yeung, S.; Singhasivanon, P.; Day, N. P.; Lindegardh, N.; Socheat, D.; White, N. J. Artemisinin Resistance in Plasmodium Falciparum Malaria. *N. Engl. J. Med.* **2009**, *361*, 455–467.

(7) Lin, J. T.; Juliano, J. J.; Wongsrichanalai, C. Drug-Resistant Malaria: The Era of ACT. *Curr. Infect. Dis. Rep.* **2010**, *12*, 165–173.

(8) Miotto, O.; Almagro-Garcia, J.; Manske, M.; MacInnis, B.; Campino, S.; Rockett, K. A.; Amaratunga, C.; Lim, P.; Suon, S.; Sreng, S.; Anderson, J. M.; Duong, S.; Nguon, C.; Chuor, C. M.; Saunders, D.; Se, Y.; Lon, C.; Fukuda, M. M.; Amenga-Etego, L.; Hodgson, A. V.; Asoala, V.; Imwong, M.; Takala-Harrison, S.; Nosten, F.; Su, X. Z.; Ringwald, P.; Ariey, F.; Dolecek, C.; Hien, T. T.; Boni, M. F.; Thai, C. Q.; Amambua-

Ngwa, A.; Conway, D. J.; Djimdé, A. A.; Doumbo, O. K.; Zongo, I.; Ouedraogo, J. B.; Alcock, D.; Drury, E.; Auburn, S.; Koch, O.; Sanders, M.; Hubbart, C.; Maslen, G.; Ruano-Rubio, V.; Jyothi, D.; Miles, A.; O'Brien, J.; Gamble, C.; Oyola S. O.; Rayner, J. C.; Newbold, C. I.; Berriman, M.; Spencer, C. C.; McVean, G.; Day, N. P.; White, N. J.; Bethell, D.; Dondorp, A. M.; Plowe, C. V.; Fairhurst, R. M.; Kwiatkowski, D. P. Multiple Populations of Artemisinin-Resistant Plasmodium Falciparum in Cambodia. *Nat. Genet.* **2013**, *45*, 648–655.

(9) Tun, K. M.; Imwong, M.; Lwin, K. M.; Win, A. A.; Hlaing, T. M.; Hlaing, T.; Lin, K.; Kyaw, M. P.; Plewes, K.; Faiz, M. A.; Dhorda, M.; Cheah, P. Y.; Pukrittayakamee, S.; Ashley, E. A.; Anderson, T. J.; Nair, S.; McDew-White, M.; Flegg, J. A.; Grist, E. P.; Guerin, P.; Maude, R. J.; Smithuis, F.; Dondorp, A. M.; Day, N. P.; Nosten, F.; White, N. J.; Woodrow, C. J. Spread of Artemisinin-Resistant Plasmodium Falciparum in Myanmar: A Cross-Sectional Survey of the K13 Molecular Marker. *Lancet Infect. Dis.* **2015**, *15*, 415–421.

(10) Burrows, J. N.; Leroy, D.; Lotharius, J.; Waterson, D. Challenges in Antimalarial Drug Discovery. *Future Med. Chem.* **2011**, *3*, 1401–1412.

(11) Aguiar, A. C. C.; Rocha, E. M. da; Souza, N. B. de; França, T. C.; Krettli, A. U. New Approaches in Antimalarial Drug Discovery and Development: A Review. *Mem. Inst. Oswaldo Cruz* **2012**, *107*, 831–845.

(12) Aguiar, A. C.; de Sousa, L. R. F.; Garcia, C. R. S.; Oliva, G.; Guido, R. V. C. New Molecular Targets and Strategies for Antimalarial Discovery. *Curr. Med. Chem.* [Online early access]. DOI: 10.2174/0929867324666170830103003. Published Online: August 29, 2017.

(13) Njoroge, M.; Njuguna, N. M.; Mutai, P.; Ongarora, D. S. B.; Smith, P. W.; Chibale, K. Recent Approaches to Chemical Discovery and Development against Malaria and the

Neglected Tropical Diseases Human African Trypanosomiasis and Schistosomiasis. *Chem. Rev.* **2014**, *114*, 11138−11163.

(14) Kumar, V.; Kaur, K.; Gupta, G. K.; Sharma, A. K. Pyrazole Containing Natural Products: Synthetic Preview and Biological Significance. *Eur. J. Med. Chem.* **2013**, *69*, 735−753.

(15) Schuck, D. C.; Ferreira, S. B.; Cruz, L. N.; Da Rocha, D. R.; Moraes, M. S.; Nakabashi, M.; Rosenthal, P. J.; Ferreira, V. F.; Garcia, C. R. Biological Evaluation of Hydroxynaphthoquinones as Anti-Malarials. *Malar. J.* **2013**, *12*, 234.

(16) Carballeira, N. M.; Bwalya, A. G.; Itoe, M. A.; Andricopulo, A. D.; Cordero-Maldonado, M. L.; Kaiser, M.; Mota, M. M.; Crawford, A. D.; Guido, R. V. C.; Tasdemir, D. 2-Octadecynoic Acid as a Dual Life Stage Inhibitor of Plasmodium Infections and Plasmodial FAS-II Enzymes. *Bioorg. Med. Chem. Lett.* **2014**, *24*, 4151−4157.

(17) Alves, E.; Iglesias, B. A.; Deda, D. K.; Budu, A.; Matias, T. A.; Bueno, V. B.; Maluf, F. V.; Guido, R. V. C.; Oliva, G.; Catalani, L. H.; Araki, K.; Garcia, C. R. Encapsulation of Metalloporphyrins Improves Their Capacity to Block the Viability of the Human Malaria Parasite Plasmodium Falciparum. *Nanomed. Nanotechnol. Biol. Med.* **2015**, *11*, 351−358.

(18) Alves, E.; Maluf, F. V.; Bueno, V. B.; Guido, R. V. C.; Oliva, G.; Singh, M.; Scarpelli, P.; Costa, F.; Sartorello, R.; Catalani, L. H.; Brady, D.; Tewari, R.; Garcia, C. R. Biliverdin Targets Enolase and Eukaryotic Initiation Factor 2 (EIF2α) to Reduce the Growth of Intraerythrocytic Development of the Malaria Parasite Plasmodium Falciparum. *Sci. Rep.* **2016**, *6*, 22093.

(19) Pereira, M.; da Silva, T.; Aguiar, A. C. C.; Oliva, G.; Guido, R. V. C.; Yokoyama-Yasunaka, J.; Uliana, S.; Lopes, L. Chemical Composition, Antiprotozoal and

Cytotoxic Activities of Indole Alkaloids and Benzofuran Neolignan of Aristolochia Cordigera. *Planta Med.* **2017**, *83*, 912–920.

(20) Baragana, B.; Norcross, N. R.; Wilson, C.; Porzelle, A.; Hallyburton, I.; Grimaldi, R.; Osuna-Cabello, M.; Norval, S.; Riley, J.; Stojanovski, L.; Simeons, F. R. C.; Wyatt, P. G.; Delves, M. J.; Meister, S.; Duffy, S.; Avery, V. M.; Winzeler, E. A.; Sinden, R. E.; Wittlin, S.; Frearson, J. A.; Gray, D. W.; Fairlamb, A. H.; Waterson, D.; Campbell, S. F.; Willis, P.; Read, K. D.; Gilbert, I. H. Discovery of a Quinoline-4-Carboxamide Derivative with a Novel Mechanism of Action, Multistage Antimalarial Activity, and Potent in Vivo Efficacy. *J. Med. Chem.* **2016**, *59*, 9672–9685.

(21) Maignan, J. R.; Lichorowic, C. L.; Giarrusso, J.; Blake, L. D.; Casandra, D.; Mutka, T. S.; LaCrue, A. N.; Burrows, J. N.; Willis, P. A.; Kyle, D. E.; Manetsch, R. ICI 56,780 Optimization: Structure-Activity Relationship Studies of 7-(2-Phenoxyethoxy)-4(1H)-Quinolones with Antimalarial Activity. *J. Med. Chem.* **2016**, *59*, 6943–6960.

(22) Yang, Y.; Yu, Y.; Li, X.; Li, J.; Wu, Y.; Yu, J.; Ge, J.; Huang, Z.; Jiang, L.; Rao, Y.; Yang, M. Target Elucidation by Cocrystal Structures of NADH-Ubiquinone Oxidoreductase of Plasmodium Falciparum (Pf NDH2) with Small Molecule To Eliminate Drug-Resistant Malaria. *J. Med. Chem.* **2017**, *60*, 1994–2005.

(23) Krake, S. H.; Martinez, P. D. G.; McLaren, J.; Ryan, E.; Chen, G.; White, K.; Charman, S. A.; Campbell, S.; Willis, P.; Dias, L. C. Novel Inhibitors of Plasmodium Falciparum Based on 2,5-Disubstituted Furans. *Eur. J. Med. Chem.* **2017**, *126*, 929–936.

(24) Burrows, J. N.; Van Huijsduijnen, R. H.; Möhrle, J. J.; Oeuvray, C.; Wells, T. N. Designing the next Generation of Medicines for Malaria Control and Eradication. *Malar. J.* **2013**, *12*, 187.

(25) Sangnoi, Y.; Sakulkeo, O.; Yuenyongsawad, S.; Kanjana-opas, A.; Ingkaninan, K.;

Plubrukarn, A.; Suwanborirux, K. Acetylcholinesterase-Inhibiting Activity of Pyrrole Derivatives from a Novel Marine Gliding Bacterium, Rapidithrix Thailandica. *Mar. Drugs* **2008**, *6*, 578–586.

(26) Okanya, P. W.; Mohr, K. I.; Gerth, K.; Jansen, R.; Müller, R. Marinoquinolines A–F, Pyrroloquinolines from *Ohtaekwangia Kribbensis* (Bacteroidetes). *J. Nat. Prod.* **2011**, *74*, 603–608.

(27) Choi, E. J.; Nam, S. J.; Paul, L.; Beatty, D.; Kauffman, C. A.; Jensen, P. R.; Fenical, W. Previously Uncultured Marine Bacteria Linked to Novel Alkaloid Production. *Chem. Biol.* **2015**, *22*, 1270–1279.

(28) Van Baelen, G.; Hostyn, S.; Dhooghe, L.; Tapolcsányi, P.; Mátyus, P.; Lemière, G.; Dommisse, R.; Kaiser, M.; Brun, R.; Cos, P.; Maes, L.; Hajós, G.; Riedl, Z.; Nagy, I.; Maes, B. U. W.; Pieters, L. Structure-Activity Relationship of Antiparasitic and Cytotoxic Indoloquinoline Alkaloids, and Their Tricyclic and Bicyclic Analogues. *Bioorg. Med. Chem.* **2009**, *17*, 7209–7217.

(29) Billingsley, K.; Buchwald, S. L. Highly Efficient Monophosphine-Based Catalyst for the Palladium-Catalyzed Suzuki-Miyaura Reaction of Heteroaryl Halides and Heteroaryl Boronic Acids and Esters. *J. Am. Chem. Soc.* **2007**, *129*, 3358–3366.

(30) Bray, B. L.; Mathies, P. H.; Naef, R.; Solas, D. R.; Tidwell, T. T.; Artis, D. R.; Muchowski, J. M. N-(Triisopropylsilyl)Pyrrole. A Progenitor "Par Excellence" of 3-Substituted Pyrroles. *J. Org. Chem.* **1990**, *55*, 6317–6328.

(31) Alvarez, A.; Guzmán, A.; Ruiz, A.; Velarde, E.; Muchowski, J. M. Synthesis of 3-Arylpyrroles and 3-Pyrrolylacetylenes by Palladium-Catalyzed Coupling Reactions. *J. Org. Chem.* **1992**, *57*, 1653–1656.

(32) Flatt, A. K.; Yao, Y.; Maya, F.; Tour, J. M. Orthogonally Functionalized Oligomers for Controlled Self-Assembly. *J. Org. Chem.* **2004**, *69*, 1752–1755.

(33) Smilkstein, M.; Sriwilaijaroen, N.; Kelly, J. X.; Wilairat, P.; Riscoe, M. Simple and Inexpensive Fluorescence-Based Technique for High-Throughput Antimalarial Drug Screening. *Antimicrob. Agents Chemother.* **2004**, *48*, 1803–1806.

(34) Van Miert, S.; Hostyn, S.; Maes, B. U. W.; Cimanga, K.; Brun, R.; Kaiser, M.; Mátyus, P.; Dommisse, R.; Lemière, G.; Vlietinck, A.; Pieters, L. Isoneocryptolepine, a Synthetic Indoloquinoline Alkaloid, as an Antiplasmodial Lead Compound. *J. Nat. Prod.* **2005**, *68*, 674–677.

(35) Lowis, D. R. HQSAR: A New, Highly Predictive QSAR Technique. *Tripos Tech. notes* **1997**, *1*, 1–17.

(36) Cramer, R. D.; Patterson, D. E.; Bunce, J. D. Comparative Molecular Field Analysis (CoMFA). 1. Effect of Shape on Binding of Steroids to Carrier Proteins. *J. Am. Chem. Soc.* **1988**, *110*, 5959–5967.

(37) Salum, L. B.; Andricopulo, A. D. Fragment-Based QSAR: Perspectives in Drug Design. *Mol. Divers.* **2009**, *13*, 277–285.

(38) Golbraikh, A.; Tropsha, A. Beware of q^2! *J. Mol. Graph. Model.* **2002**, *20*, 269–276.

(39) Fidock, D. A; Rosenthal, P. J.; Croft, S. L.; Brun, R.; Nwaka, S. Antimalarial Drug Discovery: Efficacy Models for Compound Screening. *Nat. Rev. Drug Discov.* **2004**, *3*, 509–520.

(40) Gorka, A. P.; Jacobs, L. M.; Roepe, P. D. Cytostatic versus Cytocidal Profiling of Quinoline Drug Combinations via Modified Fixed-Ratio Isobologram Analysis. *Malar. J.* **2013**, *12*, 332.

(41) Peatey, C. L.; Leroy, D.; Gardiner, D. L.; Trenholme, K. R. Anti-Malarial Drugs: How Effective Are They against Plasmodium Falciparum Gametocytes? *Malar. J.* **2012**, *11*, 34.

(42) Delves, M. J.; Straschil, U.; Ruecker, A.; Miguel-Blanco, C.; Marques, S.; Baum, J.;

Sinden, R. E. Routine in Vitro Culture of P. Falciparum Gametocytes to Evaluate Novel Transmission-Blocking Interventions. *Nat. Protoc.* **2016**, *11*, 1668–1680.

(43) Swann, J.; Corey, V.; Scherer, C. A.; Kato, N.; Comer, E.; Maetani, M.; Antonova-Koch, Y.; Reimer, C.; Gagaring, K.; Ibanez, M.; Plouffe, D.; Zeeman, A. M.; Kocken, C. H.; McNamara, C. W.; Schreiber, S. L.; Campo, B.; Winzeler, E. A.; Meister, S. High-Throughput Luciferase-Based Assay for the Discovery of Therapeutics That Prevent Malaria. *ACS Infect. Dis.* **2016**, *2*, 281–293.

(44) Fidock, D. A.; Nomura, T.; Talley, A. K.; Cooper, R. A.; Dzekunov, S. M.; Ferdig, M. T.; Ursos, L. M. B.; Sidhu, A. B. S.; Naudé, B.; Deitsch, K. W.; Su, X. Z.; Wootton, J. C.; Roepe, P. D.; Wellems, T. E. Mutations in the P. Falciparum Digestive Vacuole Transmembrane Protein PfCRT and Evidence for Their Role in Chloroquine Resistance. *Mol. Cell* **2000**, *6*, 861–871.

(45) Veiga, M. I.; Dhingra, S. K.; Henrich, P. P.; Straimer, J.; Gnädig, N.; Uhlemann, A. C.; Martin, R. E.; Lehane, A. M.; Fidock, D. A. Globally Prevalent PfMDR1 Mutations Modulate Plasmodium Falciparum Susceptibility to Artemisinin-Based Combination Therapies. *Nat. Commun.* **2016**, *7*, 11553.

(46) Kapishnikov, S.; Weiner, A.; Shimoni, E.; Schneider, G.; Elbaum, M.; Leiserowitz, L. Digestive Vacuole Membrane in Plasmodium Falciparum -Infected Erythrocytes: Relevance to Templated Nucleation of Hemozoin. *Langmuir* **2013**, *29*, 14595–14602.

(47) Combrinck, J. M.; Mabotha, T. E.; Ncokazi, K. K.; Ambele, M. A.; Taylor, D.; Smith, P. J.; Hoppe, H. C.; Egan, T. J. Insights into the Role of Heme in the Mechanism of Action of Antimalarials. *ACS Chem. Biol.* **2013**, *8*, 133–137.

(48) Gabryszewski, S. J.; Dhingra, S. K.; Combrinck, J. M.; Lewis, I. A.; Callaghan, P. S.; Hassett, M. R.; Siriwardana, A.; Henrich, P. P.; Lee, A. H.; Gnädig, N. F.; Musset, L.; Llinás, M.; Egan, T. J.; Roepe, P. D.; Fidock, D. A. Evolution of Fitness Cost-Neutral

Mutant PfCRT Conferring P. Falciparum 4-Aminoquinoline Drug Resistance Is Accompanied by Altered Parasite Metabolism and Digestive Vacuole Physiology. *PLoS Pathog.* [Online] **2016**, *12*, e1005976.

(49) Ncokazi, K. K.; Egan, T. J. A Colorimetric High-Throughput β-Hematin Inhibition Screening Assay for Use in the Search for Antimalarial Compounds. *Anal. Biochem.* **2005**, *338*, 306–319.

(50) Lorke, D. A New Approach to Practical Acute Toxicity Testing. *Arch. Toxicol.* **1983**, *54*, 275–287.

(51) Peters, W. Drug Resistance in Plasmodium Berghei Vincke and Lips, 1948. I. Chloroquine Resistance. *Exp. Parasitol.* **1965**, *17*, 80–89.

(52) Phillips, M. A; Lotharius, J.; Marsh, K.; White, J.; Dayan, A.; White, K. L.; Njoroge, J. W.; El Mazouni, F.; Lao, Y.; Kokkonda, S.; Tomchick, D. R.; Deng, X.; Laird, T.; Bhatia, S. N.; March, S.; Ng, C. L.; Fidock, D. A.; Wittlin, S.; Lafuente-Monasterio, M.; Benito, F. J.; Alonso, L. M.; Martinez, M. S.; Jimenez-Diaz, M. B.; Bazaga, S. F.; Angulo-Barturen, I.; Haselden, J. N.; Louttit, J.; Cui, Y.; Sridhar, A.; Zeeman, A. M.; Kocken, C.; Sauerwein, R.; Dechering, K.; Avery, V. M.; Duffy, S.; Delves, M.; Sinden, R.; Ruecker, A.; Wickham, K. S.; Rochford, R.; Gahagen, J.; Iyer, L.; Riccio, E.; Mirsalis, J.; Bathhurst, I.; Rueckle, T.; Ding, X.; Campo, B.; Leroy, D.; Rogers, M. J.; Rathod, M. J.; Burrows, J. N.; Charman, S. A. A Long-Duration Dihydroorotate Dehydrogenase Inhibitor (DSM265) for Prevention and Treatment of Malaria. *Sci. Transl. Med.* [Online] **2015**, *7*, 296ra111.

(53) Stickles, A. M.; Ting, L. M.; Morrisey, J. M.; Li, Y.; Mather, M. W.; Meermeier, E.; Pershing, A. M.; Forquer, I. P.; Miley, G. P.; Pou, S.; Winter, R. W.; Hinrichs, D. J.; Kelly, J. X.; Kim, K.; Vaidya, A. B.; Riscoe, M. K.; Nilsen, A. Inhibition of Cytochrome Bc 1 as a Strategy for Single-Dose, Multi-Stage Antimalarial Therapy.

Am. J. Trop. Med. Hyg. **2015**, *92*, 1195–1201.

(54) McNamara, C. W.; Lee, M. C. . S.; Lim, C. S.; Lim, S. H.; Roland, J.; Simon, O.; Yeung, B. K. S.; Chatterjee, A. K.; McCormack, S. L.; Manary, M. J.; Zeeman, A. M.; Dechering, K. J.; Kumar, T. S.; Henrich, P. P.; Gagaring, K.; Ibanez, M.; Kato, N.; Kuhen, K. L.; Fischli, C.; Nagle, A.; Rottmann, M.; Plouffe, D. M.; Bursulaya, B.; Meister, S.; Rameh, L.; Trappe, J.; Haasen, D.; Timmerman, M.; Sauerwein, R. W.; Suwanarusk, R.; Russell, B.; Renia, L.; Nosten, F.; Tully, D. C.; Kocken, C. H.; Glynne, R. J.; Bodenreider, C.; Fidock, D. A.; Diagana, T. T.; Winzeler, E. A. Targeting Plasmodium PI(4)K to Eliminate Malaria. *Nature* **2013**, *504*, 248–253.

(55) Magistrado, P. A.; Corey, V. C.; Lukens, A. K.; Lamonte, G.; Sasaki, E.; Meister, S.; Wree, M.; Winzeler, E.; Wirth, D. F. Plasmodium Falciparum Cyclic Amine Resistance Locus (PfCARL), a Resistance Mechanism for Two Distinct Compound Classes. *ACS Infect. Dis.* **2016**, *2*, 816–826.

(56) Verma, A. K.; Jha, R. R.; Kasi Sankar, V.; Singh, R. P. Selective Synthesis of 4,5-Dihydroimidazo- and Imidazo[1,5-a]Quinoxalines via Modified Pictet-Spengler Reaction. *Tetrahedron Lett.* **2013**, *54*, 5984–5990.

(57) Schwalm, C. S.; Correia, C. R. D. Divergent Total Synthesis of the Natural Antimalarial Marinoquinolines A, B, C, e and Unnatural Analogues. *Tetrahedron Lett.* **2012**, *53*, 4836–4840.

(58) Trager, W.; Jensen, J. Human Malaria Parasites in Continuous Culture. *Science* **1976**, *193*, 673–675.

(59) Lambros, C.; Vanderberg, J. P. Synchronization of Plasmodium Falciparum Erythrocytic Stages in Culture. *J. Parasitol.* **1979**, *65*, 418.

(60) Denizot, F.; Lang, R. Rapid Colorimetric Assay for Cell Growth and Survival. *J. Immunol. Methods* **1986**, *89*, 271–277.

(61) Combrinck, J. M.; Fong, K. Y.; Gibhard, L.; Smith, P. J.; Wright, D. W.; Egan, T. J. Optimization of a Multi-Well Colorimetric Assay to Determine Haem Species in Plasmodium Falciparum in the Presence of Anti-Malarials. *Malar. J.* **2015**, *14*, 253.

(62) Obach, R.S. Prediction of Human Clearance of Twenty-Nine Drugs from Hepatic Microsomal Intrinsic Clearance Data: An Examination of in Vitro Half-Life Approach and Non-Specific Binding to Microsomes. *Drug Metab. Dispos*. **1999**, *27*, 1350-1359.

(63) Powell, M. J. D. Restart Procedures for the Conjugate Gradient Method. *Math. Program.* **1977**, *12*, 241–254.

(64) Gasteiger, J.; Marsili, M. Iterative Partial Equalization of Orbital Electronegativity-a Rapid Access to Atomic Charges. *Tetrahedron* **1980**, *36*, 3219–3228.

TABLES

Table 1. Structure−Activity Relationship of the 4-Position.

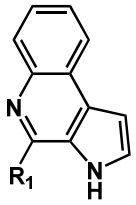

Cpd	R_1	IC_{50} (μM) *P. falciparum* (3D7 strain)	EC_{50} (μM) HepG2	SI
4	methyl	> 10	ND	ND
5	isobutyl	4.1 ± 0.2	> 250	> 61
6	benzyl	> 10	ND	ND
7	ethyl	7.3 ± 0.9	151 ± 5	21
8	phenyl	9.9 ± 0.4	> 750	> 75
chloroquine*		0.029 ± 0.01	384 ± 21	13241

ND = Not determined;
*chloroquine was used as positive control for antimalarial activity and cytotoxicity

Table 2. Structure−Activity Relationship of the 4-phenyl substituent.

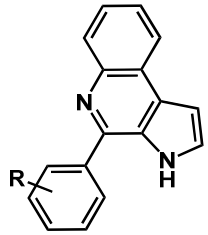

Cpd	R	IC_{50} (μM) *P. falciparum* (3D7 strain)	EC_{50} (μM) HepG2	SI
9	4-methoxy	6.7 ± 0.4	> 250	> 37
10	3,5-dimethoxy	4.9 ± 0.1	> 250	> 51
11	3,4,5-trimethoxy	9.2 ± 0.8	99 ± 7	11
12	4-chloro	10.5 ± 0.5	> 250	> 24
13	4-bromo	> 10	ND	ND
14	4-nitro	> 10	ND	ND
15	4-amino	7.7 ± 0.7	41 ± 2	5
16	4-dimethylamino	5.8 ± 0.2	> 600	> 104
17	4-COOH	12.1 ± 0.1	82 ± 4	7
18	4-CO_2Me	4 ± 2	> 250	> 63

ND = Not determined

Table 3. Structure−Activity Relationship of the 4-indole substituent.

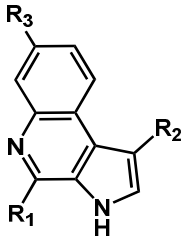

Cpd	R_1	R_2	R_3	IC_{50} (μM) *P. falciparum* (3D7 strain)	EC_{50} (μM) HepG2	SI
19	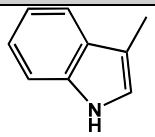	H	H	10.4 ± 0.4	> 750	72
20	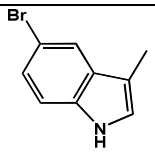	H	H	12.3 ± 0.4	93 ± 7	8
21	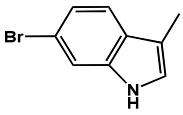	H	H	6.2 ± 0.1	42 ± 16	7
22	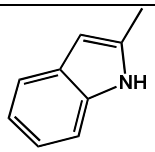	H	H	4.8 ± 0.2	746 ± 2	155
29	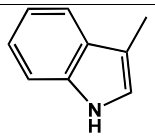	H	Br	7.9 ± 0.2	> 250	> 32
45	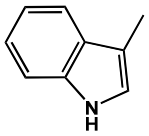	Br	H	> 10	ND	ND

ND = Not determined

Table 4. Structure−Activity Relationship of the 7-methoxy substituent

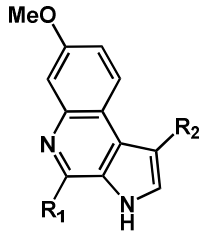

Cpd	R_1	R_2	IC_{50} (μM) *P. falciparum* (3D7 strain)	EC_{50} (μM) HepG2	SI
32	isobutyl	H	0.5 ± 0.2	35 ± 1	70
33	methyl	H	10.5 ± 0.3	> 750	71
34	ethyl	H	> 10	ND	ND
35	phenyl	H	2.4 ± 0.5	60 ± 2	25
36	3,5-dimethoxyphenyl	H	1.0 ± 0.5	> 250	> 250
37	3,4,5-trimethoxyphenyl	H	9.9 ± 0.1	> 750	75
38	4-nitrophenyl	H	1.9 ± 0.1	144 ± 38	76
39	4-aminophenyl	H	1.3 ± 0.1	> 750	> 576
40	4-dimethylamino phenyl	H	0.4 ± 0.1	20 ± 2	50
41	4-carboxyphenyl	H	> 10	ND	ND
42	methyl benzoate	H	1.3 ± 0.5	> 250	> 192
43	4-chloro phenyl	H	0.6 ± 0.3	> 250	> 417
44	benzyl	H	14.3 ± 0.7	478 ± 8	33
46	methyl	Br	5.4 ± 0.3	> 250	> 46
47	phenyl	Br	2.1 ± 0.7	111 ± 14	53

ND = Not determined

Table 5. Experimental and Predicted Activities (pIC_{50}) with Residual Values for the Test and the Prospective Set Compounds

Data Set	QSAR Method	Cpd	Experimental pIC_{50}	Predicted pIC_{50}	Residue
Test Set	HQSAR	**18**	5.40	5.36	0.04
		20	4.91	4.90	0.01
		36	6.00	5.70	0.30
	CoMFA	**18**	5.40	5.17	0.23
		20	4.91	4.92	-0.01
		36	6.00	5.97	0.03
Prospective Set	HQSAR	**48**	< 5.00	6.00	-1.00
		49	7.21	6.22	0.99
		50	7.40	6.60	0.80
	CoMFA	**48**	< 5.00	6.00	-1.00
		49	7.21	6.21	1.00
		50	7.40	6.60	0.80

Table 6. Inhibitory and cytotoxic activity of the predicted and synthesized marinoquinoline derivatives.

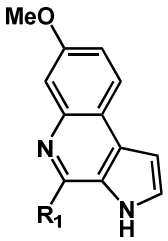

Cpd	R_1	IC_{50} (μM) *P. falciparum* (3D7 strain)	EC_{50} (μM) HepG2	SI
48	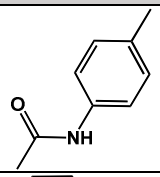	> 10	ND	ND
49	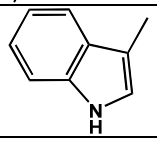	0.061 ± 0.002	20 ± 3	328
50	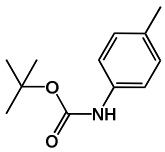	0.039 ± 0.004	> 250	> 6410

ND = Not determined

Table 7. Antiplasmodial activity of selected marinoquinoline derivatives against schizont, asynchronous and ring forms of *P. falciparum*. Parasites were synchronized twice in the week prior to the experiment using 5% D-sorbitol and the duration of the treatment was 72 h.

Compound	*P. falciparum* – 3D7 strain IC_{50} (μM)			
	asynchronous	**ring**	**trophozoite**	**schizont**
32	0.42 ± 0.03	0.50 ± 0.02	0.42 ± 0.01	0.40 ± 0.01
43	0.46 ± 0.02	0.60 ± 0.03	0.38 ± 0.08	0.50 ± 0.02
50	0.033 ± 0.003	0.039 ± 0.003	0.05 ± 0.02	0.028 ± 0.002

Table 8. Percentage of parasitemia reduction after malaria treatment with **50**.

Compound / Route	Dose	(%) of reduction			Survival
		Days after infection			
		5	7	9	Days
32 OR	50 mg/Kg	0	0	0	23 ± 6
43 OR	50 mg/Kg	0	0	0	22 ± 6
50 OR	50 mg/Kg	69 ± 8	54 ± 3	42 ± 2	25 ± 3
50 IP	50 mg/Kg	61 ± 6	34 ± 12	58 ± 8	24 ± 4
Chloroquine	20 mg/Kg	100	100	100	>30
Non-treated	-	-	-	-	19 ± 5

FIGURE 1

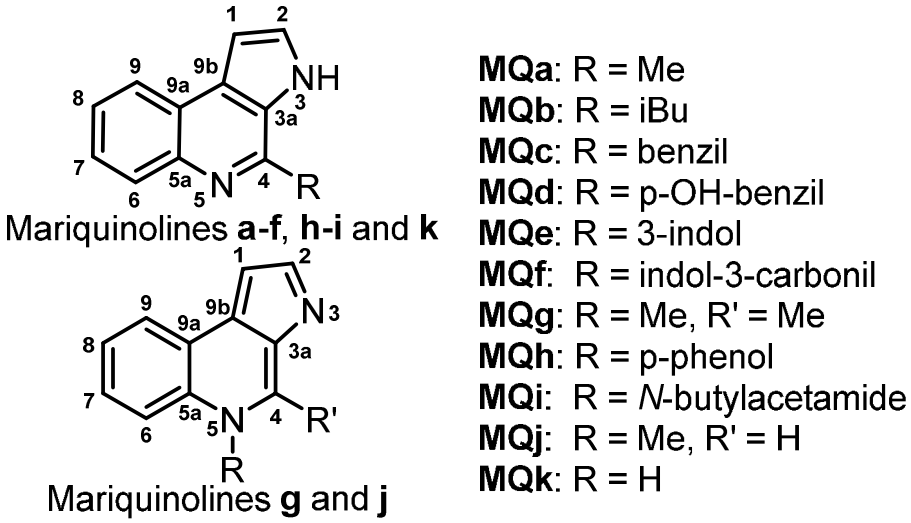

Figure 1: (**A**) 3*H*-pyrrolo[2,3-*c*]quinoline containing natural products isolated from *Ohtaekwangia kribbensis*, *Mooreia alkaloidigena* and *Catalinimonas alkaloidigena*.

FIGURE 2

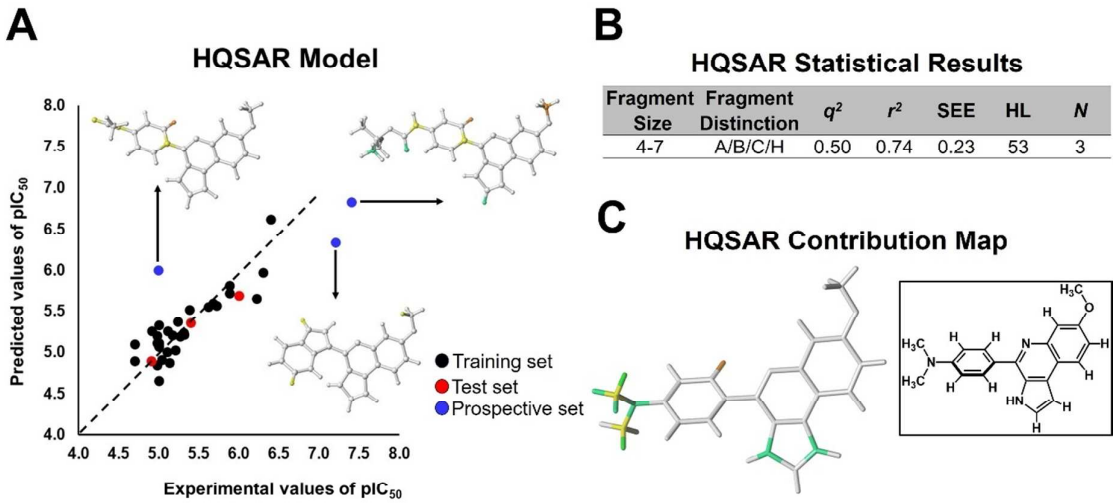

Figure 2. 2D-QSAR modeling. (**A**) Plot of predicted values of pIC_{50} versus the corresponding experimental values for the training set (black circles), test set (red circles) and prospective set (blue circles) inhibitors for the best HQSAR model. Structures and HQSAR contribution maps of the prospective inhibitors **48–50** (blue circles) are indicated. (**B**) Key statistical parameters for the best HQSAR model. (**C**) HQSAR contribution map for the most potent marinoquinoline derivative **40** (green and yellow = positive contribution of an atom to the activity of the molecules; gray = neutral contribution of an atom to the activity of the molecules; orange and red = negative contribution of an atom to the activity of the molecules). Insert: 2D structure of **40** inhibitor.

FIGURE 3

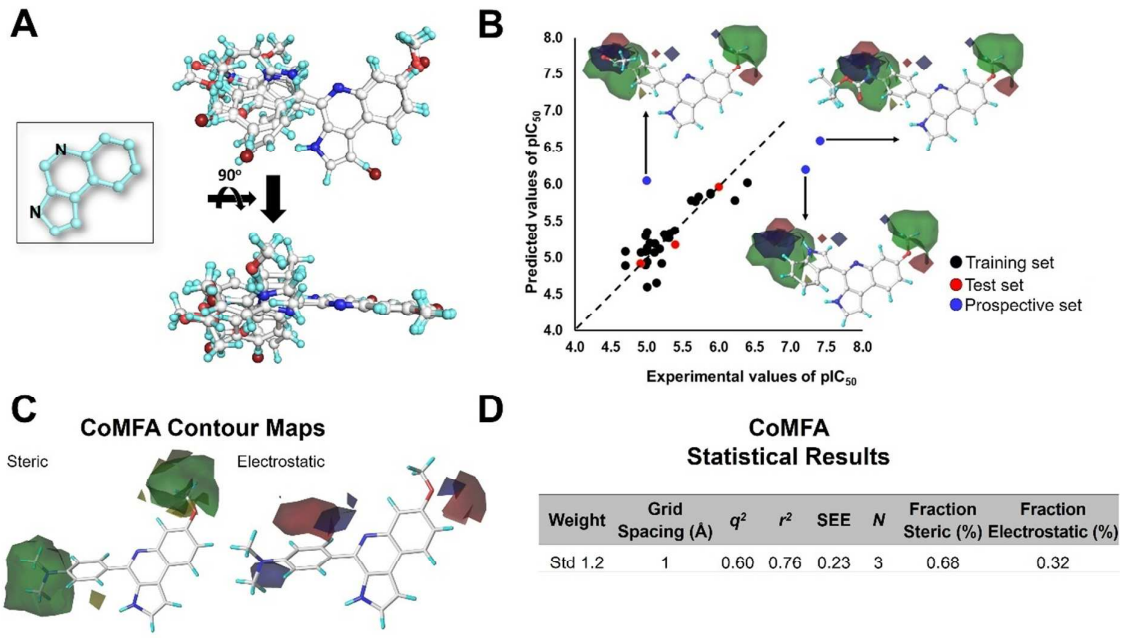

Weight	Grid Spacing (Å)	q^2	r^2	SEE	N	Fraction Steric (%)	Fraction Electrostatic (%)
Std 1.2	1	0.60	0.76	0.23	3	0.68	0.32

Figure 3. 3D-QSAR modeling. (**A**) Orthogonal view of the 3D data set alignment. Insert: maximal common scaffold used for the molecular alignment. (**B**) Plot of predicted values of pIC_{50} versus the corresponding experimental values for the training set (black circles), test set (red circles) and prospective set (blue circles) inhibitors for the best CoMFA model. Structures and CoMFA contribution maps of the prospective inhibitors **48–50** (blue circles) are indicated. (**C**) CoMFA contour maps for the most potent marinoquinoline derivative **40** (steric contributions: yellow = -0.0005 kcal/mol; green = 0.0015 kcal/mol, electrostatic contributions: red = -0.001 kcal/mol; blue = 0.001 kcal/mol). (**D**) Key statistical parameters for the best CoMFA model.

FIGURE 4

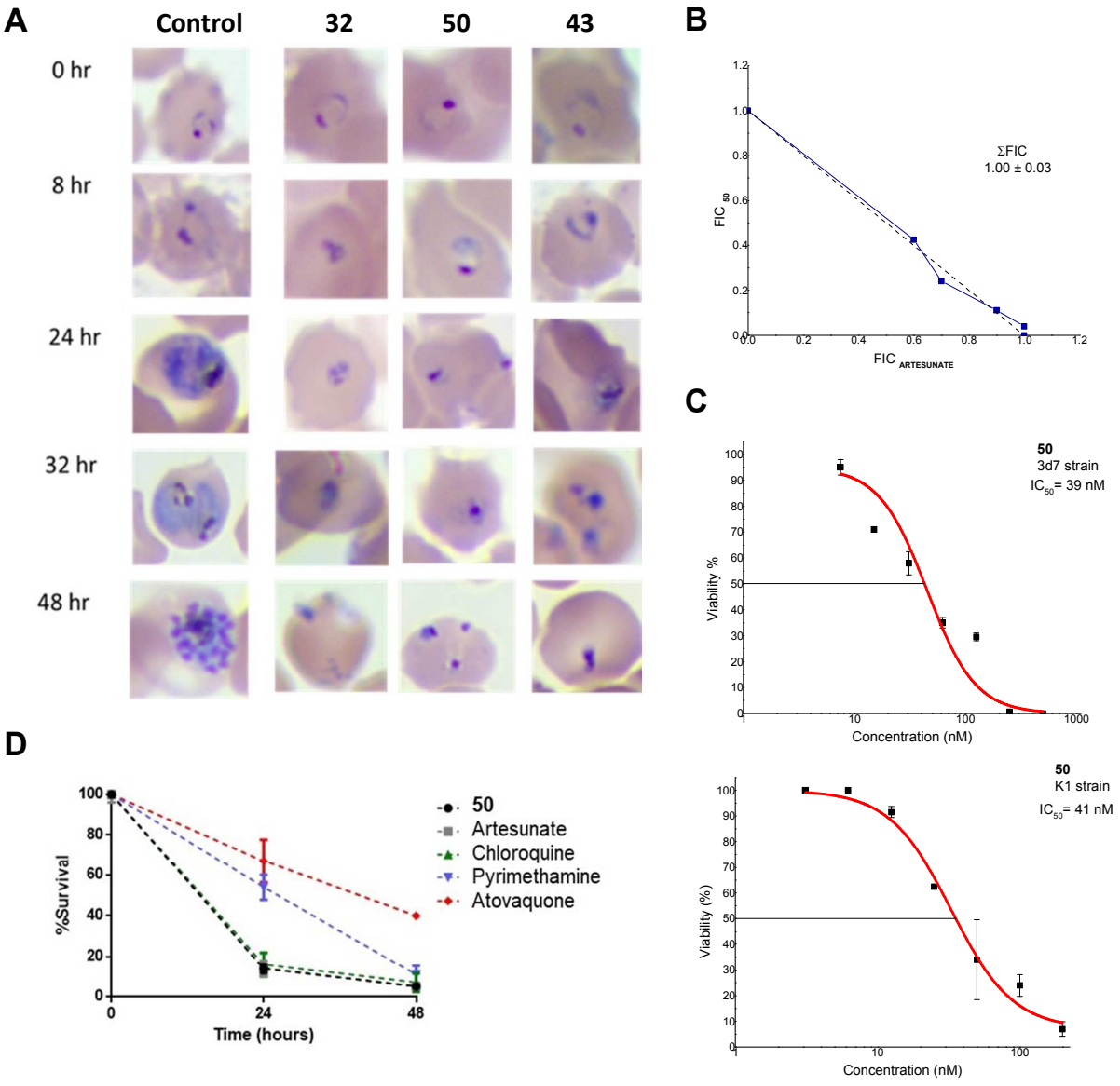

E

Cpd	Time treatment		
	0 h	24 h	48 h
	% survival	% survival ± SD	% survival ± SD
50	100	14 ± 2	6 ± 1
	Controls		
artesunate	100	14 ± 4	5 ± 1
chloroquine	100	16 ± 6	8 ± 4
pyrimethamine	100	55 ± 6	11 ± 4
atovaquone	100	68 ± 11	40 ± 1

Figure 4: (**A**) Microscopy of synchronized parasites continuously treated with **32**, **43** and **50** at concentration 10-fold the IC_{50} values and DMSO (control). Representative images of three independent experiments. (**B**) Isobologram plot for drug interaction analysis of compound **50** and artesunate. (**C**) In vitro *P. falciparum* 3d7 and K1 strains growth inhibition. Representative concentration-response curve of **50.** The fitted IC_{50}

value of 41 ($CI^{95\%}$ = 34–48) is the average of two independent experiments. (**D**) Percentage of survival parasite after treatment with **50** or standard antimalarial drugs. (**E**) Summary of percentage of survival parasite after treatment with **50.**

FIGURE 5

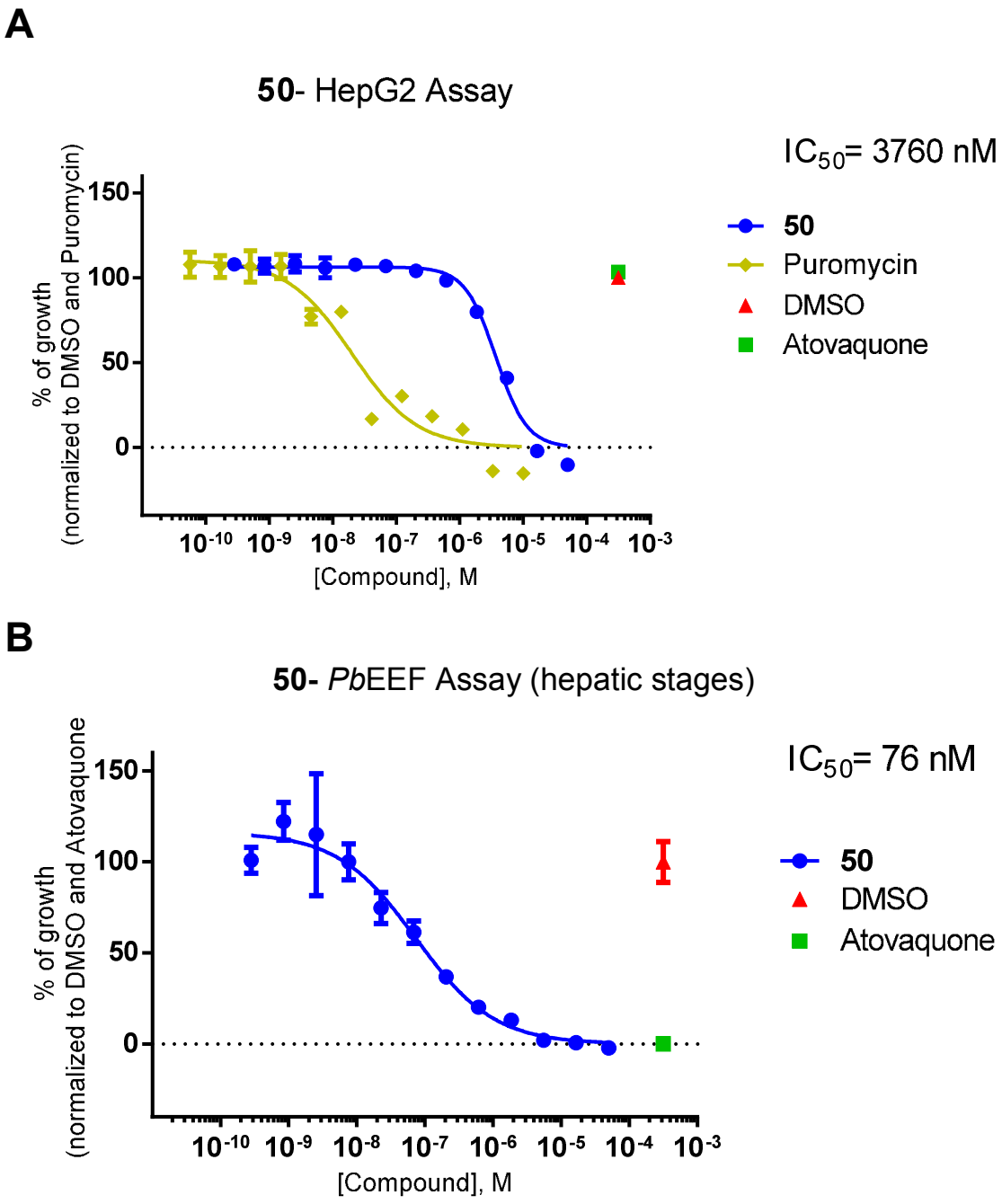

Figure 5: (**A**) Cytotoxicity evaluation of **50** against HepG2 cells, (**B**) Concentration-response curve for compound **50** in the exoerythrocytic (hepatic stages) forms of *P. berghei* by luciferase assay.

FIGURE 6

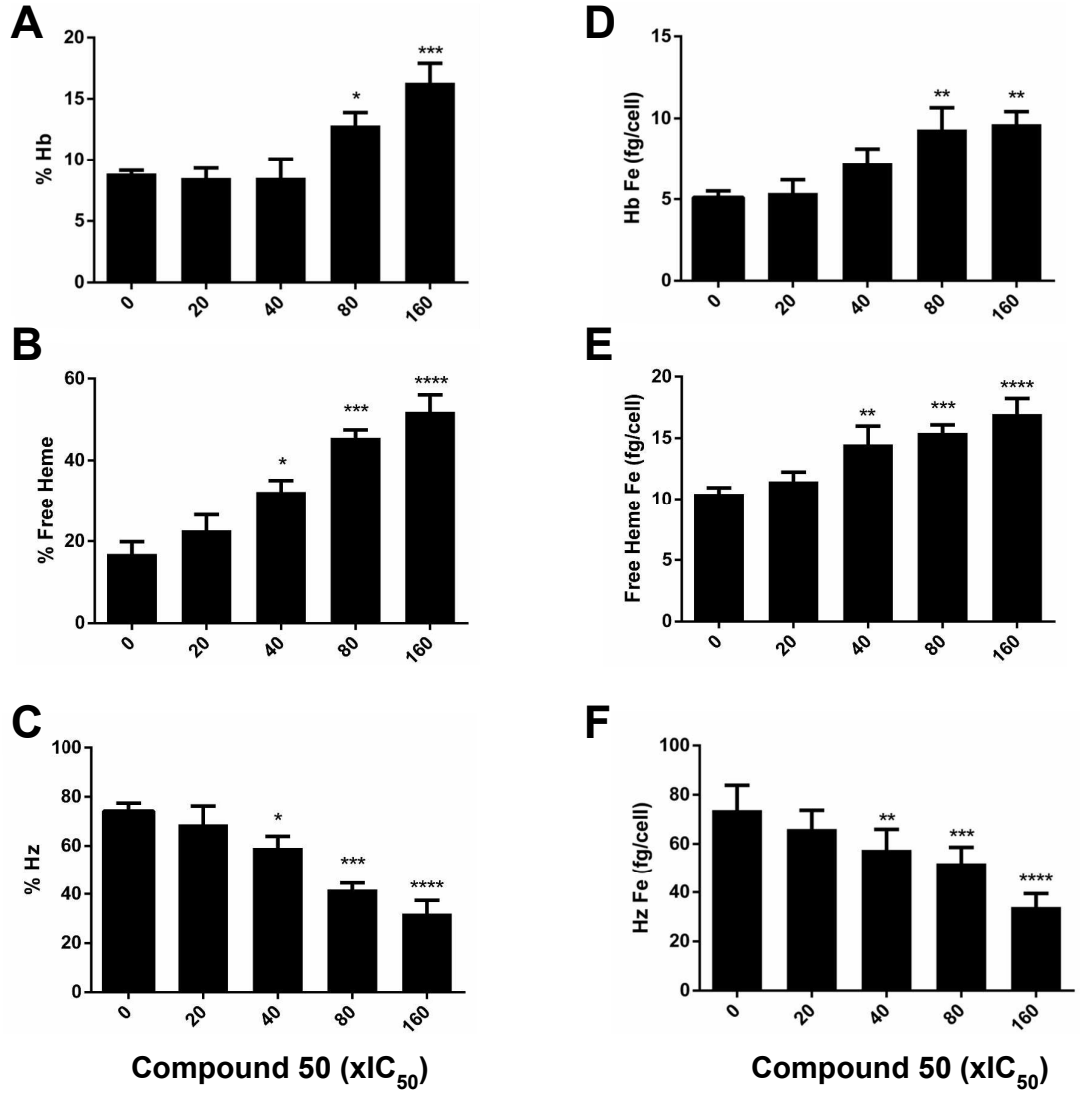

Figure 6. Heme species in compound 50-treated parasite. (**A**-**C**) Distribution of Hb (**A**), free heme (**B**), and Hz (**C**) in *P. falciparum* parasites observed in the presence of increasing concentration of **50** (20–160xIC_{50} value). (**D**–**F**) Concentration of heme species in femtogram per cell (fg/cell) was calculated after **50**-treated isolated parasites for (**D**) hemoglobin (Hb), (**E**) free heme and (**F**) hemozoine (Hz) in both untreated and treated parasites. Treated parasite was compared with untreated control parasite and statistical significance was calculated using Dunnett test (error bars showing 95 % CI). Bar graphs represents that each experiment was performed at least three times in triplicate. *P<0.05; **P<0.01; ***P<0.001; ****P<0.0001.

FIGURE 7

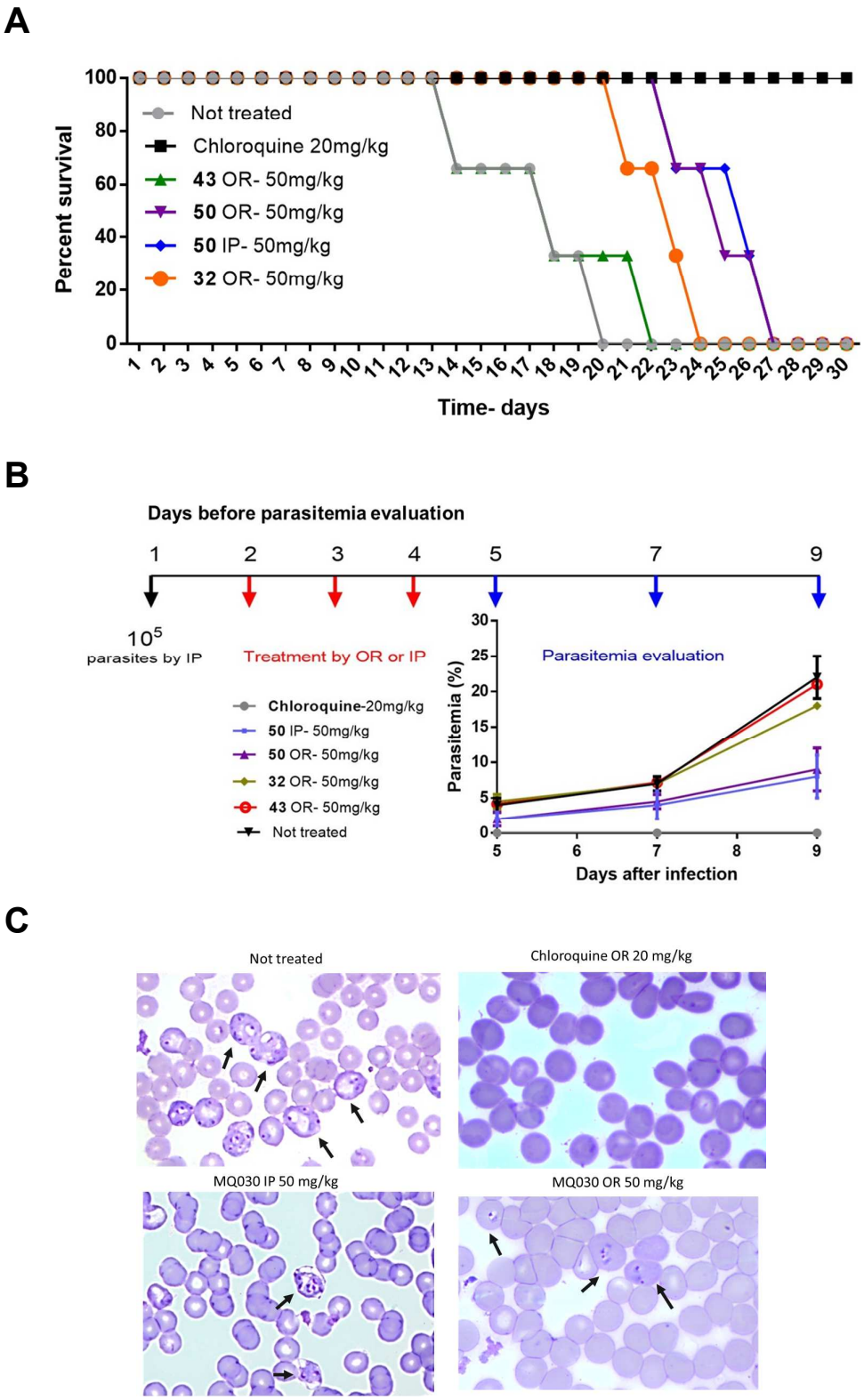

Figure 7. (**A**) In vivo survival after treatment with **32** (by OR), **43** (by OR) and **50** (by OR and IP). (**B**) Percentage of parasitemia on days 5, 7 and 9 after infection. Compound **32**, **43** and **50** were administered at 50 mg/Kg by OR or IP, chloroquine was used as a positive control 20 mg/Kg. (**C**) Microscopy of blood smears of not treated and treated mice with **50** 50 mg/Kg (OR or IP)**.** Arrows indicate infected cells.

FIGURE 8

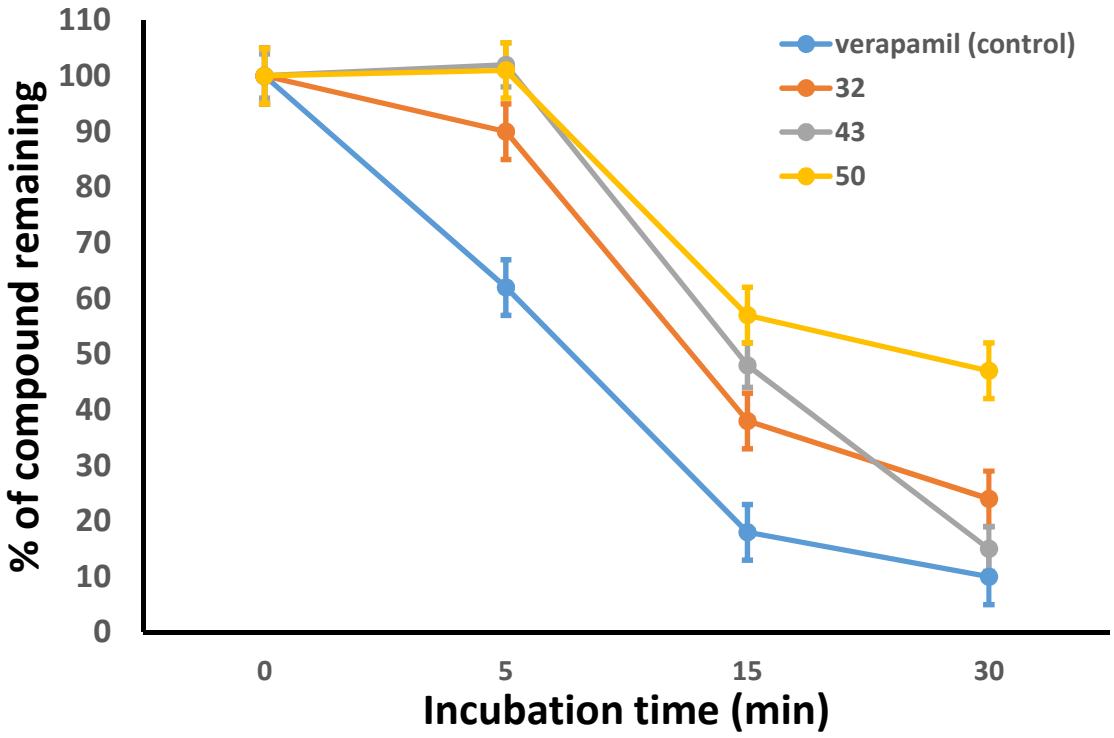

Figure 8. Metabolic stability evaluation of **32**, **43** and **50** in rat liver microsomes.

Table of Contents Graphic

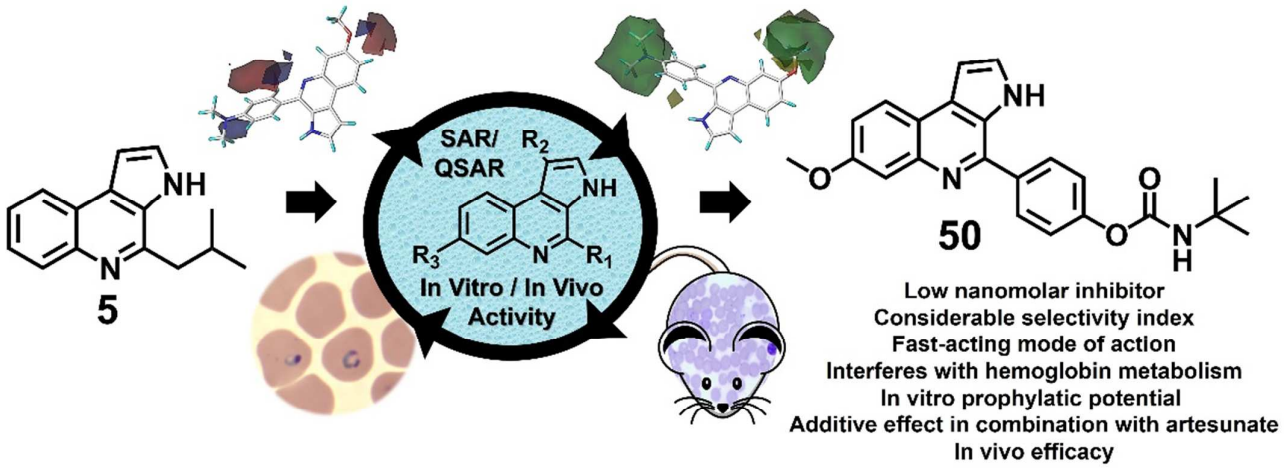

Scheme 1a: Preparation of the marinoquinolines using Suzuki Coupling and Pictet-Spengler ring closure

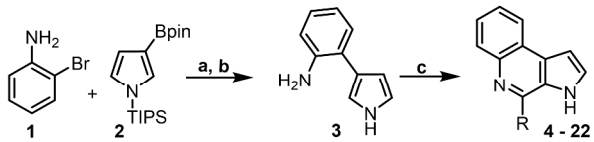

4 - methyl
5 - isobutyl
6 - benzyl
7 - ethyl
8 - phenyl
9 - 4-methoxy
10 - 3,5-dimethoxy
11 - 3,4,5-trimethoxy
12 - 4-chloro
13 - 4-bromo
14 - 4-nitro
15 - 4-amino
16 - 4-dimethylamino
17 - 4 - CO_2H
18 - 4- CO_2Me
19 - indole-3-yl
20 - 5-bromo-indol-3-yl
21 - 6-bromo-indol-3-yl
22 - indol-2-yl

Scheme 1: General scheme for the preparation of marinoquinolines (MQ).
Scheme 1a: Preparation of the marinoquinolines using Suzuki Coupling and Pictet-Spengler ring closure

338x190mm (300 x 300 DPI)

Equation 1a: Preparation of the Iodobenzenes

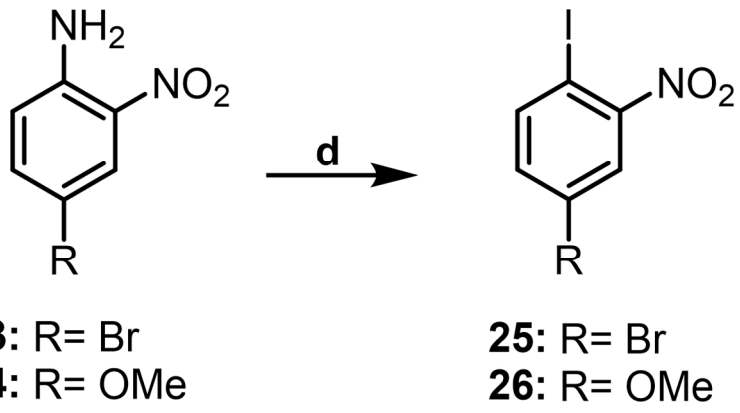

23: R= Br
24: R= OMe

25: R= Br
26: R= OMe

Equation 1a: Preparation of the Iodobenzenes

150x87mm (300 x 300 DPI)

Scheme 1b: Preparation of the brominated marinoquinoline using Suzuki Coupling and Pictet-Spengler ring closure

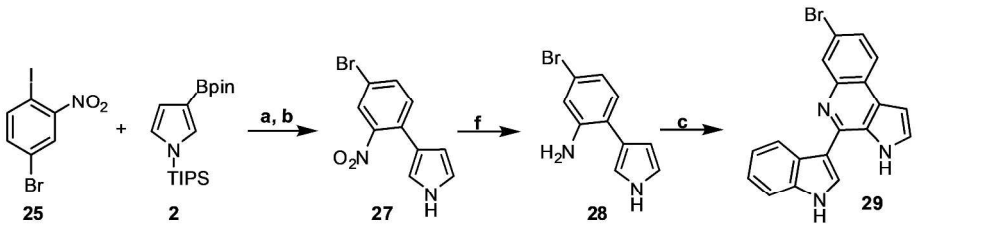

Scheme 1b: Preparation of the brominated marinoquinoline using Suzuki Coupling and Pictet-Spengler ring closure

338x190mm (300 x 300 DPI)

Scheme 1c: Preparation of the methoxylated marinoquinoline using Suzuki Coupling and Pictet-Spengler ring closure

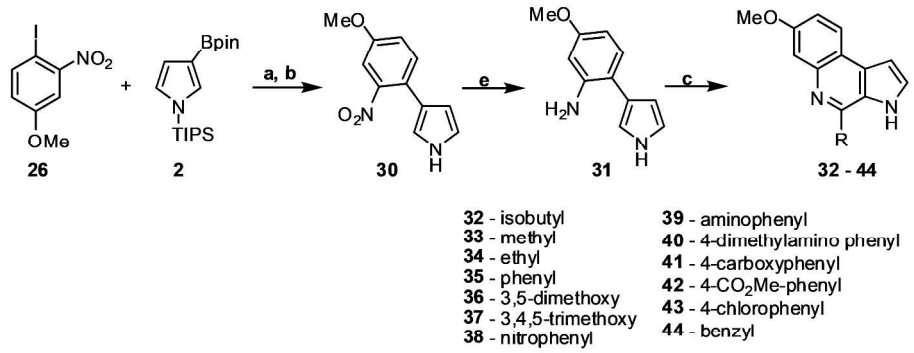

32 - isobutyl
33 - methyl
34 - ethyl
35 - phenyl
36 - 3,5-dimethoxy
37 - 3,4,5-trimethoxy
38 - nitrophenyl
39 - aminophenyl
40 - 4-dimethylamino phenyl
41 - 4-carboxyphenyl
42 - 4-CO_2Me-phenyl
43 - 4-chlorophenyl
44 - benzyl

Scheme 1c: Preparation of the methoxylated marinoquinoline using Suzuki Coupling and Pictet-Spengler ring closure

338x190mm (300 x 300 DPI)

Equation 1b: Regioselective bromination of marinoquinolines **19** and 33

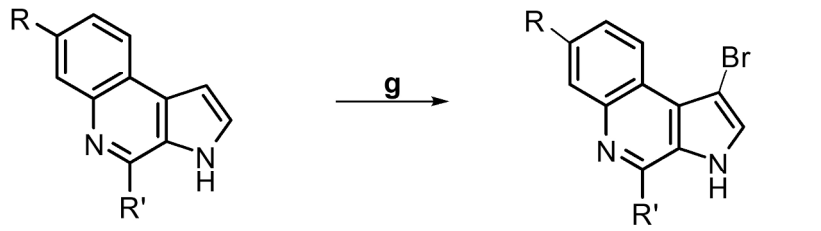

19: R= H, R' = indole-3-yl
33: R= OMe, R' = methyl
35: R= OMe, R' = phenyl

45: R= H, R' = indole3-yl
46: R= OMe, R' = methyl
47: R= OMe, R' = phenyl

Equation 1b: Regioselective bromination of marinoquinolines 19 and 33

220x109mm (300 x 300 DPI)

Equation 1c: Preparation of the theoretically predicted marinoquinolines derivatives

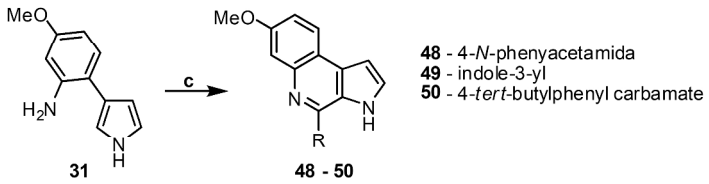

Equation 1c: Preparation of the theoretically predicted marinoquinolines derivatives

338x190mm (300 x 300 DPI)

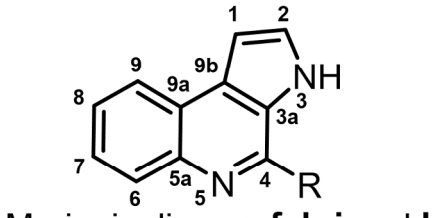

Mariquinolines **a-f**, **h-i** and **k**

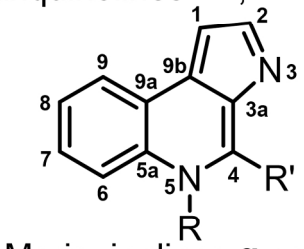

Mariquinolines **g** and **j**

MQa: R = Me
MQb: R = iBu
MQc: R = benzil
MQd: R = p-OH-benzil
MQe: R = 3-indol
MQf: R = indol-3-carbonil
MQg: R = Me, R' = Me
MQh: R = p-phenol
MQi: R = *N*-butylacetamide
MQj: R = Me, R' = H
MQk: R = H

Figure 1: (A) 3H-pyrrolo[2,3-c]quinoline containing natural products isolated from Ohtaekwangia kribbensis, Mooreia alkaloidigena and Catalinimonas alkaloidigena.

177x103mm (300 x 300 DPI)

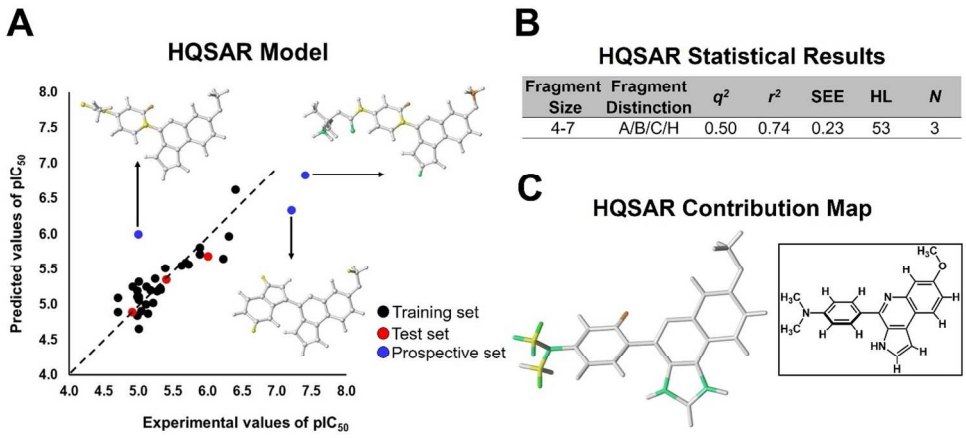

Figure 2. 2D-QSAR modeling. (A) Plot of predicted values of pIC50 versus the corresponding experimental values for the training set (black circles), test set (red circles) and prospective set (blue circles) inhibitors for the best HQSAR model. Structures and HQSAR contribution maps of the prospective inhibitors 48–50 (blue circles) are indicated. (B) Key statistical parameters for the best HQSAR model. (C) HQSAR contribution map for the most potent marinoquinoline derivative 40 (green and yellow = positive contribution of an atom to the activity of the molecules; gray = neutral contribution of an atom to the activity of the molecules; orange and red = negative contribution of an atom to the activity of the molecules). Insert: 2D structure of 40 inhibitor.

325x147mm (300 x 300 DPI)

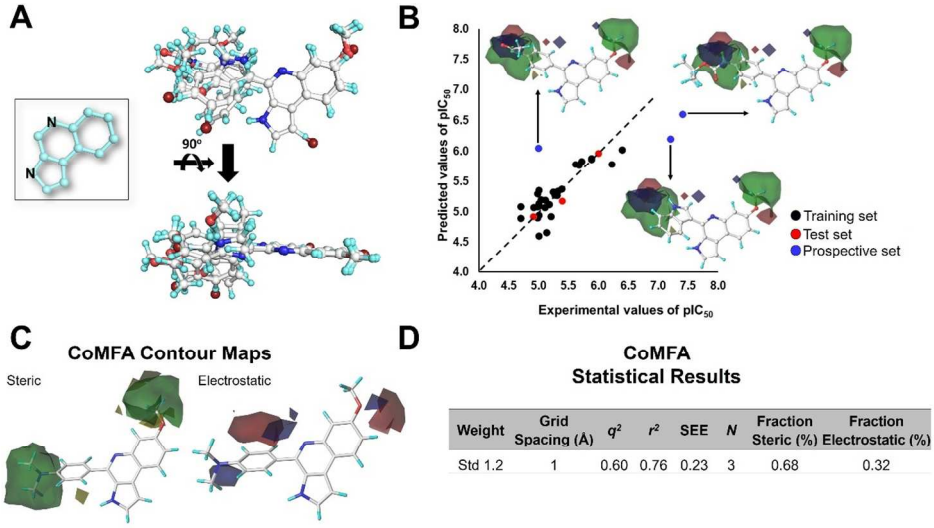

Weight	Grid Spacing (Å)	q^2	r^2	SEE	N	Fraction Steric (%)	Fraction Electrostatic (%)
Std 1.2	1	0.60	0.76	0.23	3	0.68	0.32

Figure 3. 3D-QSAR modeling. (A) Orthogonal view of the 3D data set alignment. Insert: maximal common scaffold used for the molecular alignment. (B) Plot of predicted values of pIC50 versus the corresponding experimental values for the training set (black circles), test set (red circles) and prospective set (blue circles) inhibitors for the best CoMFA model. Structures and CoMFA contribution maps of the prospective inhibitors 48–50 (blue circles) are indicated. (C) CoMFA contour maps for the most potent marinoquinoline derivative 40 (steric contributions: yellow = -0.0005 kcal/mol; green = 0.0015 kcal/mol, electrostatic contributions: red = -0.001 kcal/mol; blue = 0.001 kcal/mol). (D) Key statistical parameters for the best CoMFA model.

338x190mm (300 x 300 DPI)

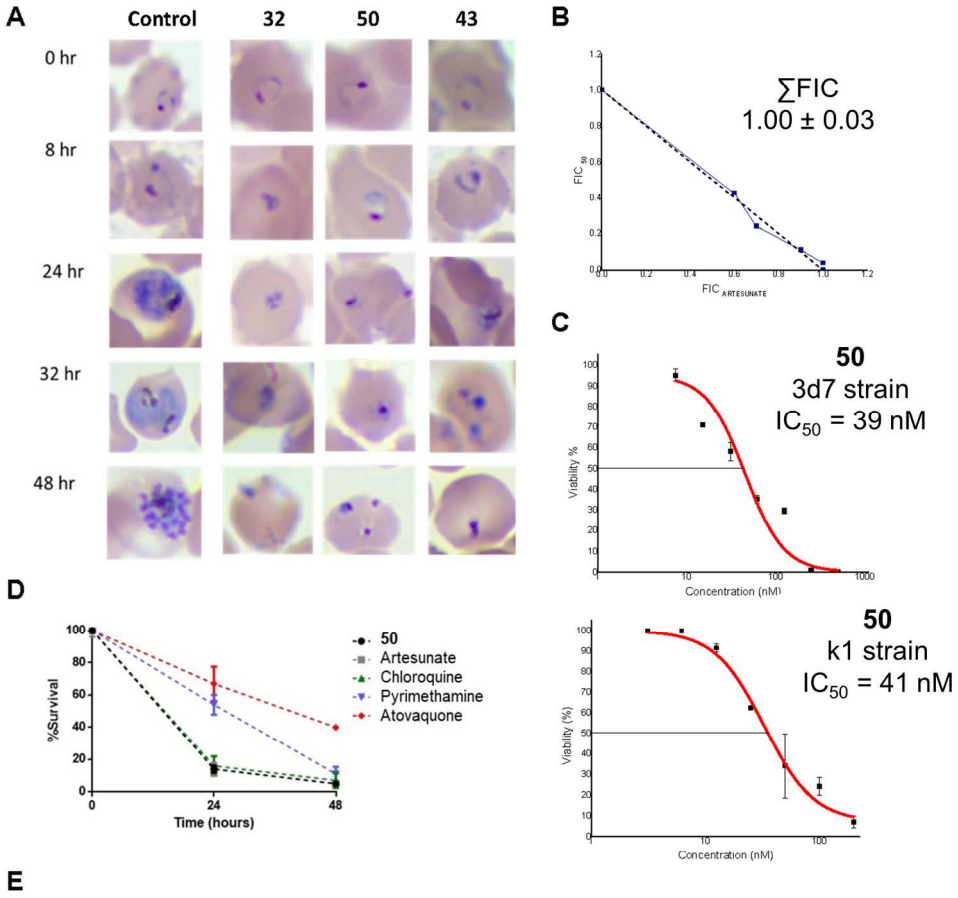

E

Cpd	Time treatment		
	0 h	24 h	48 h
	% survival	% survival ± SD	% survival ± SD
50	100	14 ± 2	6 ± 1
	Controls		
artesunate	100	14 ± 4	5 ± 1
chloroquine	100	16 ± 6	8 ± 4
pyrimethamine	100	55 ± 6	11 ± 4
atovaquone	100	68 ± 11	40 ± 1

Figure 4: (A) Microscopy of synchronized parasites continuously treated with 32, 43 and 50 at concentration 10-fold the IC50 values and DMSO (control). Representative images of three independent experiments. (B) Isobologram plot for drug interaction analysis of compound 50 and artesunate. (C) In vitro P. falciparum 3d7 and K1 strains growth inhibition. Representative concentration-response curve of 50. The fitted IC50 value of 41 (CI95% = 34–48) is the average of two independent experiments. (D) Percentage of survival parasite after treatment with 50 or standard antimalarial drugs. (E) Summary of percentage of survival parasite after treatment with 50.

155x190mm (300 x 300 DPI)

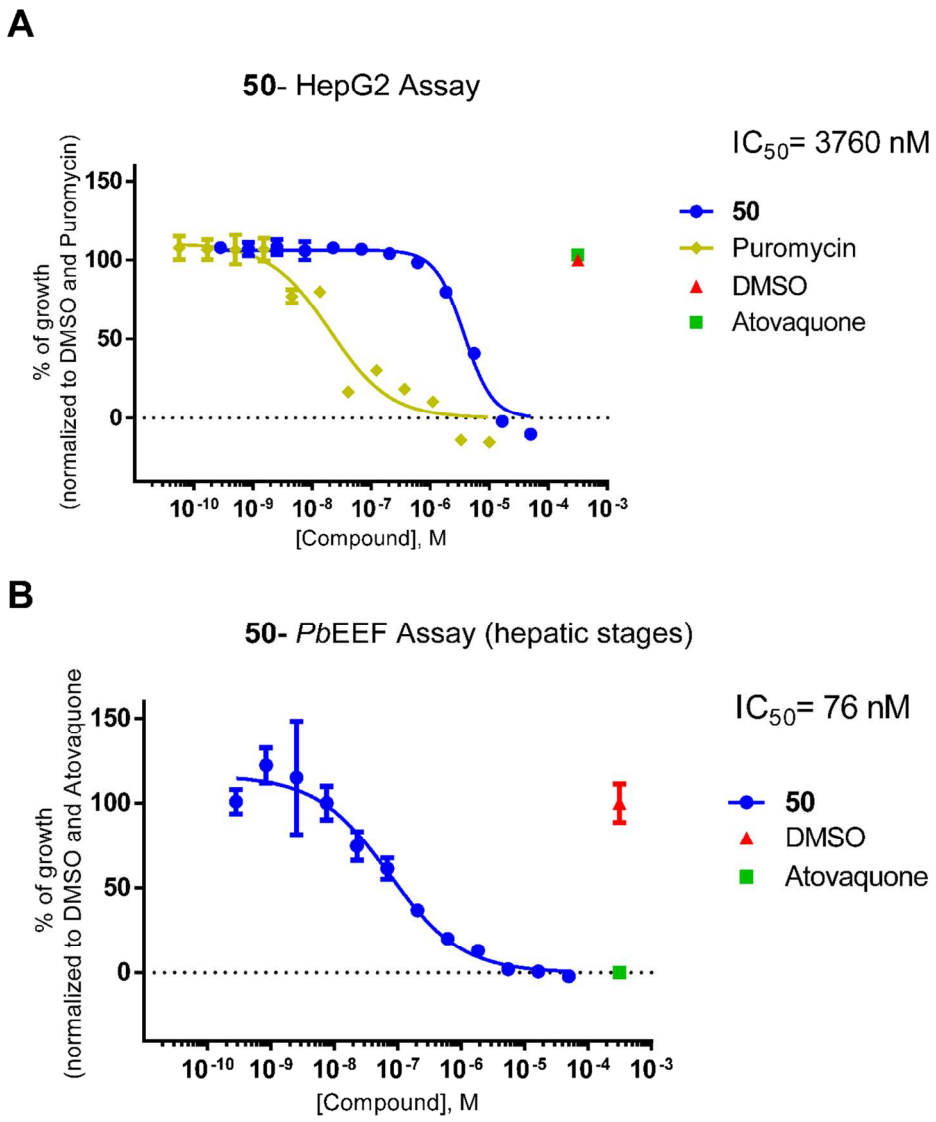

Figure 5: (A) Cytotoxicity evaluation of 50 against HepG2 cells, (B) Concentration-response curve for compound 50 in the exoerythrocytic (hepatic stages) forms of P. berghei by luciferase assay.

158x186mm (300 x 300 DPI)

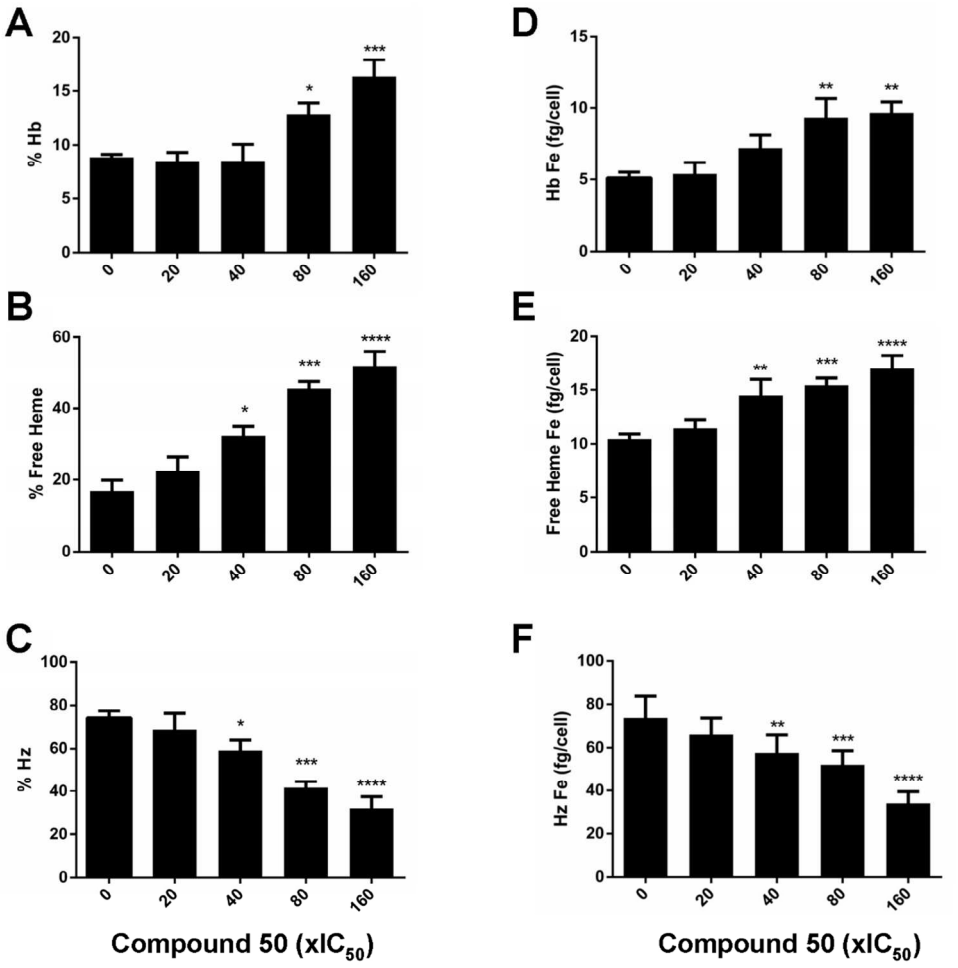

Figure 6. Heme species in compound 50-treated parasite. (A-C) Distribution of Hb (A), free heme (B), and Hz (C) in P. falciparum parasites observed in the presence of increasing concentration of 50 (20–160xIC50 value). (D–F) Concentration of heme species in femtogram per cell (fg/cell) was calculated after 50-treated isolated parasites for (D) hemoglobin (Hb), (E) free heme and (F) hemozoine (Hz) in both untreated and treated parasites. Treated parasite was compared with untreated control parasite and statistical significance was calculated using Dunnett test (error bars showing 95 % CI). Bar graphs represents that each experiment was performed at least three times in triplicate. *P<0.05; **P<0.01; ***P<0.001; ****P<0.0001.

184x190mm (300 x 300 DPI)

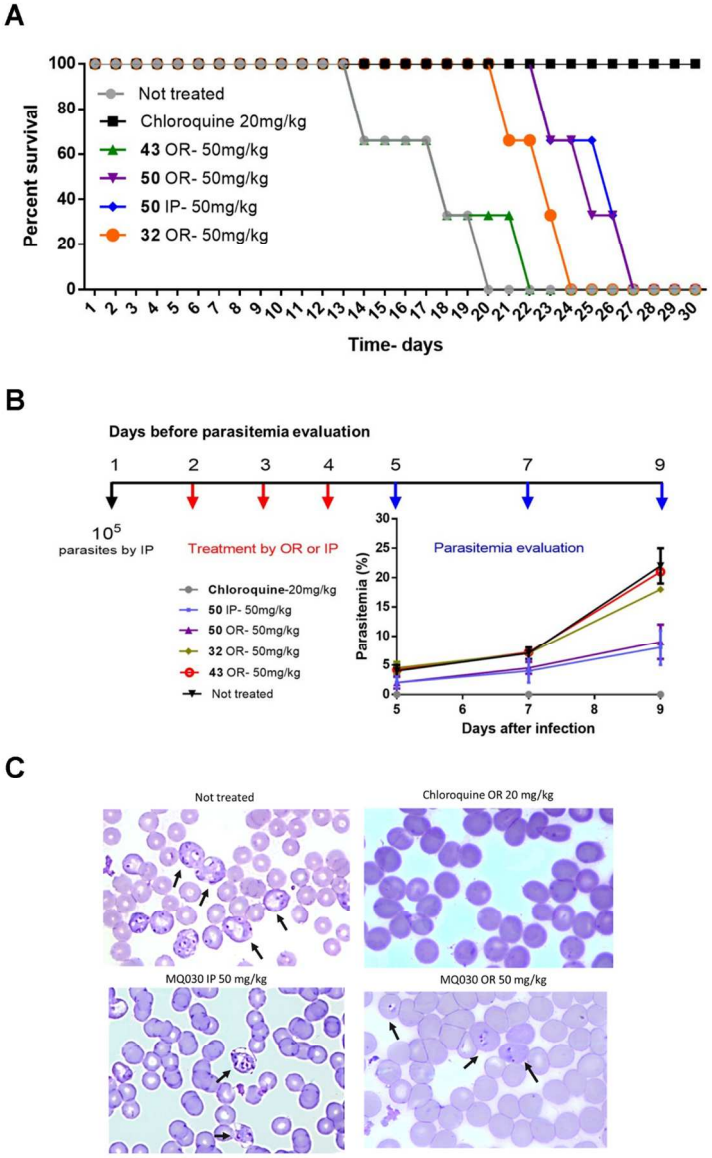

Figure 7. (A) In vivo survival after treatment with 32 (by OR), 43 (by OR) and 50 (by OR and IP). (B) Percentage of parasitemia on days 5, 7 and 9 after infection. Compound 32, 43 and 50 were administered at 50 mg/Kg by OR or IP, chloroquine was used as a positive control 20 mg/Kg. (C) Microscopy of blood smears of not treated and treated mice with 50 50 mg/Kg (OR or IP). Arrows indicate infected cells.

118x190mm (300 x 300 DPI)

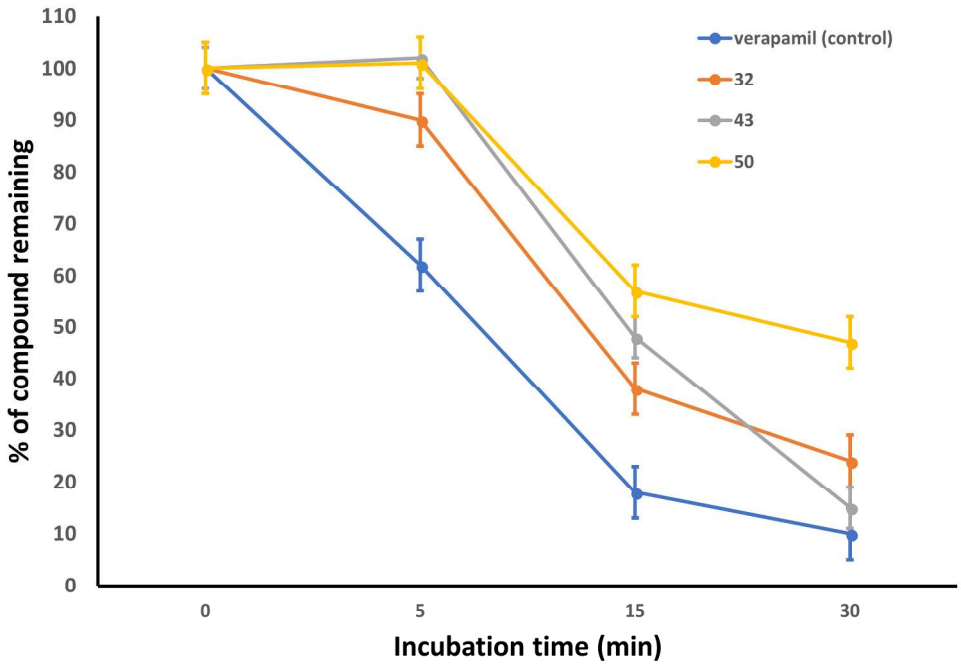

Figure 8. Metabolic stability evaluation of 32, 43 and 50 in rat liver microsomes.

213x150mm (300 x 300 DPI)

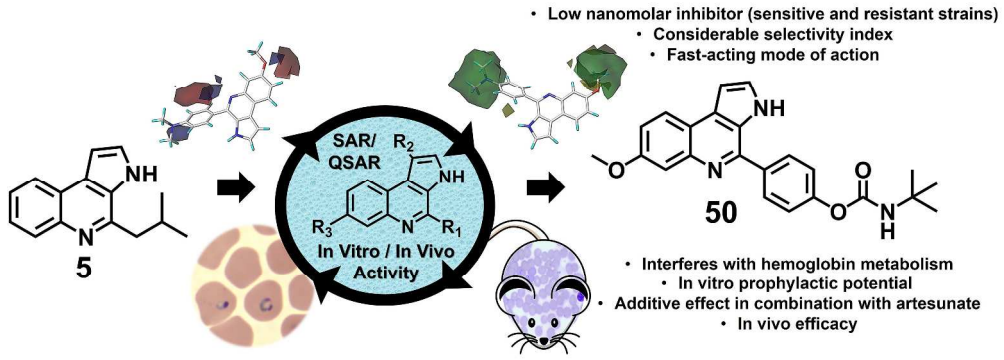

Table of Contents Graphic

338x127mm (300 x 300 DPI)